AD-783 898

ADAPTIVE ARRAY PROCESSING OF HF
BACKSCATTER RADAR SIGNALS

Lloyd J. Griffiths

Colorado University

Prepared for:

Rome Air Development Center
Advanced Research Projects Agency

May 1974

AD- 783 898

REPORT DOCUMENTATION PAGE		READ INSTRUCTIONS BEFORE COMPLETING FORM
1. REPORT NUMBER RADC-TR-74-194	2. GOVT ACCESSION NO.	3. RECIPIENT'S CATALOG NUMBER
4. TITLE *(and Subtitle)* Adaptive Array Processing of HF Backscatter Radar Signals		5. TYPE OF REPORT & PERIOD COVERED Semi-Annual (to 30 Mar 74) 6. PERFORMING ORG. REPORT NUMBER
7. AUTHOR(s) Lloyd J. Griffiths		8. CONTRACT OR GRANT NUMBER(s) F30602-72-C-0386
9. PERFORMING ORGANIZATION NAME AND ADDRESS University of Colorado Boulder CO 80302		10. PROGRAM ELEMENT, PROJECT, TASK AREA & WORK UNIT NUMBERS 62301E 14235101
11. CONTROLLING OFFICE NAME AND ADDRESS Defense Advanced Research Projects Agency 1400 Wilson Blvd Arlington VA 22209		12. REPORT DATE May 1974 13. NUMBER OF PAGES 105
14. MONITORING AGENCY NAME & ADDRESS(if different from Controlling Office) Rome Air Development Center (OCSE) ATTN: Leonard Strauss Griffiss AFB NY 13441		15. SECURITY CLASS. (of this report) UNCLASSIFIED 15a. DECLASSIFICATION/DOWNGRADING SCHEDULE

16. DISTRIBUTION STATEMENT *(of this Report)*

Approved for public release; distribution unlimited.

17. DISTRIBUTION STATEMENT *(of the abstract entered in Block 20, if different from Report)*

Approved for public release; distribution unlimited.

18. SUPPLEMENTARY NOTES

None

19. KEY WORDS *(Continue on reverse side if necessary and identify by block number)*

adaptive antenna arrays
HF arrays
interference rejection
range-doppler displays
tapped delay line filters

20. ABSTRACT *(Continue on reverse side if necessary and identify by block number)*

This report summarizes the results obtained during an
investigation directed toward the use of adpative antenna
array beamforming techniques in HF backscatter radar systems.
The work reported covers the period January 1, 1973 through
February 28, 1974 and is a continuation of previously reported
studies. Data for this investigation were obtained using the Side-

DD FORM 1 JAN 73 1473   EDITION OF 1 NOV 65 IS OBSOLETE   UNCLASSIFIED

Aperture HF Radio Research Facility which is located near Los Banos in the central valley of California and is operated by Stanford Research Institute, Menlo Park, California. Simultaneous digitized recordings were taken at four subarray outputs, with each subarray consisting of 32 vertical monopole elements which were combined using a conventional time delay and sum beamforming system. Total aperture for the study was 1.3km. Individual receivers with 1 kHz bandwidth and common local oscillator were used at the four subarray outputs. Transmitting facilities at Lost Hills, California and Bearden, Arkansas were used during the experiment.

Three transmit/receive formats were used during these investigations: 1) CW signals transmitted at Bearden, Arkansas at a frequency selected to provide one-hop ionospheric propagation were received at Los Banos in the presence of strong teletype interference. 2) CW signals transmitted at Lost Hills, California were used to provide one-hop backscatter geometry. A repeater, located at Bearden, provided 100 Hz DSB modulation for purposes of target simulation. 3) FM/CW radar format signals were transmitted from Lost Hills and the radar was used to search for targets of opportunity.

In all three cases, data were processed at the University of Colorado using a CDC 6400 computer. No real-time processing was attempted during the course of this study. Comparison of adaptive and conventional beamforming techniques on these data demonstrated that an output signal-to-noise ratio (SNR) improvement of 25-30 dB may be achieved using adaptive techniques in the presence of CW transmissions. This improvement was achieved for both the forward scatter and backscatter geometries. Adaptation performance in the presence of clutter was identical to that in an interference only environment. Total time for adaptation from zero coefficient values to steady-state optimum values was shown to be less than 40msec. Substantial noise reduction improvement in the range/doppler display obtained from an FM/CW transmitted signal was demonstrated.

The conclusion drawn from this study is that simple adaptive beamforming methods can easily be employed to operate in real-time on the SRI WARF array and that such methods will significantly improve overall radar performance.

ADAPTIVE ARRAY PROCESSING OF HF BACKSCATTER RADAR SIGNALS

Lloyd J. Griffiths

PUBLICATION REVIEW

This technical report has been reviewed and is approved.

RADC Project Engineer

ii

ABSTRACT

This report summarizes the results obtained during an investigation directed toward the use of adaptive antenna array beamforming techniques in HF backscatter radar systems. The work reported covers the period January 1, 1973 through February 28, 1974 and is a continuation of previously reported studies.

Data for this investigation were obtained using the Wide-Aperture HF Radio Research Facility which is located near Los Banos in the central valley of California and is operated by Stanford Research Institute, Menlo Park, California. Simultaneous digitized recordings were taken at four subarray outputs, with each subarray consisting of 32 vertical monopole elements which were combined using a conventional time delay and sum beamforming system. Total aperture for the study was 1.3 km Individual receivers with 1 kHz bandwidth and common local oscillator were used at the four subarray outputs. Transmitting facilities at Lost Hills, California and Bearden, Arkansas were used during the experiment.

Three transmit/receive formats were used during these investigations: 1) CW signals transmitted at Bearden, Arkansas at a frequency selected to provide one-hop ionospheric propagation were received at Los Banos in the presence of strong teletype interference. 2) CW signals transmitted transmitted at Lost Hills, California were used to provide one-hop backscatter geometry. A repeater, located at Bearden,

provided 100 Hz DSB modulation for purposes of target simulation. 3) FM/CW radar format signals were transmitted from Lost Hills and the radar was used to search for targets of opportunity.

In all three cases, data were processed at the University of Colorado using a CDC 6400 computer. No real-time processing was attempted during the course of this study. Comparison of adaptive and conventional beamforming techniques on these data demonstrated that an output signal-to-noise ratio (SNR) improvement of 25-30 dB may be achieved using adaptive techniques in the presence of CW transmissions. This improvement was achieved for both the forward scatter and backscatter geometries. Adaptation performance in the presence of clutter was identical to that in an interference only environment. Total time for adaptation from zero coefficient values to steady-state optimum values was shown to be less than 40 msec. Substantial noise reduction improvement in the range/doppler display obtained from an FM/CW transmitted signal was demonstrated.

The conclusion drawn from this study is that simple adaptive beamforming methods can easily be employed to operate in real-time on the SRI WARF array and that such methods will significantly improve overall radar performance.

CONTENTS

TABLES

ILLUSTRATIONS

I. SUMMARY

This report outlines the technical results obtained under RADC Contract No. F 30602-72-C-038C during the period January 1, 1973 to February 28, 1974. The work reported is a continuation of that previous reported.[1] This section presents a summary of the primary results obtained during the course of this study and the conclusions drawn from these results. Detailed information is presented in the sections following.

The objective of this work was to obtain quantitative measurements of the improvement provided by an adaptive array beamforming system in HF radar applications. Results were obtained using experimental data recorded in a relatively noisy HF environment. This work is a continuation of a previously reported study[1] which utilized CW, one hop, forward scatter ionospheric signals, and extends these results to the case of realistic HF backscatter radar environment. Data for this investigation were recorded using the Wide-Aperture HF Radio Research Facility (WARF) operated by Stanford Research Institute, Menlo Park, California. A complete description of this facility is given in Reference 2. An improved receiving system was employed for the present investigation. This system had 1 kHz bandwidth receivers at each of four subarray outputs at the WARF receiving site at

1

Los Banos. Simultaneous sample and hold circuitry was installed to provide a 2 kHz sampling rate at each receiver output. All data were recorded on seven track computer compatible magnetic tape and mailed to the University of Colorado for processing. Computations were carried out using the CDC 6400 facility at Colorado. Data for the present study were recorded during August, 1973.

Data were taken simultaneously from four adjacent subarray outputs of the WARF receiving array. Each subarray contains 32 vertical monopole elements at 10 meter spacing. These elements are combined using a remotely controlled time delay and sum beamforming system. The total aperture spanned by the four subarrays is 1.3 km. Transmitting facilities at Lost Hills, California were used to generate the radar signals and a low power repeater at Bearden, Arkansas was used for purposes of target simulation. In all tests, transmitter frequencies were selected so as to provide a one-hop ionospheric path between Bearden and Los Banos. All tests were conducted with the subarray elements steered in the boresight -- i.e., 90 degrees true -- direction. Transmitter frequencies were intentionally chosen near high interference regions of the HF spectrum for purposes of determining the SNR improvement capabilities of the adaptive beamforming system. All tests were conducted at approximately local noon at the ionospheric midpath point.

Three different experimental configurations were implemented during the course of this study:

1. CW forward scatter test-low power CW signals were transmitted from Bearden and received at Los Banos. Frequencies were selected to provide both high and low SNR conditions.

2. CW backscatter test-fixed frequency transmissions were generated at Lost Hills and received in a one-hop backscatter mode at Los Banos. A repeater at Bearden was used to produce 100 Hz sideband modulation for purposes of simulating a target. Both high and low SNR conditions were provided.

3. FM/CW backscatter test - a radar waveform format consisting of a sweep over 8 1/3 kHz at a 60 Hz repitition rate was transmitted from Lost Hills. The Los Banos array was then used to locate targets of opportunity in the backscatter signal. Once such a target had been located, data were recorded at the eight sub-array outputs.

These data were processed at Colorado to evaluate the performance improvement provided by an adaptive beamforming system. In each case, an adapted beam output was computed at a given data sample as the sum of delayed and weighted signals out of the four subarray receivers. The number of delayed signals from each subarray -- i.e., the total memory duration per subarray -- was preselected as 1,3,5, or 9 samples. Thus, the total number of variable weights in the adaptive array processor was 4,12,20, or 36. These weights were updated as each new data sample was received using

3

the P-vector adaptive algorithm described in the sections
following. The resulting beam output was then compared with
a conventional beam output formed by applying fixed Tchebsychev
weights to the four subarray outputs and summing the result.

Average output SNR improvement of adaptive over conven-
tional beamforming was measured for both the forward and back-
scatter CW tests described above. The results obtained were
as follows:

1. CW forward scatter at low received SNR (-25 dB at a
subarray output)

no. of wts/subarray	SNR improvement
1	3.2 dB
3	5.5 dB
5	9.6 dB
9	11.1 dB

2. CW backscatter at high received SNR (-38 dB)

5	25.5 dB

3. CW backscatter at low received SNR (-44 dB)

5	27.9 dB

It should be noted that the received SNR's shown above for
the backscatter signals are computed as signal-to-noise plus
interference plus clutter ratios. The total time to reach
steady-state adaptation was measured for each of the above
cases. This measurement was carried out by setting the
adaptive coefficients to zero and monitoring the output SNR
as a function of time as the weights adapted. The results
varied between 15 m sec for 9 weights per subarray in the

4

forward-scatter experiment to 30 m sec for 5 weights in the low SNR backscatter test.

Comparisons were also derived for the FM/CW tests. For these data, range/doppler maps were computed using a 0.5 sec. integration interval. Maps were computed for the same data set using both fixed, conventional beamforming at the four subarray outputs and a time variable, continuously adapting beamformer. In all cases, the adaptive range/doppler displays exhibit substantial noise improvement. Specific examples are presented in the sections following.

Several conclusions may be drawn from the results of this study:

1. Output SNR improvements of 20-30 dB may be achieved using four adaptive subarrays.

2. Total time to adapt is less than 40 m sec.

3. Five adaptive weights per subarray is sufficient to provide substantial improvement.

4. Adaptive improvement against clutter is identical to that achieved for interference -- i.e., the fact that the clutter is correlated with the desired signal does not degrade adaptive performance.

5. The P-vector algorithm can be used effectively for FM/CW radar formats.

Thus, adaptive processing of HF radar array signals appears to offer considerable improvement over conventional beam-forming systems. Further investigations should now be carried out to implement and demonstrate an on-line, real-time adaptive system.

5

II. INTRODUCTION

The investigation described herein is a continuation of a program which was initiated early in 1972. Previous results obtained during this program are summarized in References 1 and 3. These reports contain bibliographies and background information relevant to the general area of adaptive beamforming techniques. The primary objective of the overall program is to define the improvement provided by an adaptive beamforming system in HF radar applications. The work has been directed toward an investigation of the use of adaptive methods in the radar receiving array only. Thus, the transmitting system is presumed to consist of both fixed antenna hardware and fixed transmitter waveform format. In effect, the proposed adaptive array beamformer is to be considered as a component which will be added to an existing radar system with minimal change in the overall configuration. The questions which must be answered during the course of this program are 1) What is the improvement offered by the proposed system and 2) What are the costs associated with its implementation.

The specific objective of the research reported in this report was to obtain quantitative measurements which provide an answer to the first of these questions. The measurements were taken under conditions representative of

the environment in which an HF system must operate. Specifically, one-hop backscatter signals generated by an FM/CW transmitter format were received in the presence of relatively high noise and interference levels. Adaptive beamforming techniques are ideally suited to these conditions and can provide time variable null-tracking of both the frequency and spatial direction of arrival of interference sources.

A partial answer to the second question stated above may also be inferred from the results of the present study. The specific equipment configuration used to obtain the results consisted of an all digital system similar to that shown in Fig. 1. The cost of this system is easily ascertained and bears a direct relationship to the number of adaptive sub-arrays used and the complexity of the adaptive processing algorithm. Further investigations, however, are required to evaluate hybrid configurations of the type shown in Fig. 2 which may have significant advantages for wide bandwidth and/or multiple element systems.
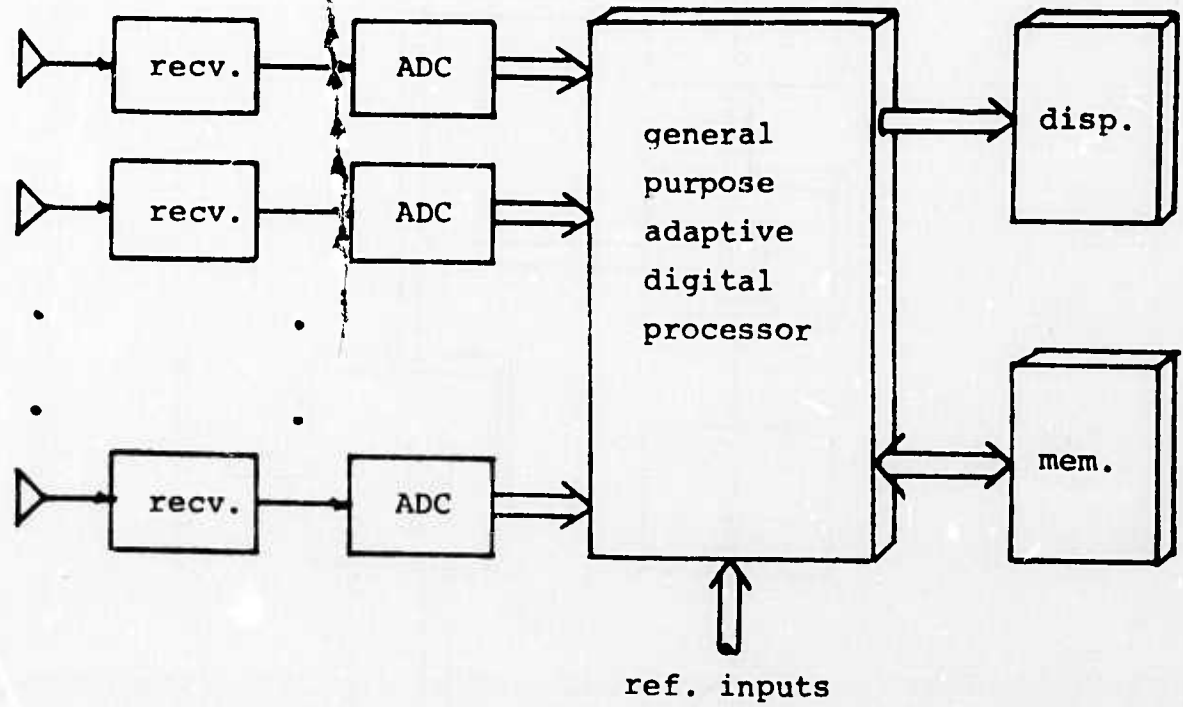
Fig. 1   General form of all digital adaptive receiving
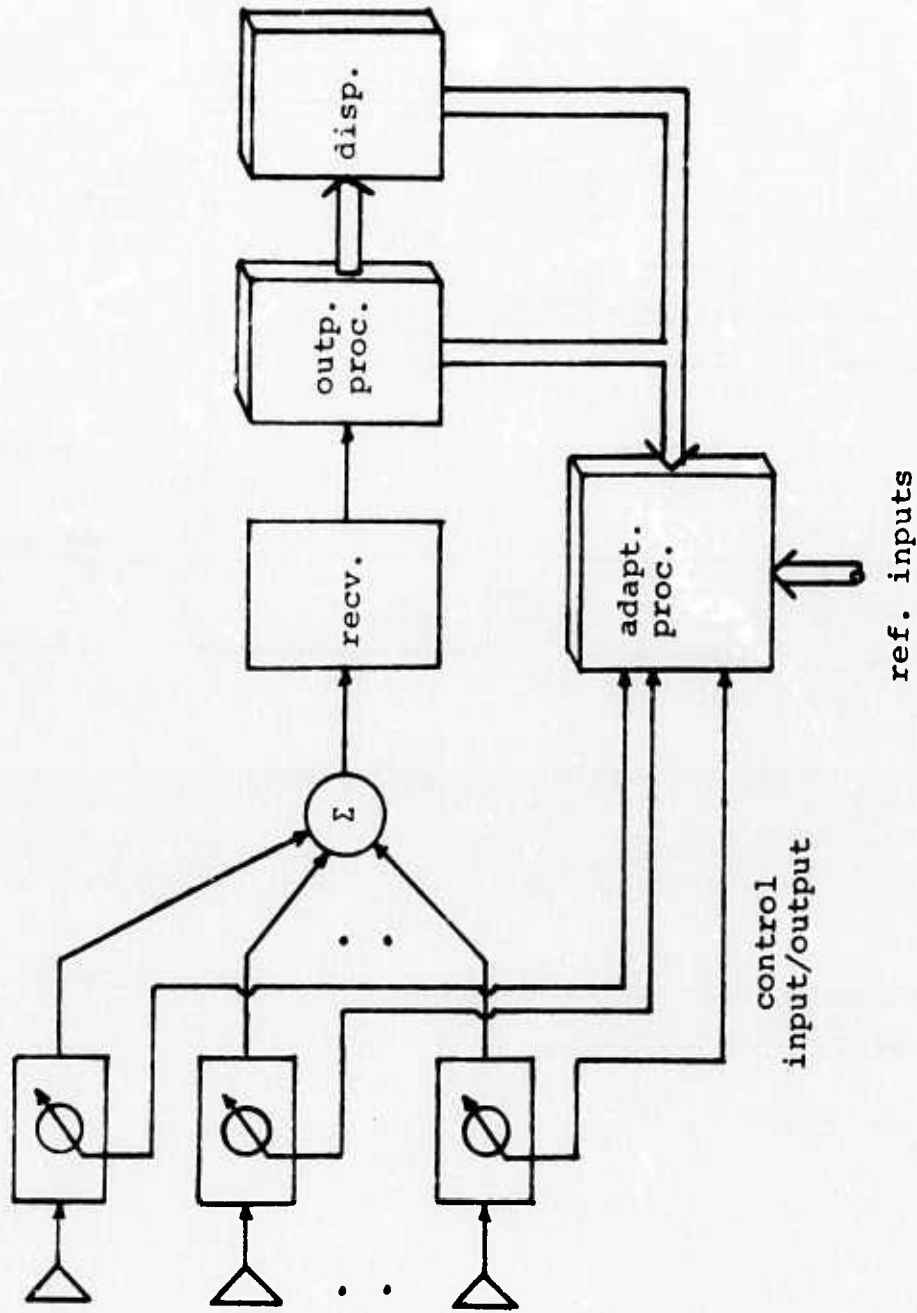array beamforming system.

Fig. 2 General form of hybrid analog/digital adaptive receiving array beamforming system

9

III. EXPERIMENTAL FACILITIES AND DATA BASE

A. EQUIPMENT

All data for the present study were recorded at the Los Banos receiving site of the WARF facility operated by the Ionospheric Dynamics Group at Stanford Research Institute, Menlo Park, California. Active transmitters at Bearden, Arkansas and Lost Hills, California were used during the course of the study. Figure 3 illustrates the relative locations of these facilities and summarizes their parameters. All tests were conducted with both the Los Banos and the Lost Hills arrays steered in the 90° true direction.

The receiving system at Los Banos utilized the outputs of four spatially separated adjacent subarrays. Each output consisted of the sum of 32 vertical monopole elements with a 10 meter spacing between elements. The array is linear and oriented in the North-South direction. Thus, a given subarray aperture was 320 meters and the total aperture spanned was 1.28 km. It should be noted that this aperture represents one half of the total available at Los Banos and that the entire system contains eight subarray outputs. Equipmental difficulties at the time of the tests, however, prevented utilization of the full array.

Figure 4 illustrates the receiving and recording system used in this work. The subarray output signals were de-
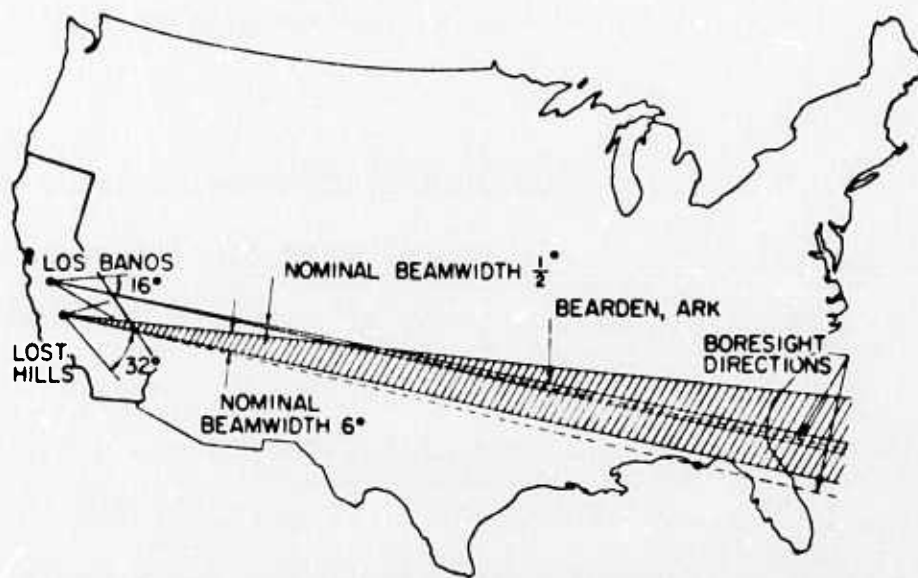
10

FIGURE 3 Location map.

WIDE-APERTURE RECEIVING STATION AT LOS BAÑOS, CALIFORNIA:
   256 vertical monopole antenna elements in 8 sub-arrays.
   Total length of array, 2.5 km.
   Frequency range, 9 to 27 MHz.
   Beamwidth at 20 MHz, 0.5 deg.
   Array is bidirectional, broadside.
   Boresight, 90 deg and 270 deg true.
   Direction of main lobe of sensitivity pattern may be repetitively slewed ± 16 deg in
      0.25 deg steps.
   Terrain eastward, flat.

TRANSMITTING AND REPEATING STATION AT BEARDEN, ARKANSAS:
   Average power capability, 1 kW
   Antennas:
      One single-element ITT FTM;
      Two horizontally polarized Collins LPA's (rotatable; 13 dB gain).

TRANSMITTING STATION AT LOST HILLS, CALIFORNIA:
   Average power capability, 30 kW.
   Antenna, 18-element ITT LDAA.
   Nominal gain, 18 dB.
   Midband beamwidth, 6 deg.
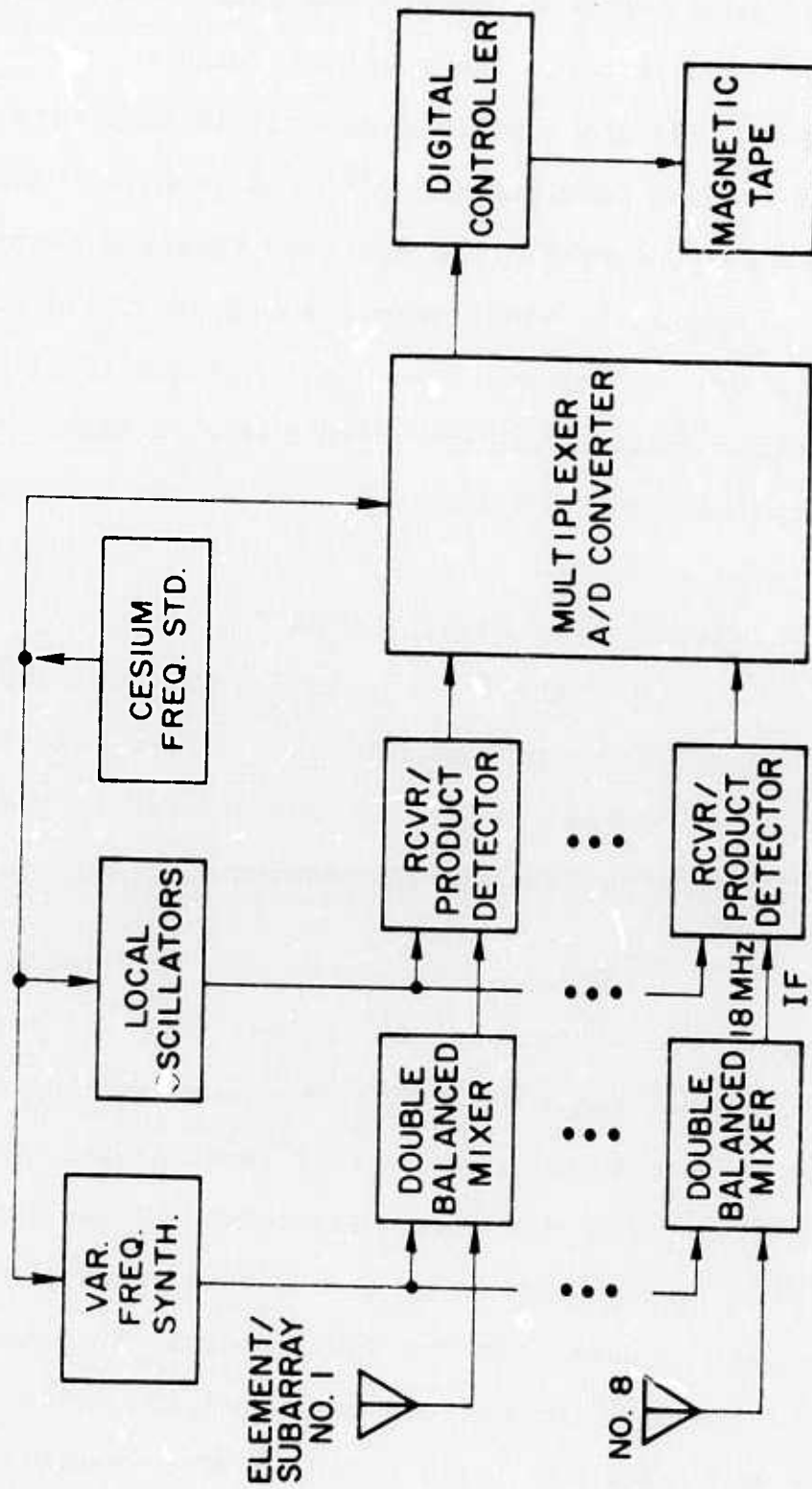   Boresight, 90 deg true, slewable ± 32 deg in 4 deg steps.

11

Figure 4   Block diagram of the eight-channel receiving and digital recording system for the Los Banos array.

12

modulated using four identical mixers and receivers driven by a common local oscillator. The receivers used were installed in March, 1973 and contained several improvements over those used for the previous study[1]. A receiver bandwidth of 1.0 kHz was selected. The detected baseband output signals served as inputs to simultaneous sample and hold circuits which were then digitized using a multiplexed 12 bit analog to digital converter and stored on magnetic tape. Thus, simultaneous samples were recorded from each of the four subarrays and the skew correction used previously[1] to compensate for a successive element A/D conversion was not required. The effective sampling rate of the system was 2.0 kHz per subarray output. The magnetic tapes produced in this manner were later converted to CDC 6400 compatible format and shipped to the University of Colorado for further processing.

B. DATA BASE

The magnetic tape format used to collect data was segmented into individual files with each file representing a time continuous recording of a particular experimental configuration. A given data file contained between 2 and 1000 physical magnetic tape records with each record consisting of 64 milliseconds of data from the four subarray outputs.

Table I is the data log written on August 17, 1974. Local time for the tests was 12:00 to 15:00 PST. Twelve files of data were recorded on this date and may be grouped into the following four experimental configurations:

13

TABLE I: Data log for WARF data collection
on August 17, 1973 during 12:00 - 15:00 PST.

Tape File No.	No. of Records	Sample Frequency	Tx Frequency	Tx Mode	Description
1	2	2000	-	off	500 Hz calibration signal
2	10	2000	17.124	off	TTY interference only 650-710 Hz
3	100	2000	17.124	off	Low SNR Bearden Tx @ 500 Hz
4	10	2000	17.124	off	High SNR Bearden Tx @ 500 Hz
5	10	2000	17.124	off	Repeat of File 4 with 1000 Hz broad band modulation at Bearden
6	50	2000	17.124	off	
7	100	2000	16.295	CW	High SNR Bearden repeater at ±100 Hz
8	100	2000	16.295	CW	Low SNR Bearden repeater at ±100 Hz
9	100	2000	16.295	FM/CW	Low SNR Bearden repeater at ±15 Hz
10	150	1920	16.295	FM/CW	Same as File 9 with different sampling
11	150	1920	16.355	FM/CW	High SNR Bearden repeater at ±15 Hz
12	1000	1920	11.640	FM/CW	Pseudo-operational test

14

1. File 1 Calibration:

Simultaneous, in phase, equal amplitude sinusoidal test sig-
nals were inserted into the system shown in Fig. 4 at the
locations normally used to connect the subarray output signals
to the double balanced mixers. These signals are used for in-
dividual gain/phase matching of the receivers and serve as an
indication of the system spurious levels.

2. Files 2-6 Forward scatter CW tests:

Transmitting facilities located at Bearden were used to gen-
erate signals at 17.124 MHz. This frequency was selected to
provide one-hop ionospheric propagation over the Bearden to Los
Banos path as well as a moderate amount of interference in the
1 kHz operating bandwidth. The data recorded on files 3 and 4
consisted of CW transmissions with the carrier offset by 500
Hz so as to appear in the center of the 1000 Hz analysis band.
Signal-to-noise ratio was varied by reducing the transmitter
power. Files 5 and 6 were recorded in a similar fashion with
the addition of a 1000 Hz broadband noise modulation imposed
on the CW carrier for purposes of simulating a spread spectrum
source. The objective of this series of experiments was to
obtain data under conditions similar to those taken during
the 1972 study and to use the data as a basis for comparison.

3. Files 7-8 Backscatter CW tests:

The Lost Hills facility was used to transmit CW signals at
16.295 MHz. A low power repeater at Bearden induced a ±100 Hz
offet prior to retransmission of the received signal. The
operating frequency provided one-hop propagation over the
path. Received SNR was varied during this experiment by re-

15

ducing the repeater output power. These data were collected for the purposes of comparing adaptive eprformance in the presence of clutter with that obtained under conditions of interference only (Files 2-6).

4. Files 9-12 FM/CW radar experiments:

The purpose of these experiments was to collect data using transmitter waveforms identical to those which would be used in an operational HF radar system. The waveform transmitted from Lost Hills consisted of a sawtooth linear FM sweep over a 8 1/3 kHz frequency range, centered at 16.3 MHz, and a sweep repetition rate of 60 Hz as shown in Fig 5. A repeater at Bearden was employed to simulate a 15 Hz. doppler offset target. The experiments consisted of tests under both low and high SNR conditions and a "pseudo-operational" experiment at 11.64 MHz with the repeater turned off. During this test, the radar was used to search for targets of opportunity. As shown in Table I, the sampling rate was reduced to 1.920 kHz to provide synchronization with the 60 Hz chirp repetition rate.

C. DATA PROCESSING AND EVALUATION

One method which may be used to examine spatially dis- tributed digital data which has been obtained from uniformly spaced linear array is the two-dimensional digital Fourier transform (2D DFT) described in a previous report[1]. In this technique, a two-dimensional data matrix A is formed as follows:
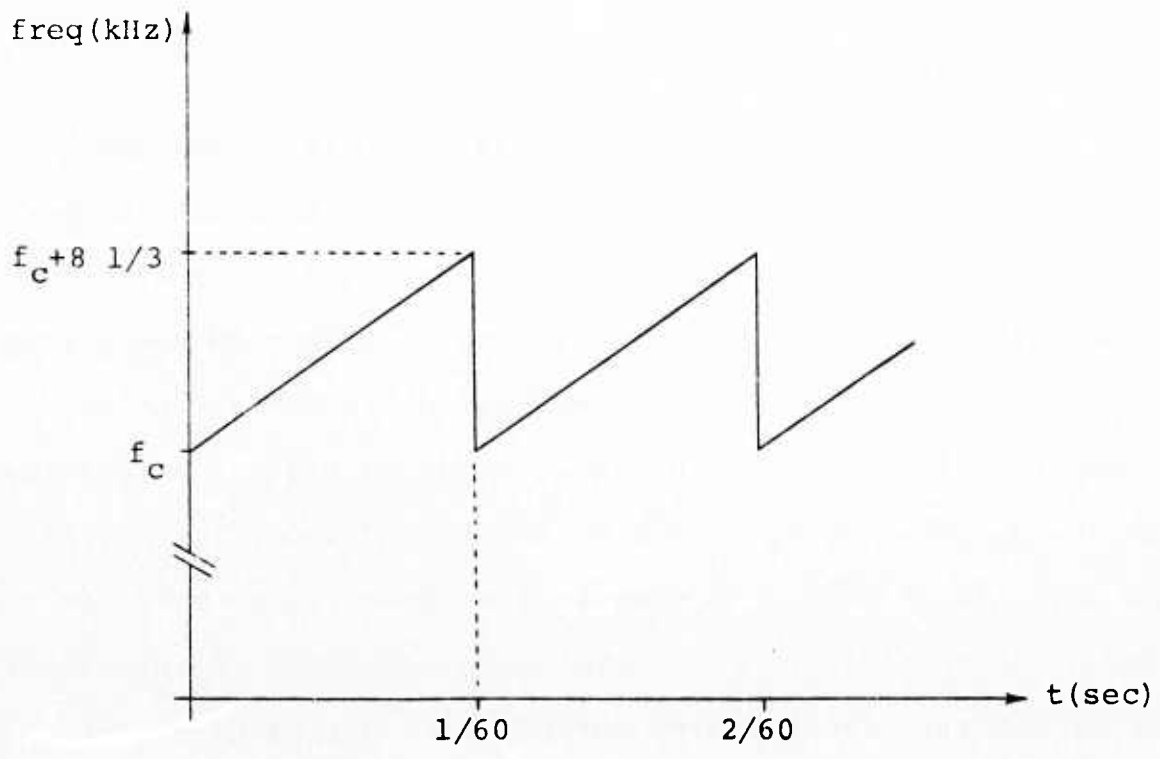
16

Fig. 5   Instantaneous frequency of transmitted
         waveform used during FM/CW tests

$$A = \begin{bmatrix} x_1(k) & x_1(k-1) & \cdots & x_1(k-N+1) \\ x_2(k) & x_2(k-1) & \cdots & x_2(k-N+1) \\ x_3(k) & & & \\ x_4(k) & & & x_4(k-N+1) \end{bmatrix} \quad (1)$$

where $x_\ell(k-j)$ = sample at time $(k-j)$ from ℓ^{th} subarray and N is the number of samples per element processed. Transforming the rows and columns of A produces a new matrix in which the elements of the ℓth row may be interpreted as the frequency spectrum for signals received from the ℓth resolvable azimuth. In a four element array, there are four resolvable azimuths spaced by

$$\Delta\theta = \sin^{-1}\left[\frac{C}{Lfd}\right] \quad (2)$$

where

C = velocity of propagation

L = no. of elements (subarrays)

f = received frequency

d = element spacing.

For the 4 subarray system used in the present study the spacing at 17 MHz is 0.80 degrees.

Figure 6 shows the results obtained with this technique for the calibration signal recorded in File 1. A total of 256 samples per element were processed to produce the display, thus providing a frequency resolution of about 8 Hz. The first eight zimuthal lines shown were obtained by interpolation of the four lines provided by the data. (The 9th line is a reproduction of the first included to maintain symmetry.) A

18
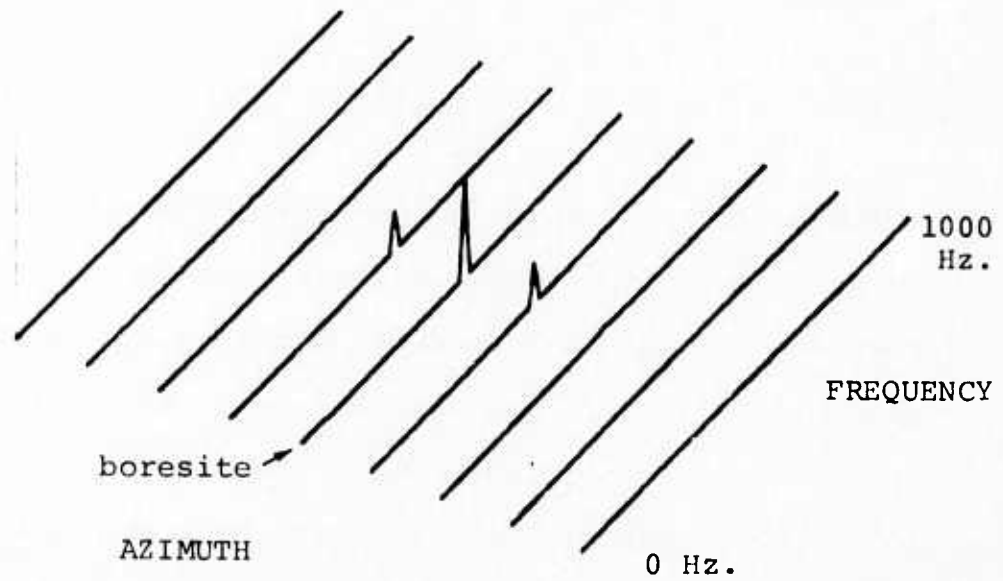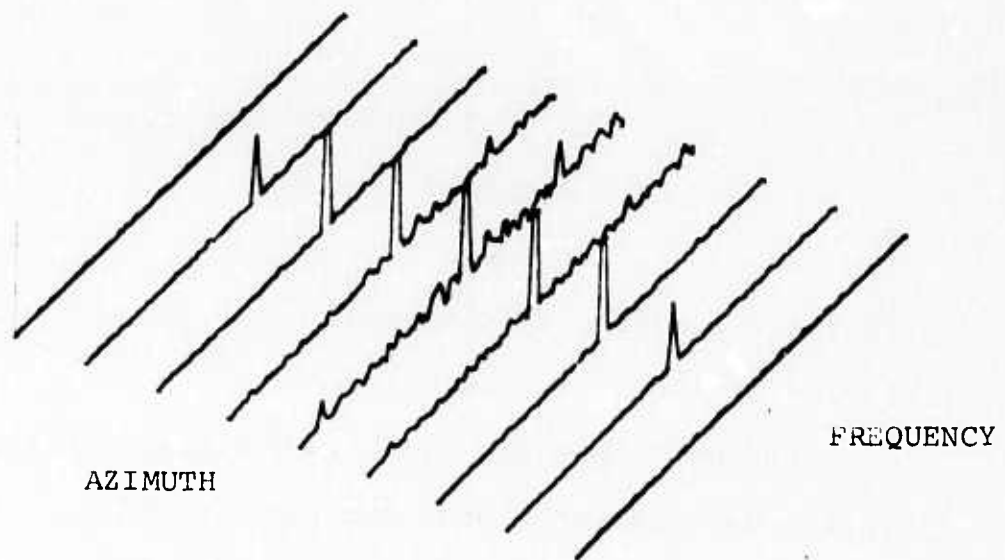
a) Display gain = 1.0

b) Display gain = 100.0

Fig. 6   Azimuth/frequency display for calibrate signal.

19

nine line display was generated for purposes of comparison with the previous work which resulted from eight element data.

Fig. 6a) has been normalized to the maximum computed value, and 6b) is the same display with all values multiplied by a factor of 100. Large amplitude values in Fig. 6b) have been clipped. The calibration signal is located at 500 Hz and has an apparent broadside direction of arrival. The sidelobes shown are produced by a raised cosine weighting which was applied to the data prior to 2D-DFT. Note that relatively few spurious signals are present in the data. The noise floor exhibits the same spatial characteristics as the calibration signal and was most likely produced by the calibration signal generator. These results represent a considerable improvement over the receiving system used in the previous study. The signal amplitude relative phase, and D.C. offset measured at each receiver output during calibration is summarized in Table II.

Table II: Calibration Summary

Channel	Amplitude	Phase	DC Offset
1	4.88	0	0.059
2	4.86	0.021°	0.015
3	4.84	-0.042°	0.012
4	4.87	0.005°	0.079

Figs. 7-10 illustrate 2D DFT's of some typical sample of the raw data recorded during the present study. The forward-

20

scatter CW transforms shown in Fig. 7 were computed using a total of 512 time samples from each subarray output. The resulting frequency resolution in the display is 4 Hz and enables identification of the desired signal in the high SNR case. Similar labelling for the low SNR case, however, is not readily obtained. Many of the remaining transforms presented in this report were computed using only 128 samples per element and a resulting resolution of 16 Hz. The transform equivalent to Fig. 7b) is presented in Fig. 8 for comparison. Note that although much of the fine scale frequency structure can no longer be identified, spatial and frequency domain characteristics of the interference field are readily apparent. The broadband signal shown in the 600-750 Hz frequency range was a teletype interference identified at the time date were recorded.

Figs. 9 and 10 illustrate the clutter-dominated data observed during the CW backscatter tests. The repeater offset signal can be seen in the high SNR experiment (arrow) and interference lines appear in the low SNR display. Transform results for the FM/CW experiment are shown in Fig. 11. The multiplicity of clutter lines which appear at 60 Hz separations corresponds to the chirp repetition rate.
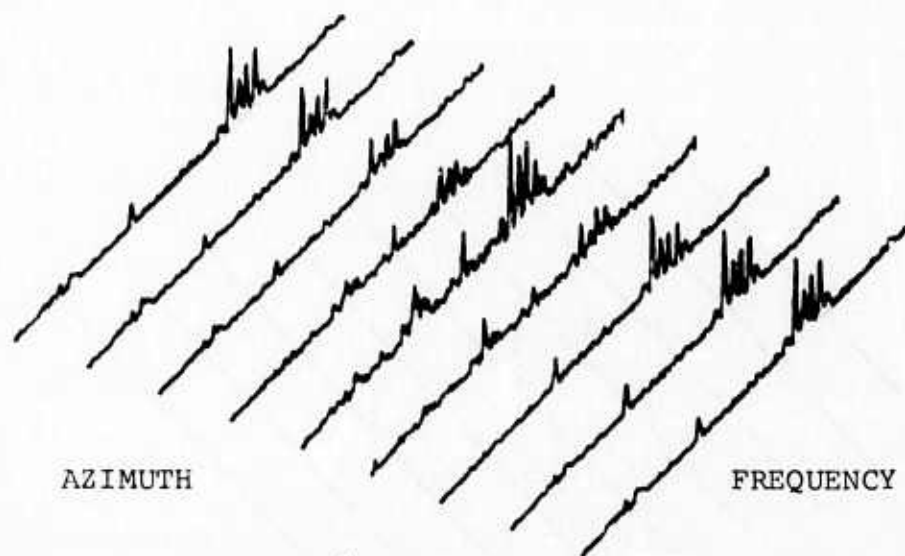
Fig. 7 a)
Azimuth/frequency
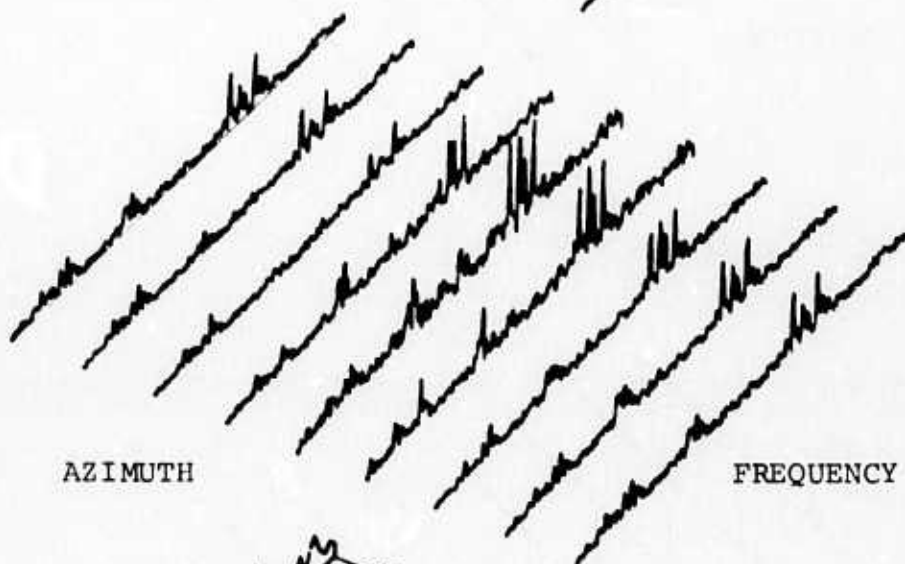display for high
SNR forward scatter
data.

Fig. 7 b)
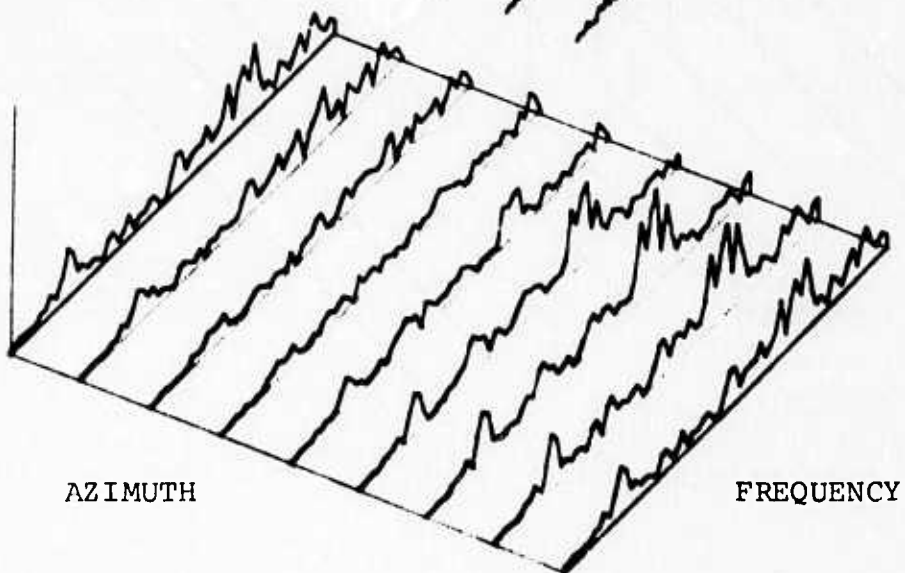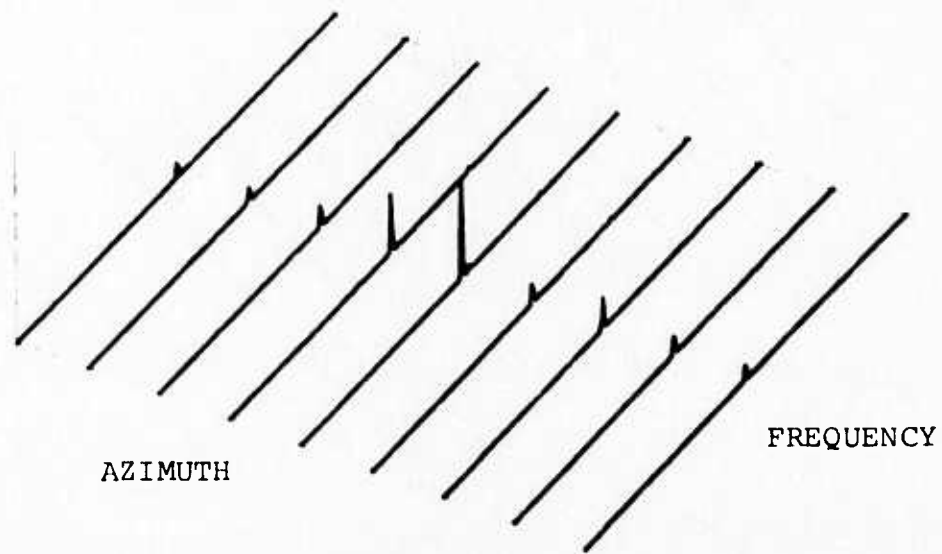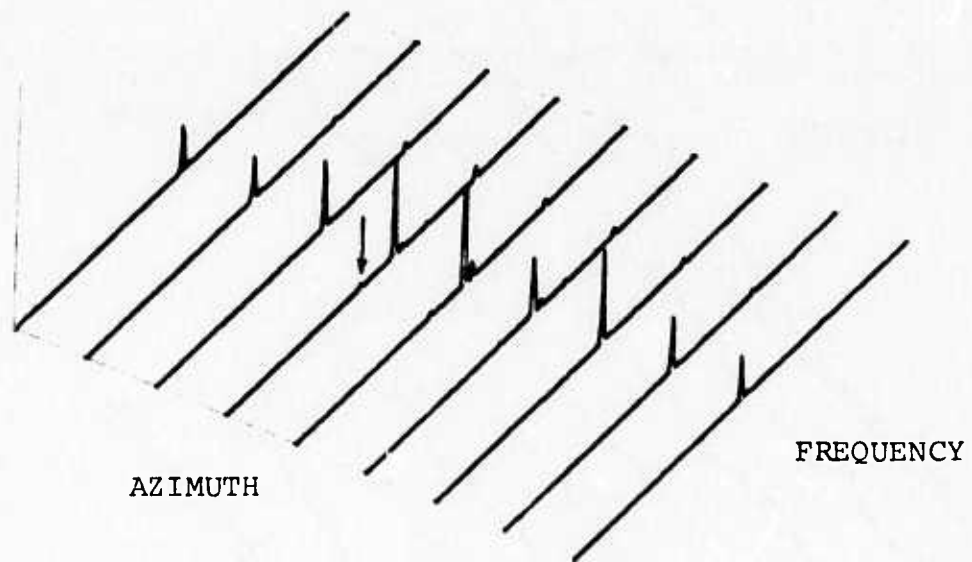Azimuth/frequency
display for low
SNR forward scatter
data.

Fig. 8
Azimuth/frequency
display for low
SNR forward scatter
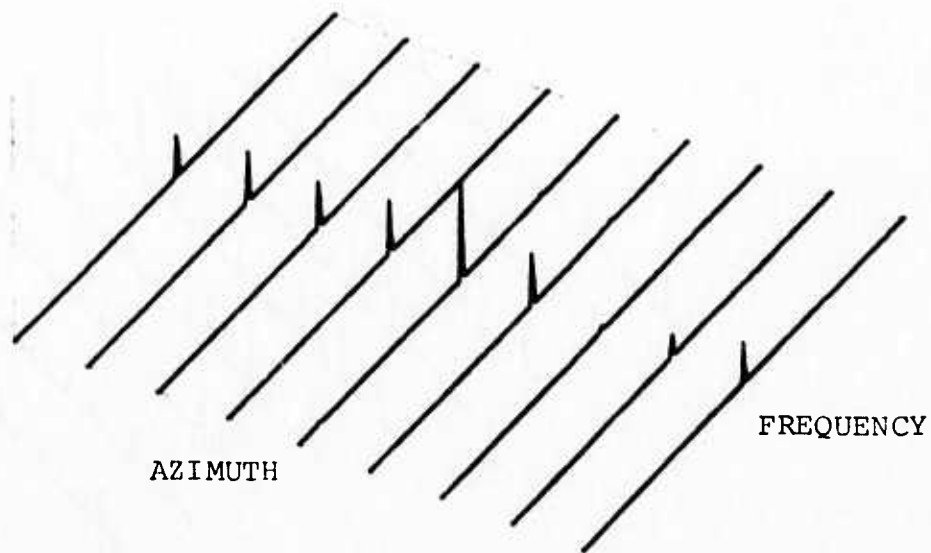data using 128 pt.
transform.

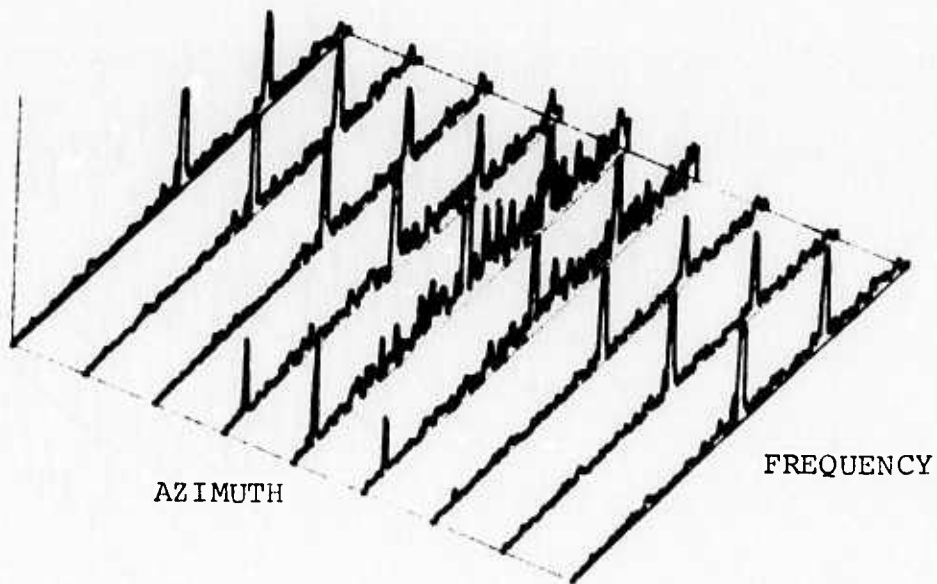22

a)   Di. ᵆlay gain = 1.0

b)   Display gain = 3.0

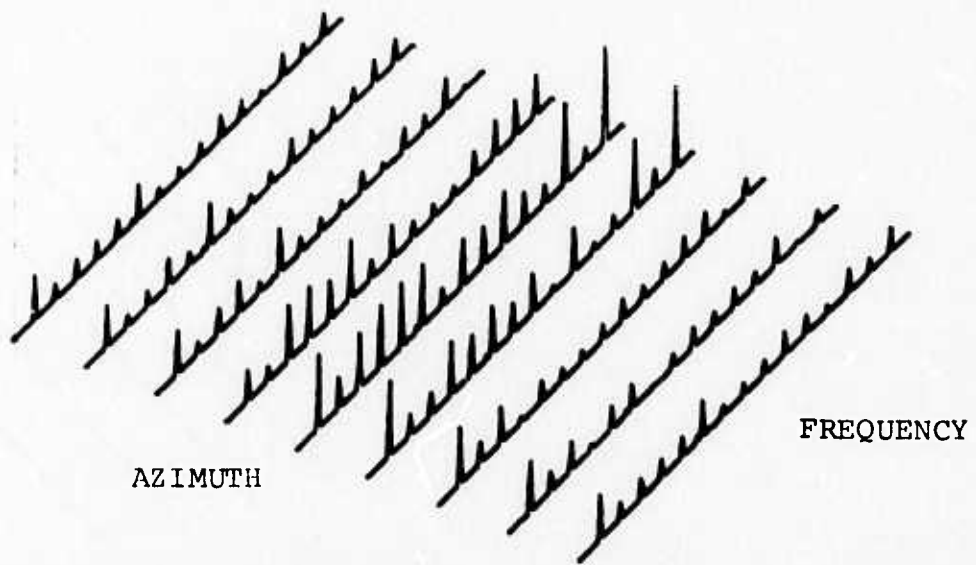Fig. 9   Azimuth/frequency display for high SNR backscatter data.

23

a)   Display gain = 1.0
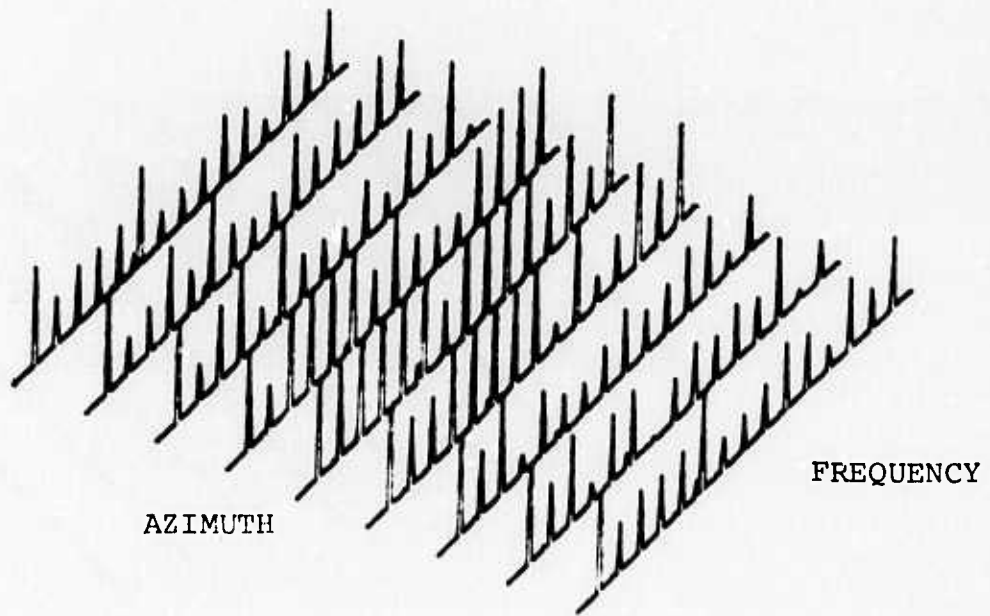

b)   Display gain = 30.0

Fig. 10   Azimuth/frequency display for low SNR backscatter data.

24

a)   Display gain = 1.0

b)   Display gain = 30.0

Fig. 11   Azimuth/frequency display for FM/CW experiment.

25

IV. ARRAY PROCESSING THEORY

The basic theory of array processing of interest in the present study has been developed in a previous report[1]. The theory presented below extends this work to include a calculation of the adaptive convergence time and the effects of adaptation in the presence of an FM/CW transmitted waveform.

A GAIN-PHASE BEAMFORMING VS. FREQUENCY-DEPENDENT BEAMFORMING

The beamforming system presented in this study is an all digital system in which successive samples from the down-converted subarray outputs are weighted and summed to produce a single sampled beam output signal. Figure 12 illustrates the basic processor. Note that each antenna "element" is actually a 32 element subarray. This processor is capable of filtering signals incident on the array both in terms of the frequency of the received signal and the direction of arrival. Thus, the beamformer acts as a combined spatial/temporal filter.

To illustrate, assume a planar sinusoidal signal at frequency $f_c + f_m$ arrives from azimuthal angle 0. Let the relative phase delay, in radians, between two successive elements be denoted by $\Delta\theta$. We further assume that the mixers are driven with a common local oscillator at frequency f_c Hz and that $f_c + f_m$ is within the operating bandwidth of the system (i.e., $|f_m| \leq 500$ Hz). The signal observed after down con-
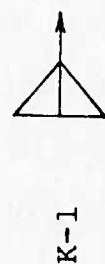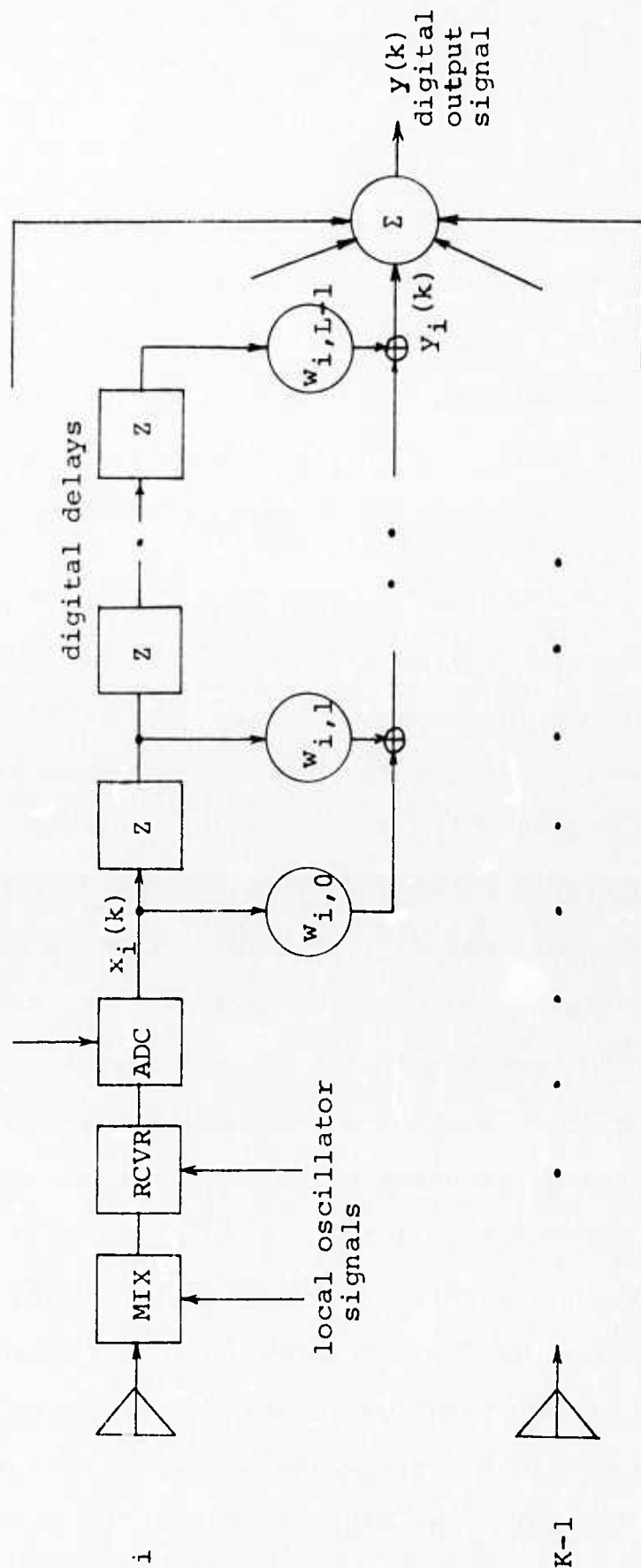
Fig. 12 Tapped-delay-line digital array processing configuration.

27

version is then a sinusoidal signal at frequency f_m and the relative phase between successive outputs remains at $\Delta\theta$ radians due to the use of a common local oscillator. Using phasar notation the kth sample out of the ith element $x_i(k)$ may be represented as

$$x_i(k) = e^{j[\omega_m k\Delta T - i\Delta\theta]} \qquad i=0,1,..K-1 \tag{3}$$

where ΔT is the sampling interval and K elements have been assumed. Note that the zeroth element is taken as the phase reference. Denoting the ℓth coefficient in the digital filter at the ith element as $w_{i,\ell}$ --see Fig. 12-- , the filtered output signal $y_i(k)$ is [4]

$$y_i(k) = e^{jw_m k\Delta T} \sum_{\ell=0}^{L-1} w_{i,\ell} \, e^{-j(\ell\omega_m\Delta T + i\Delta\theta)} \tag{4}$$

The total beamformer output signal at the kth sample is then

$$z(k) = \sum_{i=0}^{K-1} y_i(k)$$

$$= e^{j\omega_m k T} \sum_{i=0}^{K-1}\sum_{\ell=0}^{L-1} w_{i,\ell} \, e^{-j(\ell\omega_m\Delta T + i\Delta\theta)} \tag{5}$$

Thus, the gain and phase response $T(\Delta\theta,\Delta\emptyset)$ of the processor to signals incident from "directional angle" $\Delta\theta$ and oscillating at "digital frequency" $\Delta\emptyset = \omega_m\Delta T$ may be expressed as

$$T(\Delta\theta,\Delta\emptyset) = \sum_{i=0}^{K-1}\sum_{\ell=0}^{L-1} w_{i,\ell} e^{-ji\Delta\theta} \, e^{-j\ell\Delta\emptyset} \tag{6}$$

Equation (6) illustrates the spatial-temporal duality

28

of the digital beamformer shown in Fig. 12. Complete

symmetry is obtained for the case $L = K$ -- i.e., the number

of digital coefficients per element is equal to the number

of spatial elements. To illustrate the duality, assume $L = K$

and that a set of coefficients $\{w_{i,\ell}\}$ has been determined

such that the array frequency response to signals incident

from direction Θ_o and having a $\Pi/2$ phase shift between
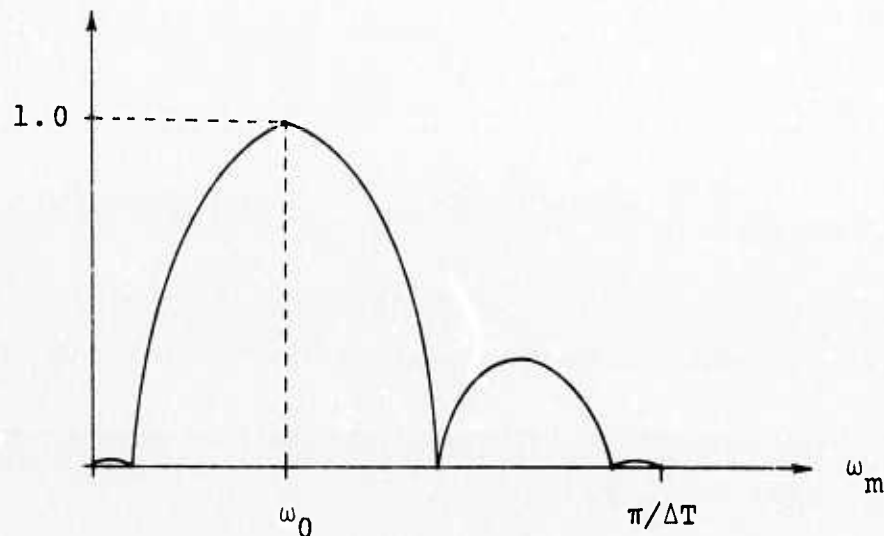
successive elements is as shown below.

Fig. 13   Assumed processor frequency response for signal
arriving from direction Θ_o.

Further assumed that a new processor is implemented with com-

plementary coefficients $\{\tilde{w}_{i,\ell} = w_{\ell,i}\}$. This system will then

have a spatial beam pattern for signals incident at frequency

$\omega_m \Delta T = \Pi/2$ which is identical to that shown in Fig. 13.
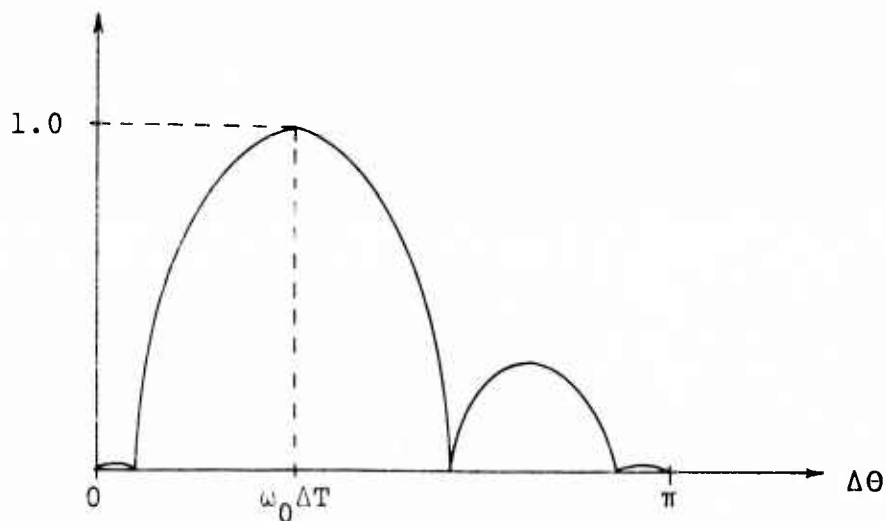
Fig. 14   Processor spatial beam pattern for system con-
taining complementary coefficients.

Note that the horizontal axis in this plot is the inter-
element progressive phase shift and is not necessarily the
direction of arrival.

An alternative all-digital array processor which uti-
lizes quadrature receivers is shown in Fig. 15. For the
narrow bandwidths of interest in the present study, it is
presumed that the quadrature relationship is preserved for all
received signals. Adjustment of the coefficients in this
system will provide only spatial processing -- i.e., frequency
selectivity within the bandwidth cannot be achieved.

To illustrate, using the assumptions given prior to (3)
above, the kth sample of the downconverted in-phase and quad-
rature   components $p_i(k)$ and $q_i(k)$, respectively, observed at
the output of the ith element will be

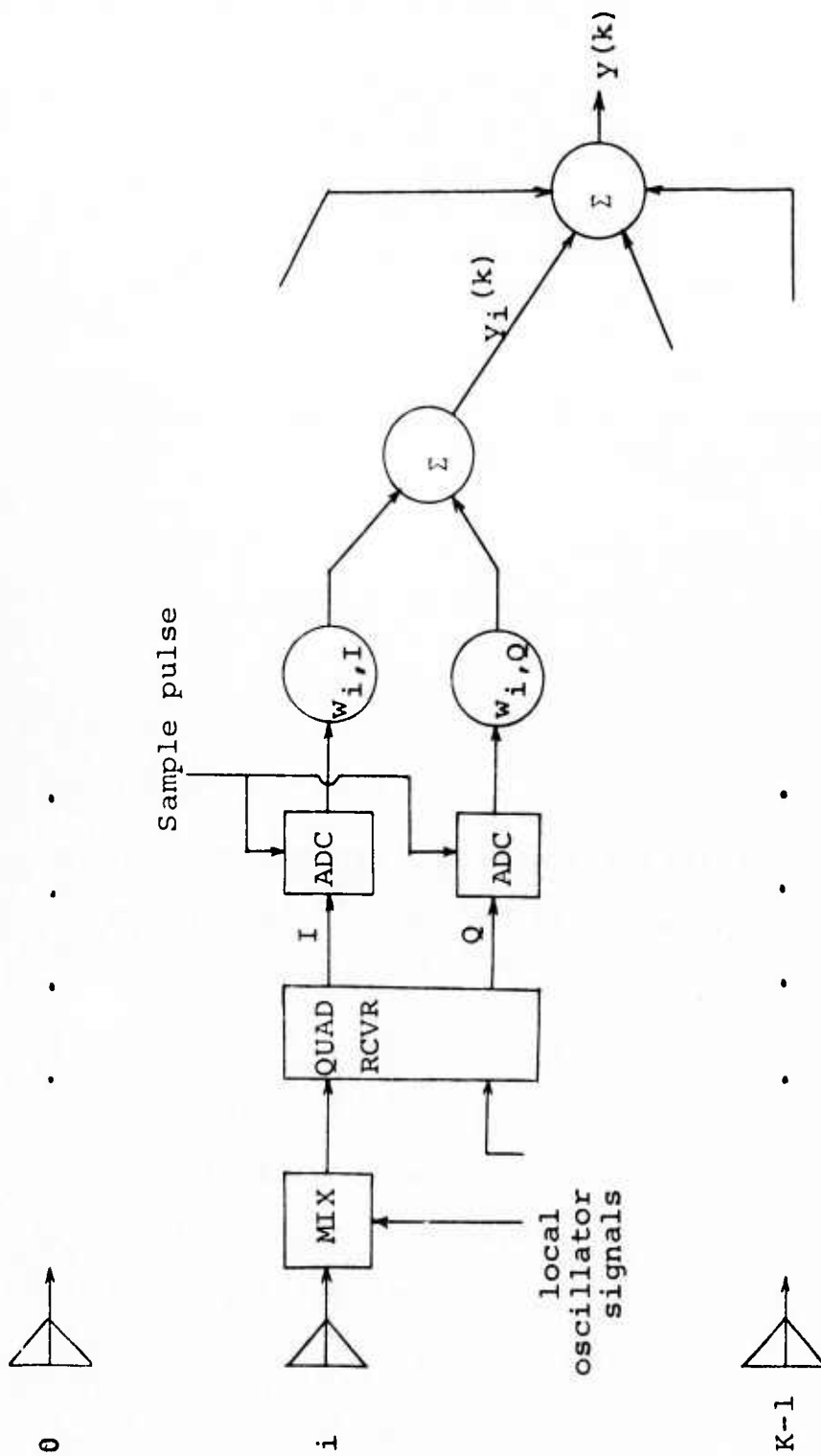$$p_i(k) = e^{j[\omega_m k\Delta T - i\Delta\theta]} \qquad (7a)$$

30

Fig. 15 Digital quadrature receiver beamforming system

31

$$q_i(k) = e^{j[\omega_m k\Delta T - i\Delta\Theta - \Pi/2]}$$

$$= -j \, p_i(k) \tag{7b}$$

Denoting $w_{i,1}$ and $w_{i,2}$ as the in phase and quadrature coefficients, the beamformer output signal is

$$z(k) = \sum_{i=0}^{K-1} w_{i,1}p_i(k) + w_{i,2}q_i(k)$$

$$= e^{j\omega_m k\Delta T} \sum_{i=0}^{K-1} (w_{i,1} - jw_{i,2})e^{-ji\Delta\Theta}. \tag{8}$$

Thus, the transfer function $T(\Delta\Theta)$ of the system depends only on the progressive phase shift $\Delta\Theta$ of the incident waveform,

$$T(\Delta\Theta) = \sum_{i=0}^{K-1} (w_{i,1} - jw_{i,2})e^{-ji\Delta\Theta}. \tag{9}$$

and is independent of the frequency of the received signal.

The processor shown in Fig. 12 is preferred over that shown in Fig. 15 because the additional degrees of free om -- e.g., the filter coefficients -- can be utilized to obtain greater noise and interference rejection. Although frequency selectivity within the receiver bandwidth for signals received from the desired direction is clearly not a desirable characteristic, such selectivity in other directions allows deeper nulls in both spatial and temporal domains and consequently, decreased output noise power. Examples of this phenomenon are presented in the sections following. It

32

should be noted that constrained digital processors[5] and associated adaptive algorithms[6] have been presented which force the system shown in Fig. 12 to provide a flat frequency response in the desired direction. These methods, however, require a greater number of digital calculations per adaptive step than the unconstrained procedure used in both the present and the previous study[1]. The constraint imposed on the system also causes a corresponding reduction in null depth in other directions. A complete comparison of constrained and unconstrained methods using experimental data, however, was not included within the scope of the present program.

B NON-ADAPTIVE DETERMINATION OF BEAMFORMER COEFFICIENTS

It is presumed in this research that the subarrays shown in Fig. 12 have been steered in the direction of the desired target return to the extent that this signal appears in phase at the inputs to the digital filters. Thus, the kth sample from the ith subarray may be expressed as the sum of a target signal term $S(k)$ and an unwanted component $n_i(k)$

$$x_i(k) = S(k) + n_i(k). \tag{10}$$

Note that $n_i(k)$ is the result of noise, interference, and clutter returns received by the ith subarray. The objective of the beamforming system is to produce an output signal which closely approximates $S(k)$ -- i.e., an output which does not contain components produced by the $n_i(k)$. The conventional approach to beamforming utilizes only the first set of weights shown in Fig. 12. Thus, all other weights have zero value,

$$w_{i,\ell} = 0 \qquad i = 0,1, \,.. \, K-1; \; \ell = 1,2, \,..L-1 \tag{11}$$

and the first set form a Tchebychev or other desired amplitude taper. For example, in the four subarray system of interest in the present study, the Tchebychev weights are given by

$$
\begin{aligned}
w_{0,0} &= 0.6 \\
w_{1,0} &= 1.0 \\
w_{2,0} &= 1.0 \\
w_{3,0} &= 0.6.
\end{aligned} \tag{12}
$$

34

An alternative method of beamforming is the array processor studied in this research in which the filter coefficients are chosen to minimize the average squared difference between the beamformer output signal $z(k)$ and a desired output signal $d(k)$. The desired response is taken as the target signal at a delay of one-half of the digital filter length used to process each subarray output. Thus,

$$d(k) = S(k-L/2).\tag{13}$$

and the quantity to be minimized is given by $\overline{\epsilon}^2$, where

$$\overline{\epsilon}^2 = E\{[d(k)-z(k)]^2\}.\tag{14}$$

The set of filter coefficients which minimizes (14) is derived in Ref. 1 and may be expressed in matrix notation as

$$W^* = R_{xx}^{-1} \quad P_{xd}\tag{15}$$

where W^* is the vector of optimum filter coefficients

$$W^* = \begin{bmatrix} w^*_{0,0} \\ w^*_{1,0} \\ \vdots \\ w^*_{K,0} \\ \vdots \\ w^*_{K,L} \end{bmatrix}\tag{16}$$

The square matrix R_{xx} is the matrix of cross-correlation values of the data in the processor and P_{xd} is the steering

35

vector formed as the average of the product of the desired array response and the data vector in the processor. By assuming the $S(k)$ and $n_i(k)$ are uncorrelated in (10), the vector P_{xd} is completely determined from a knowledge of the spectral properties of the target signal. For example, if $S(k)$ is sinusoidal at frequency ω_d radians/sec and the ADC sampling interval is ΔT seconds,

$$
P_{xd} = \begin{bmatrix} \cos\ (\omega_d \Delta T\ L/2) \\ \cos\ (\omega_d \Delta T\ L/2) \\ \cdot \\ \cdot \\ \cos\ (\omega_d \Delta T\ L/2) \\ \cos\ [\omega_d \Delta T (L-1)/2] \\ \cdot \\ \cdot \\ \cdot \\ \cos\ (-\omega_d \Delta T\ L/2) \end{bmatrix} \tag{17}
$$

In summary, the optimum processor (16) may be calculated from a knowledge of the received data cross correlation values and the spectral properties of the desired beamformer output. This method of selecting the coefficient values in Fig. 12 will result in a combined spatial/temporal filter. The precise nature of this filter is determined by the properties of the $n_i(k)$ components in (10). In general, however, the processor will have a broadside mainlobe at frequency ω_d while placing pattern nulls in the direction and frequency of the stronger interfering noise sources. This is in contrast with the conventional beamformer defined in (11) and (12) which has

36

broadband nulls formed in predetermined directions, inde-
pendent of the spatial nature of the interference.

C ADAPTIVE DETERMINATION OF BEAMFORMER COEFFICIENTS

For a given desired frequency of the target signal, the
optimum set of filter coefficients given in (15) is completely
determined from a knowledge of the cross-correlation matrix
R_{xx}. The elements of this matrix are unknown a priori but
may be estimated directly using finite time averages on the
received signals. For example, an estimate of the cross-
correlation between the kth sample from the ith subarray
$x_i(k)$ and the $(k-2)^{nd}$ sample from the jth subarray may be
computed as

$$\hat{r}_{i,j}(2) = \frac{1}{N} \sum_{\ell=0}^{N-1} x_i(k-\ell) x_j(k-2-\ell) \qquad (18)$$

There are several difficulties associated with this approach.
First, the estimate (18) is the average over the previous N
samples of received data, a value chosen sufficiently large
to provide a good statistical estimate but not so large as
to mask the effects of slowly varying noise parameters such
as direction of arrival of the interference. Selecting the
appropriate value is not an easy task. A second difficulty
arises in the use of (18) to track time varying intereference.
Unless a large amount of data memory is available, the
estimates (18) must be applied to data received after the
estimates are formed. Thus, after each block of N samples

37

is used to compute cross-correlation values, the optimum coefficients (15) are calculated and applied to process succeeding data samples. At some later time, new correlation values are computed and the filter coefficients are reset to the appropriate values. Since the filter is always applied to data at a time after that used to compute correlation values, it is necessarily suboptimum for the case of time-varying data.

The adaptive method of computing filter coefficients used in this and the previous study overcomes these difficulties in that the coefficients are updated as each new data sample is received. A single, easily adjusted parameter in the algorithm controls the rate of adaptation or, equivalently, the correlation averaging time of the processor. The algorithm[1] is

$$W(k+1) = W(k) + \mu[P_{xd} - z(k) X(k)] \qquad (19)$$

where $W(k)$ is the set of filter coefficients used to produce the kth sample of the beamformer output signal $z(k)$ and $X(k)$ is the set of data samples observed at these coefficients, i.e.,

$$X(k) = \begin{bmatrix} x_0(k) \\ x_1(k) \\ \cdot \\ \cdot \\ x_K(k) \\ x_0(k-1) \\ \cdot \\ \cdot \\ \cdot \\ x_K(k-L+1) \end{bmatrix} \qquad (20)$$

38

The derivation of this algorithm is based on a modi-
fication of gradient descent techniques. Details of the
derivation may be found in references 1 and 7. Repeated use
of (19) results in a sequence of coefficient values $\underline{W}(k)$,
$\underline{W}(k+1)$, ... which may be characterized as random vectors.
For the case of stationary input statistics, the mean value
$M_W(k+1)$ of the coefficient vector at time k+1 may be computed
from (19) as

$$M_W(k+1) = E[W(k+1)]$$

$$= E[W(k)]+\mu\{P_{xd}-E[z(k)X(k)]\}$$

$$= M_W(k)+\mu[P_{xd}-R_{xx}M_W(k)]. \qquad (21)$$

Evaluation of the last term in (21),

$$E[z(k)X(k)] = E[x(k)X^T(k)W(k)]$$

$$= E[X(k)X^T(k)]E[W(k)]$$

$$= R_{xx}M_W(k), \qquad (22)$$

is based on the assumption that X(k) is a stationary, zero-
mean gaussian vector and that the resulting coefficients
are also gaussian [8]. Further detailed discussion of these
assumption may be found in references [9] and [10].

The difference equation (21) for the mean coefficient
vector may be expressed in the form

$$M_W(k+1) = [I-\mu R_{xx}]M_W(k)+\mu P_{xd}. \qquad (23)$$

39

Repetitive application of (23) using an initial mean value $M_W(0)$ yields

$$M_W(k) = W* + [I - \mu R_{xx}]^k M_W(0). \tag{24}$$

Thus, the mean value of the adapted coefficients obtained by iteration converges to the optimum set, provided that the term in square brackets converges to zero. It can be shown [9] that such convergence is guaranteed provided that

$$0 < \mu < \frac{2}{\lambda_{max}}, \tag{25}$$

where λ_{max} is the maximum eigenvalue of the autocorrelation matrix R_{xx}. A more practical bound may be obtained by utilizing the positive definite properties of this matrix. Thus

$$0 < \mu < \frac{2}{K \cdot L \cdot \sigma_x^2}, \tag{26}$$

where σ_x^2 is the maximum variance observed in the array signals, also insures convergence.

For the purposes of this study, a digital automatic gain control was employed at each element output to ensure unit variance for all channels. The proportionality constant was selected as

$$\mu = \frac{\alpha}{K \cdot L}, \tag{27}$$

where KL is the total number of adaptive coefficients in the beamformer and $0 < \alpha < 2$ to ensure convergence.

A measure of the adaptive time constant for this processor can be obtained from (24). In general, the adaptation transient

40

will consist of a sum of terms of the form

$$(1-\mu\lambda_i)^k \tag{28}$$

where $0<\lambda_i\leq\lambda_{max}$ is the ith eigenvalue of R_{xx}. The adaptive time constant τ_a is defined as that value of k which reduces the transient term to 1/e of its original value. Thus, from (28), we obtain

$$\frac{-1}{\ln(1-\mu\lambda_{max})} \leq \tau_a \leq \frac{-1}{\ln(1-\mu\lambda_{min})}. \tag{29}$$

These bounds may be simplified using (27) and the fact that the minimum eigenvalue of the autocorrelation matrix cannot be less than the total power σ_N^2 of the uncorrelated noise component at the processor inputs. Further, the maximum eigenvalue cannot exceed the maximum variance times the number of filter coefficients and when $\sigma_x^2 = 1$, the bounds (29) are given by

$$\frac{-1}{\ln(1-\alpha)} \leq \tau_a \leq \frac{-1}{\ln(1-\frac{\alpha\sigma_N^2}{KL})} \tag{30}$$

It has been observed in practice that a reasonable single estimate for λ_a is obtained by using an "average" eigenvalue. Since all eigenvalues must sum to the trace of R_{xx} [7]

$$\sum_{i=1}^{KL} \lambda_i = KL\sigma_x^2 = KL, \tag{31}$$

and an average value is $\lambda_{av} \simeq 1.0$ when $\sigma_x^2 = 1.0$. The corresponding time constant is then given by

$$\tau_a \simeq \frac{-1}{\ln(1-\frac{\alpha}{KL})} \tag{32}$$

41

For example, a processor with five adaptive weights at each of the four subarray outputs can be expected to yield a time constant of about 200 samples when $\alpha = 0.10$ or 1000 samples when $\alpha = 0.02$. At a 2.0 kHz sampling rate, these times correspond to 0.1 and 0.5 seconds, respectively. It should be noted, however, that rates considerably faster have been observed in practice, particularly for the case of highly coherent -- e.g., sinusoidal -- signals. Examples of this phenomenon are presented in the sections following.

The discussion presented above has shown that the mean values of the coefficients obtained using the adaptive algorithm (19) will converge to the optimum values W*(10) provided that two conditions are met

i) the proportionality constant satisfies (26)

ii) the P_{xd} vector used in (19) is identical to the true cross correlation vector defined in (17).

It can be further shown [9]-[10], that the variance of the adapted solution can be made arbitrarily small through sufficiently small choice of μ. Of course, reduced values of μ imply corresponding increases in the convergence rate as shown by Eq. (29).

D   ADAPTATION FOR FM/CW WAVEFORMS

The adaptive algorithm described above was designed for operation in a CW environment and as such can be expected to perform well for both the forward scatter and backscatter CW data files recorded during this study. The data format of

42

interest in an operational HF backscatter radar, however, is that of FM/CW transmissions. Specifically, the transmitted signal consists of a sinusoid in which the instantaneous frequency is changed linearly with time for the duration of one sweep. At the completion of each sweep, the frequency is returned to its initial value with a phase coincident with that used at the beginning of the previous sweep. Figure 5 illustrates the instantaneous time history of the specific FM/CW format used in this study. The sweep duration of 1/60 sec provided 32 digital samples per sweep.

The receiver output signal generated by a stationary target at range r_d consists of a constant-frequency sinusoid which may be set to a prescribed value f_d through appropriate choice of the local oscillator waveform. An example is presented in Fig. 16. Note that for a brief portion of the sweep (τ_d sec.) the beat frequency falls outside of the receiver passband. The time waveform observed at the receiver output for this signal is shown in Fig. 17. Dashed lines are used to indicate portions of the sweep in which the frequency is outside the passband of the receiver. For the parameters used in this study, 1kHz receiver bandwidth and 8 1/3 kHz sweep range, the maximum allowable time period outside the passband is 1/(8 1/3) of the sweep period or about 2 milliseconds.

Inspection of 17 shows that the receiver output waveform for a stationary target consists of a sinusoid during each sweep with the phase of the sinusoid held constant with

43
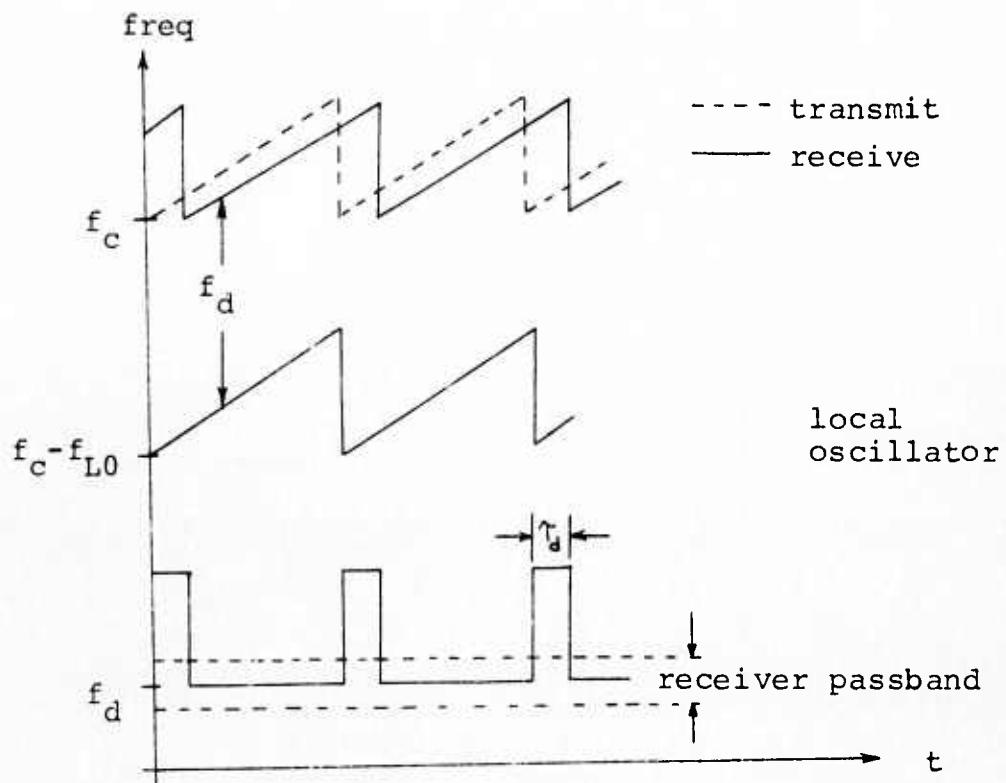
Fig. 16   Receiver output frequency generated by
a stationary target in a FM/CW system

44
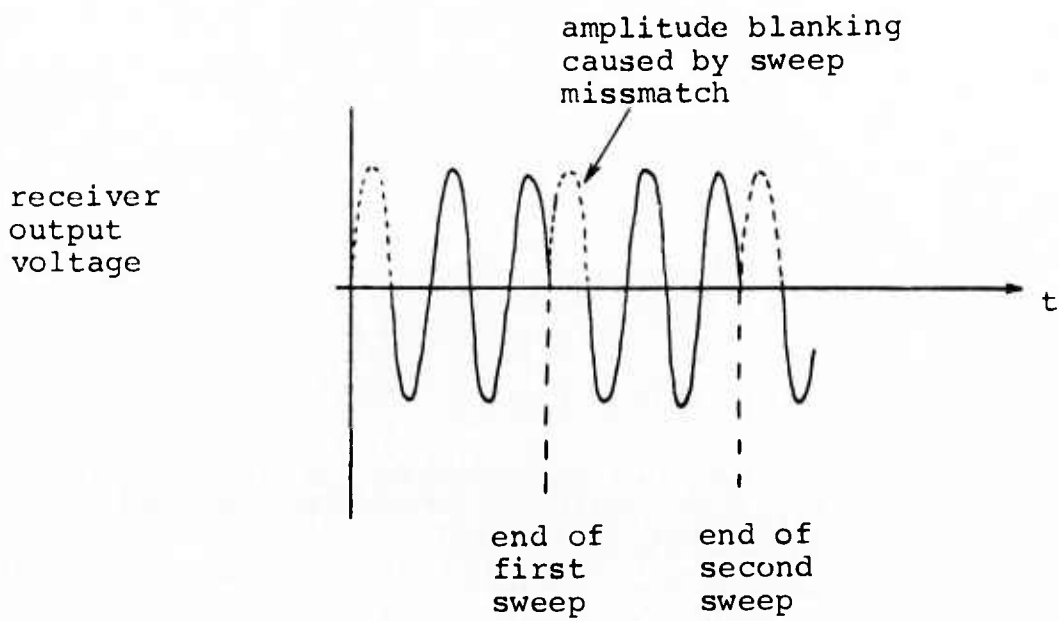
Fig. 17   Receiver output time waveform for
           stationary target shown in Fig. 16

45

respect to the start time of the sweep. A moving target at the same range would produce a similar waveform except that the phase reference of the sinusoid would drift with respect to the start time of the sweep. In Fig. 18, successive sweeps are arranged vertically to illustrate this property. Note that the above discussion is based on the assumption that the doppler frequency caused by target motion produces only a small frequency change during one sweep. This assumption is consistent with the targets of interest in the HF environment.

The signal observed at the output of an FM/CW radar during any one sweep may thus be approximated by a sinusoid at frequency f_d, determined by the target range, and at phase ϕ_d, determined by the target range and doppler, and by the sweep number. The transient observed after frequency flyback consists of both an amplitude change and a phase shift. An adaptive system which is designed to operate in the presence of a sinusoidal desired output signal can be expected to perform well during the mid-sweep portions of the received signals. The effect of the flyback transient on adaptive performance, however, is not so easily analyzed. One method of avoiding the influence of these transients, is to cease adaptation for the period in which the transients reside in the processor. This procedure has beem implemented and tested on recorded FM/CW data. The results indicate that adaptive performance is unaffected by these transients. Specific examples are presented in the sections following.

46
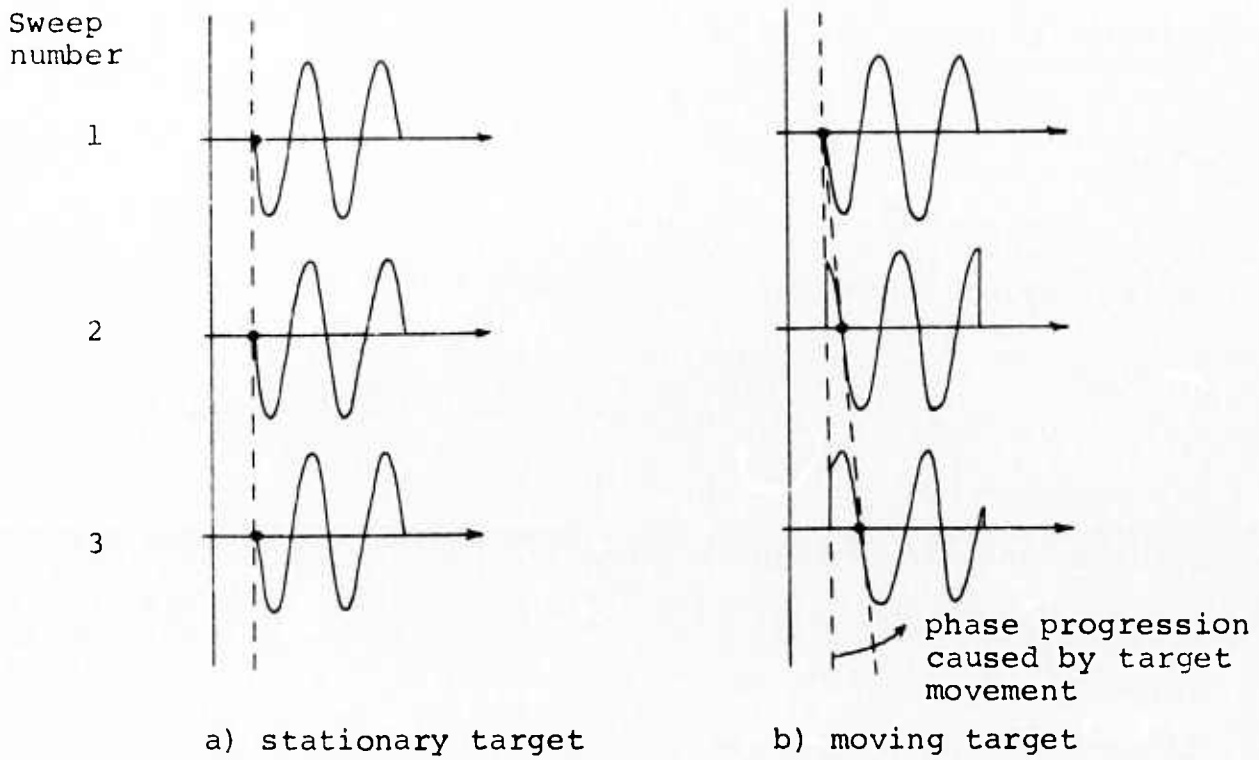
Fig. 18   Receiver output waveforms for fixed and
moving targets in an FM/CW system

V.   RESULTS

The results presented below are divided into three categories according to the experimental data configuration used to record the data -- i.e., forward scatter CW tests, backscatter CW tests and backscatter FM/CW tests. In each case examples are presented comparing the performance of the adaptive beamformer with that of the conventional beamformer. The results presented were derived using a wide variety of adaptive parameters and input signal configurations. All computations were carried out using the CDC 6400 computing facility at the University of Colorado.

A.   FORWARD-SCATTER CW TESTS

In order to demonstrate the spatial-temporal filtering capabilities of the tapped-delay-line processor shown in Fig. 12, a number of non-adaptive computations were carried out using the optimal coefficient relationship defined in Eq. (15). In each case, a total of 128 data samples per element were used to estimate the autocorrelation matrix values. All time averages were carried out using the method shown in Eq. (18). The inverse of the resulting matrix was then multiplied by the steering vector in Eq.(17). A desired output frequency $\omega d/2\pi = 500$ Hz corresponding to the downconverted CW Bearden signal was used in these calculations.

The input data were taken from File 3 and consisted of

48

a low SNR forward scatter CW signal received in the presence of teletype interference (see Table I, Section III). Figure 8 shows the azimuth/frequency content of the first 128 sample data block recorded on this file. Optimal filter coefficient values were computed for processors containing 1, 3, 5, and 9 taps per array element. A display of the azimuthal response of the resulting processor, plotted as a function of frequency within the received bandwidth, was generated using two-dimensional Fourier Transform techniques.

The calculation proceeds by arranging the filter coefficients in a two-dimensional array with each row containing the coefficient values for the tapped-delay-line attached to a particular antenna element. Thus, with reference to Figure 12 and Eq. (16), the matrix is

$$
\begin{bmatrix}
w_{0,0} & . & w_{0,1} & \cdot & \cdot & w_{0,L-1} \\
w_{1,0} & & & & & w_{1,L-1} \\
. & & & & & \\
. & & & & & \\
w_{K-1,0} & & & & & w_{K-1,L-1}
\end{bmatrix}
\tag{33}
$$

Transforming the rows and columns of (33) leads to a matrix in which each row is the frequency response of the processor in a particular azimuthal direction. The azimuthal spacing is determined by the original received frequency and the subarray separation. It should be noted that the validity of this procedure is based on the assumption that the sub-

49

array spacing in wavelengths remains constant over the bandwidth of the received signals. Thus, the technique may readily be applied to narrowband HF arrays operating at bandwidths less than 50 kHz.

The azimuth/frequency responses obtained with this method for the optimal filters derived from the first 128 data samples in File 3 is shown in Figs. 19-22. In each case, the product of the data transform in Fig. 8 and the appropriate processor transform is also illustrated. The desired CW signal is indicated by the vertical arrow. Inspection of this series of plots shows that the received signal-to-noise ratio, determined by a summation over the product pattern, improves as the number of filter coefficients increases. The improvement results from an increased selectivity in both azimuthal and temporal filtering. Thus, a comparison of Figure 19 with Figure 22 shows that the strong teletype signal is eliminated at all azimuths in the latter case but only on two azimuths in Fig. 19.

An indication of the time variability of the optimal pattern for the 5 tap per element case is shown in Fig. 23. In this series, optimal coefficients were computed for 4 successive blocks of 128 data samples from File 3. Substantial plot-to-plot variation is evident, particularly in the sidelobe structure. For example, compare the frequency response in the azimuthal direction for Figs. (23b) and (23c). This variation cannot be attributed to statistical fluctua-

a) Optimal processor response.
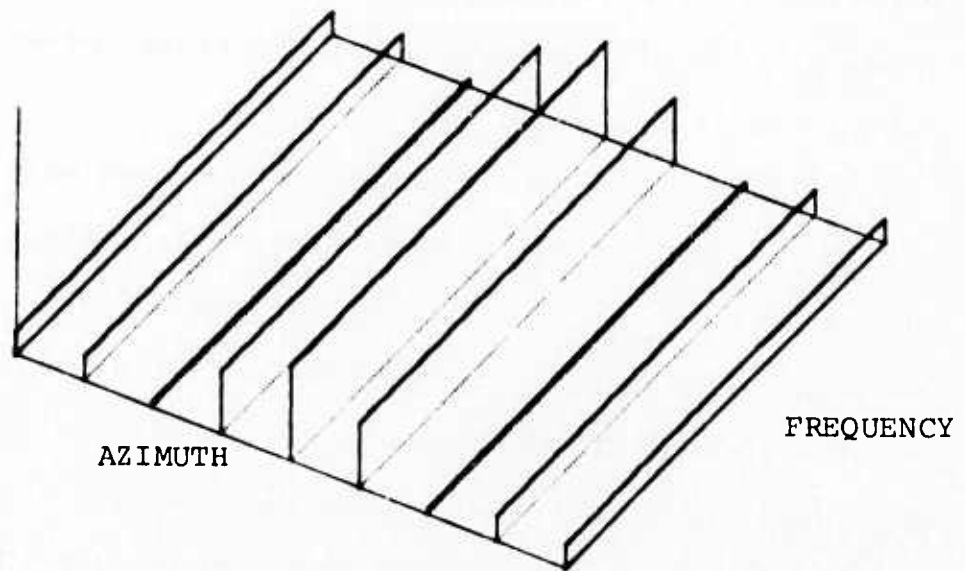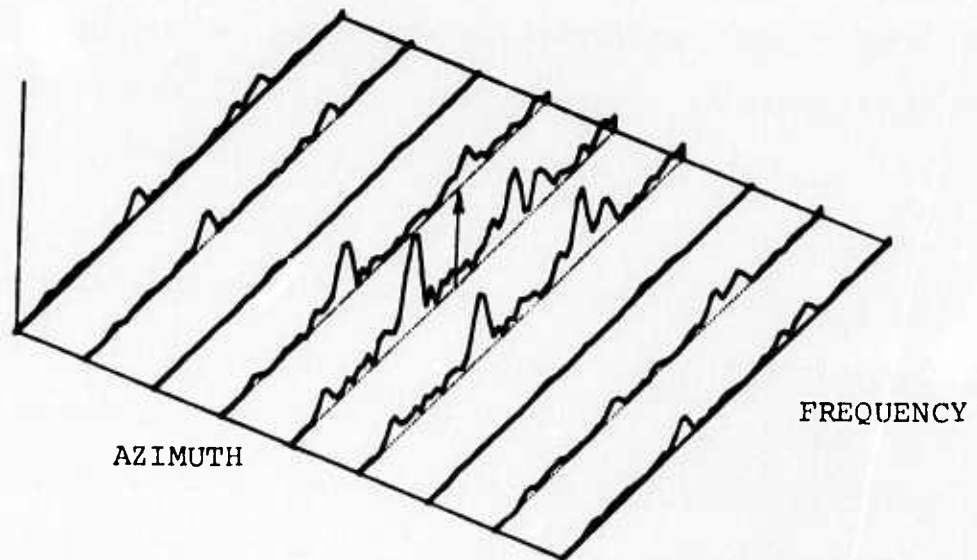
b) Product response.

Fig. 19 Azimuth/frequency response for File 3, Record 1 with one coefficient per element.
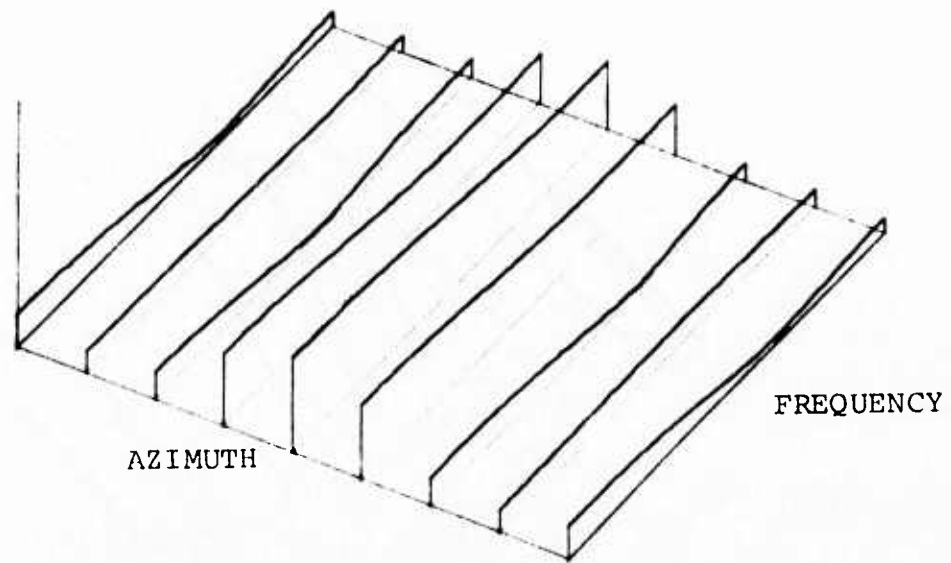
a) Optimal processor response.
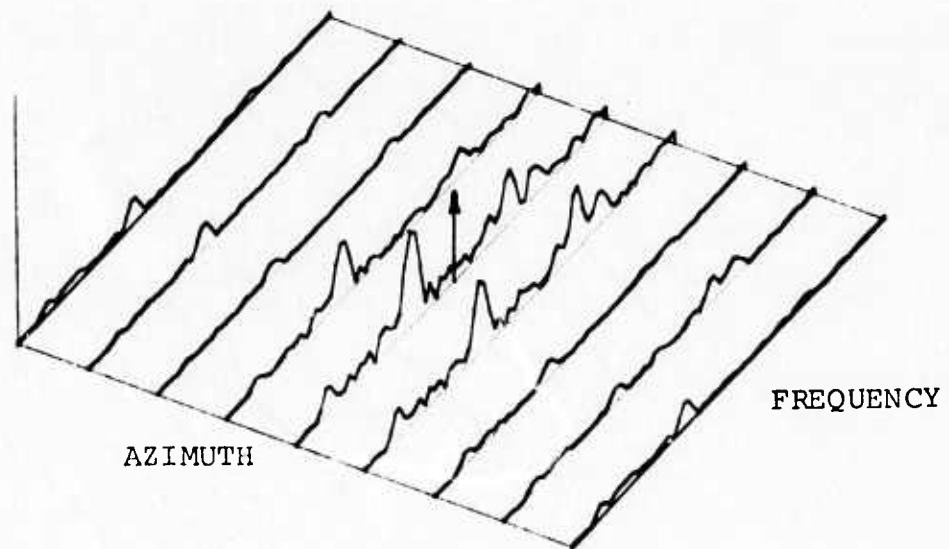
b) Product response

Fig. 20 Azimuth/frequency response for File 3, Record 1
with three coefficients per element.
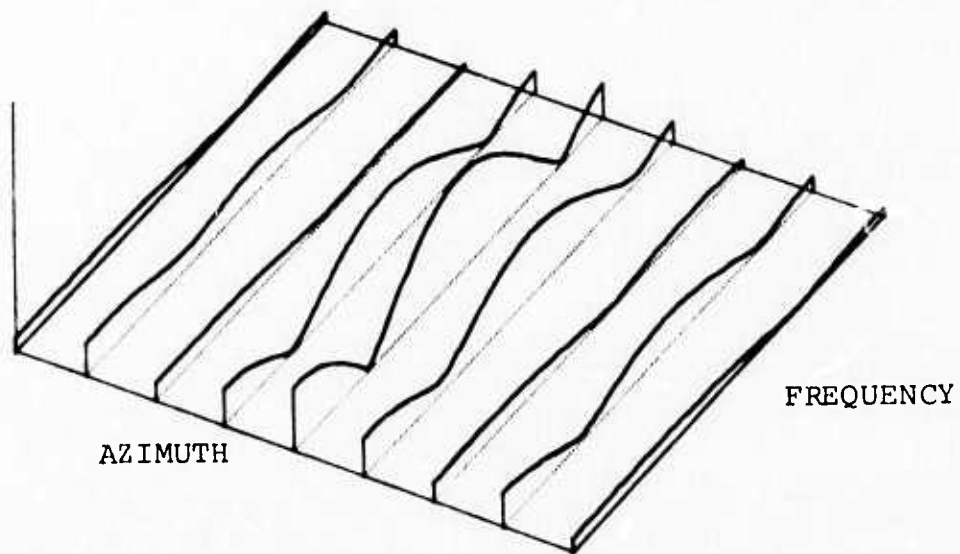
a) Optimal processor response.
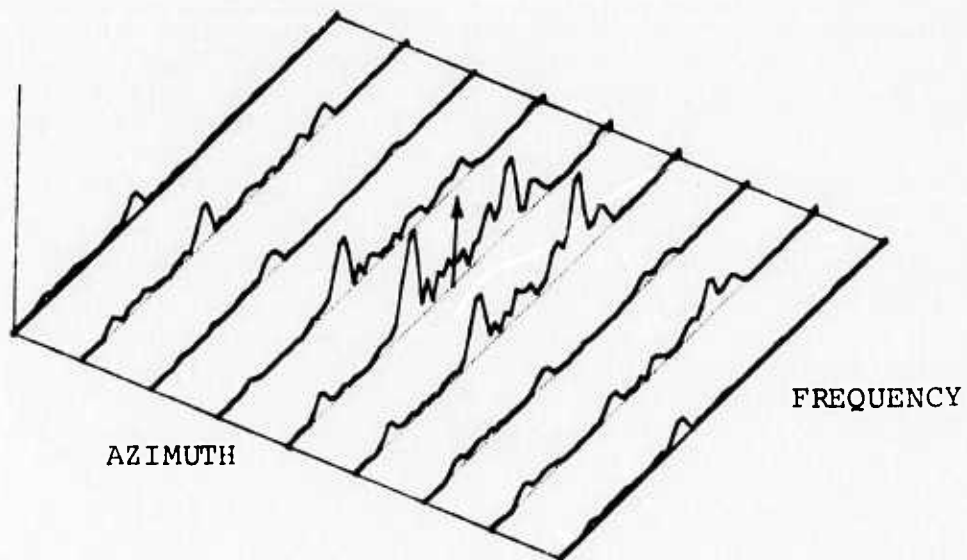
b) Product response.

Fig. 21 Azimuth/frequency response for File3, Record 1
with five coefficients per element.

53
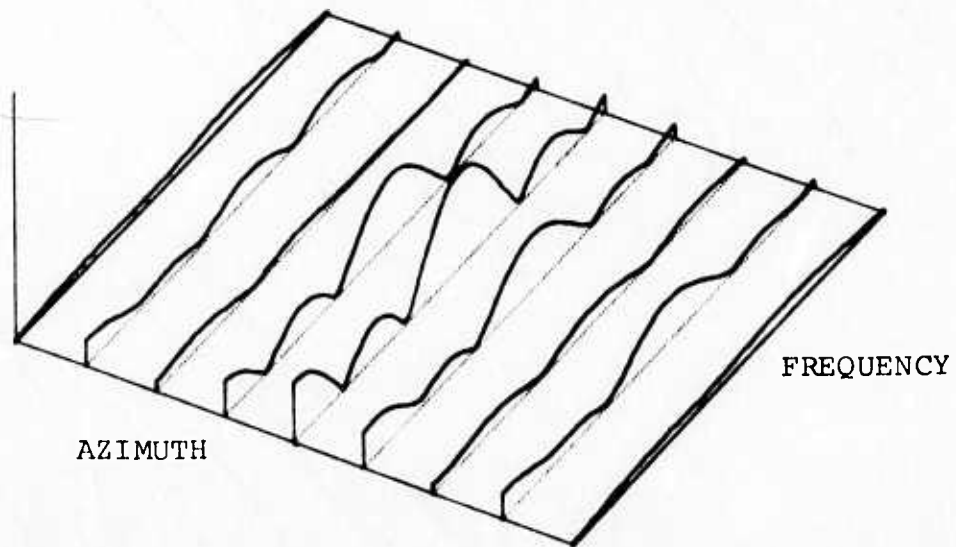
a) Optimal processor response.
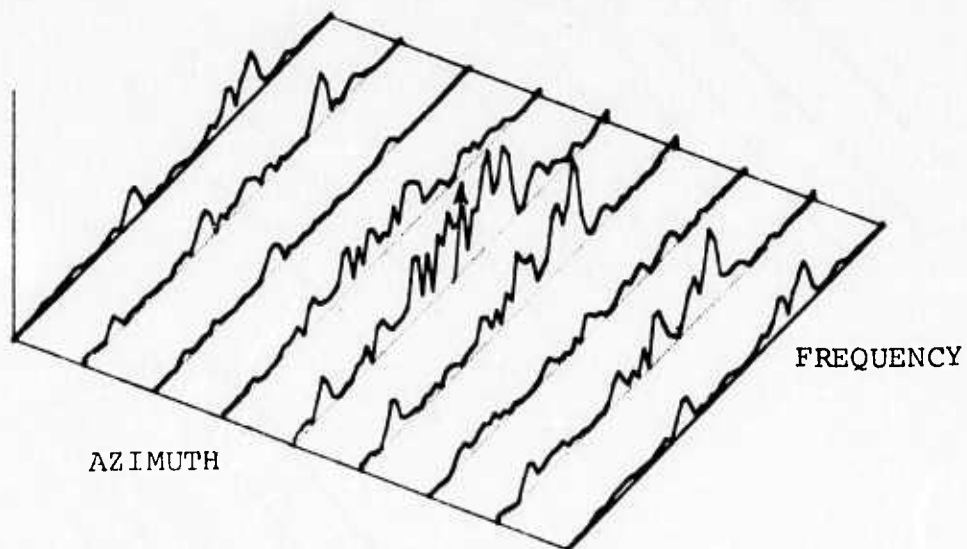
b) Product response.

Fig. 22   Azimuth/frequency response for File 3, Record 1
with nine coefficients per element.

a) File 3, Record 1

b) File 3, Record 2

c) File 3, Record 3

d) File 3, Record 4
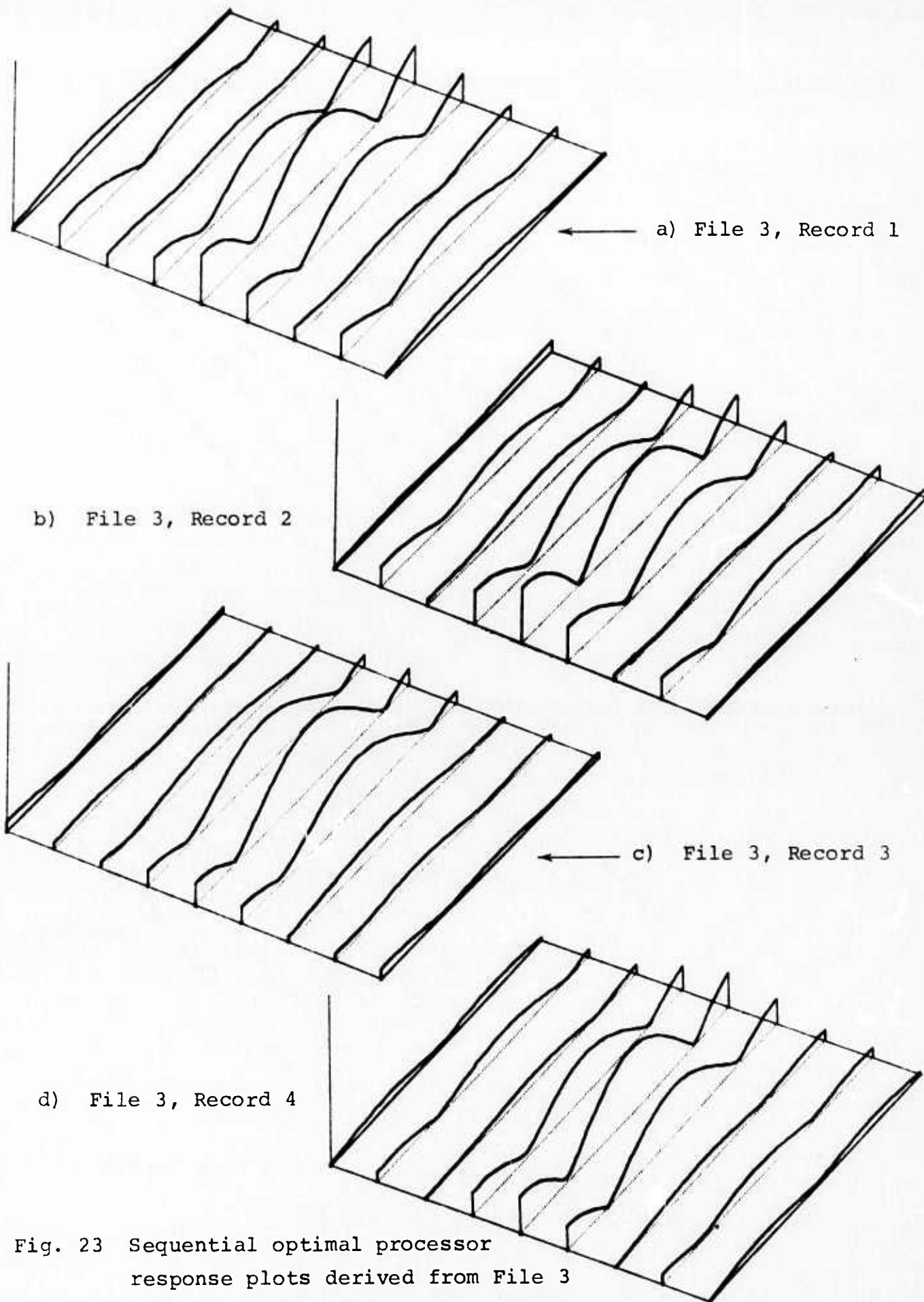
Fig. 23 Sequential optimal processor
response plots derived from File 3
with five coefficients per element.

55

tions in the autocorrelation estimates and is therefore indicative of changes in the azimuth/temporal structure of the received data.

The P-vector adaptation algorithm (19) was also implemented on these data. At intervals of 128 samples, the adapted weight vector was read out and azimuth/frequency displays were generated. Figure 24 illustrates the results obtained at four successive intervals by adapting on the same data as used to compute the optimal patterns in Fig. 23. The adapted processor contained 5 coefficients per element and the value of α selected [see Eq. (27)] was 0.4. Although the adapted and time-averaged plots are markedly similar, differences in the sidelobe structure can be detected. These differences can be attributed to the fact that time-averaging is a block-time process taken over 128 samples and adaptation is equivalent to exponential averaging with the length of the average being determined by the adaptive time constant. Using the method presented in Section IV, the average time constant for this set of parameters is about 50 samples.

Time history plots of the received signal-to-noise ratio for File 3 were computed for both conventional and adaptive processors. The SNR was computed from time averages on the received data as the ratio of output sinusoidal power at the desired frequency to total output power. Thus, the maximum possible output SNR was unity or zero db. Figures 25 and 26 illustrate this quantity during the first 140 m.sec. of File 3 for adaptive processors containing one weight and
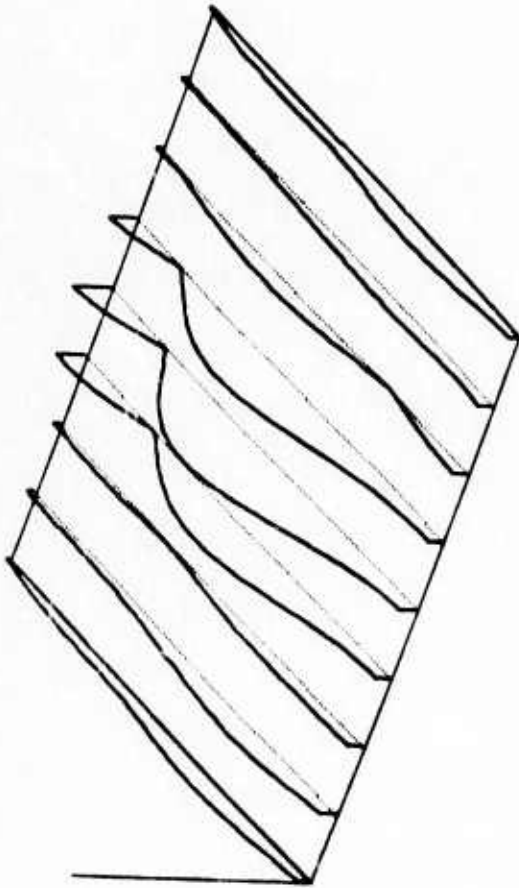
a) File 3, Record 1
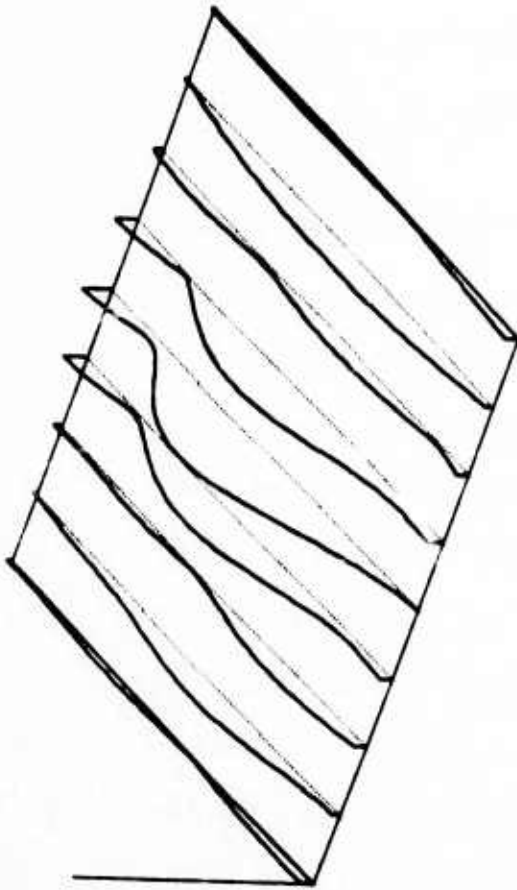
b) File 3, Record 2
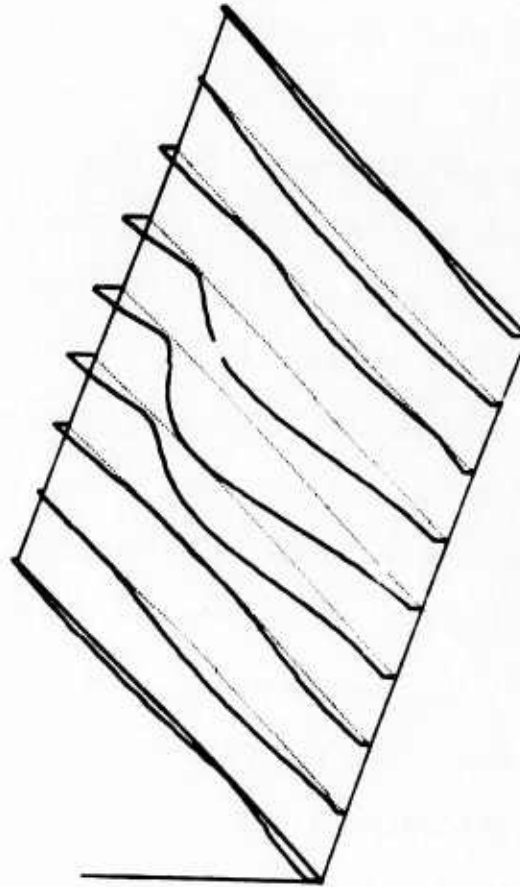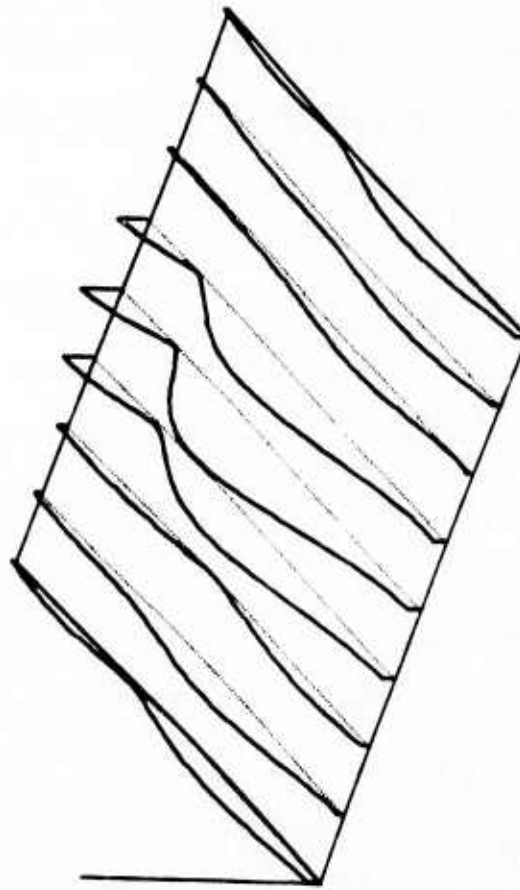
c) File 3, Record 3

d) File 3, Record 4

Fig. 24   Sequential adaptive processor response plots derived from File 3 with five coefficients per element.

57
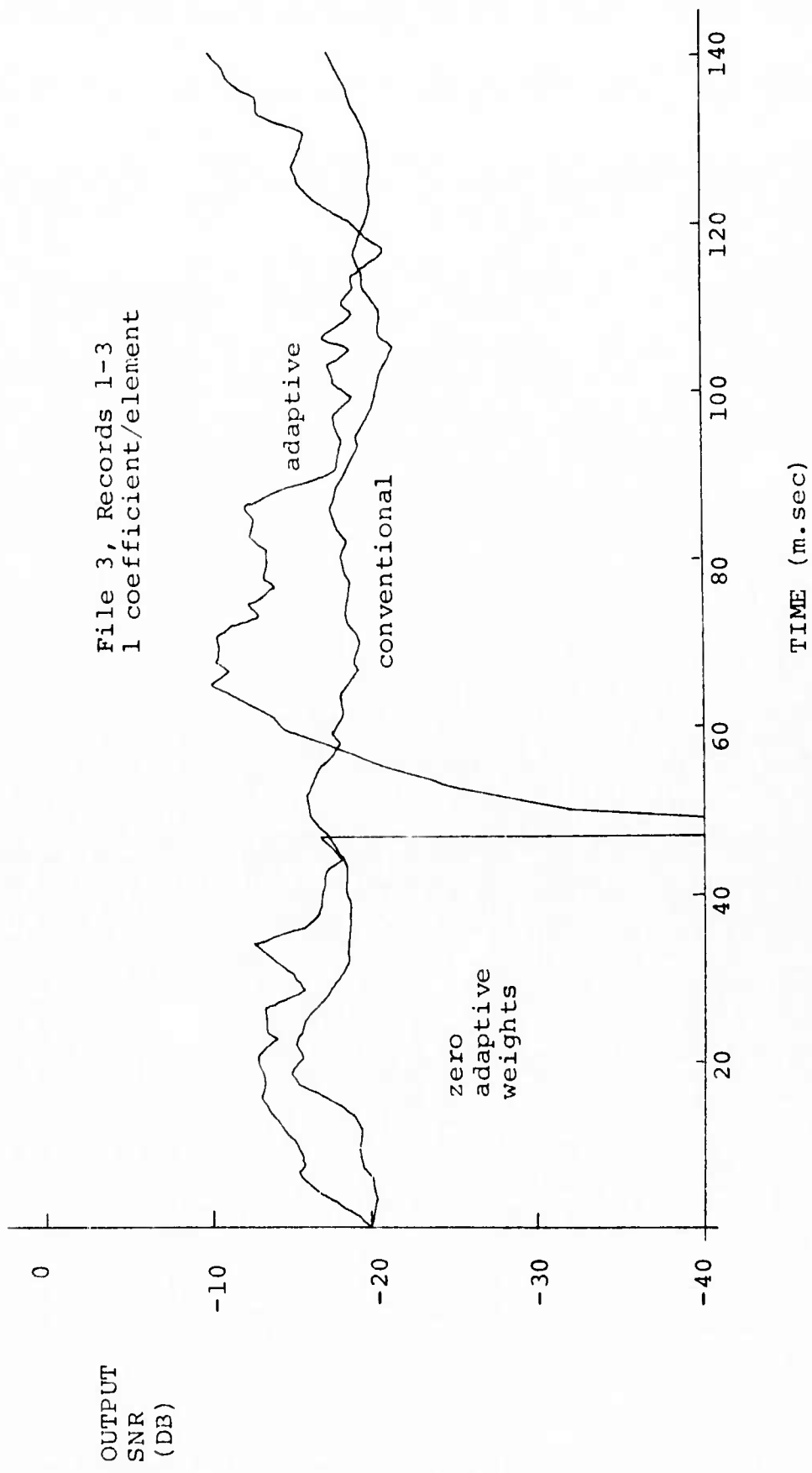
Fig. 25 Time history of output SNR for forward-scatter CW test
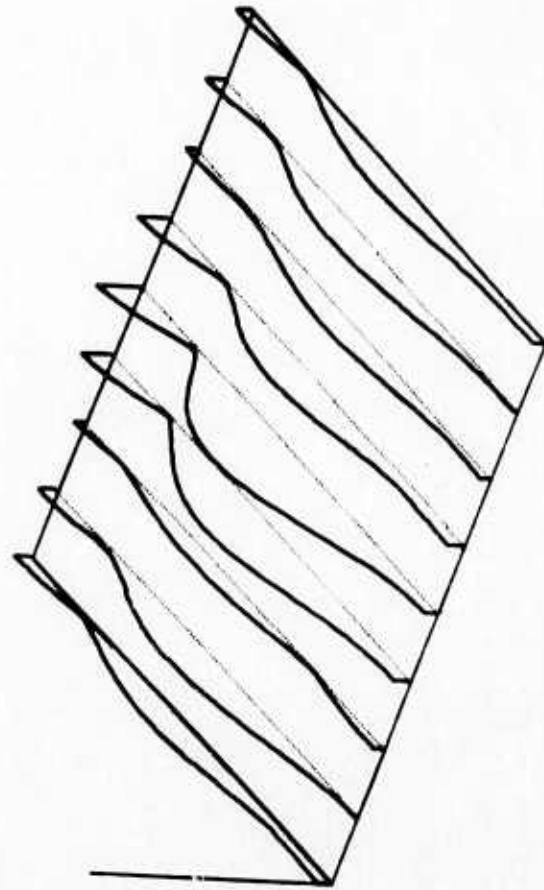with 1 coefficient per element
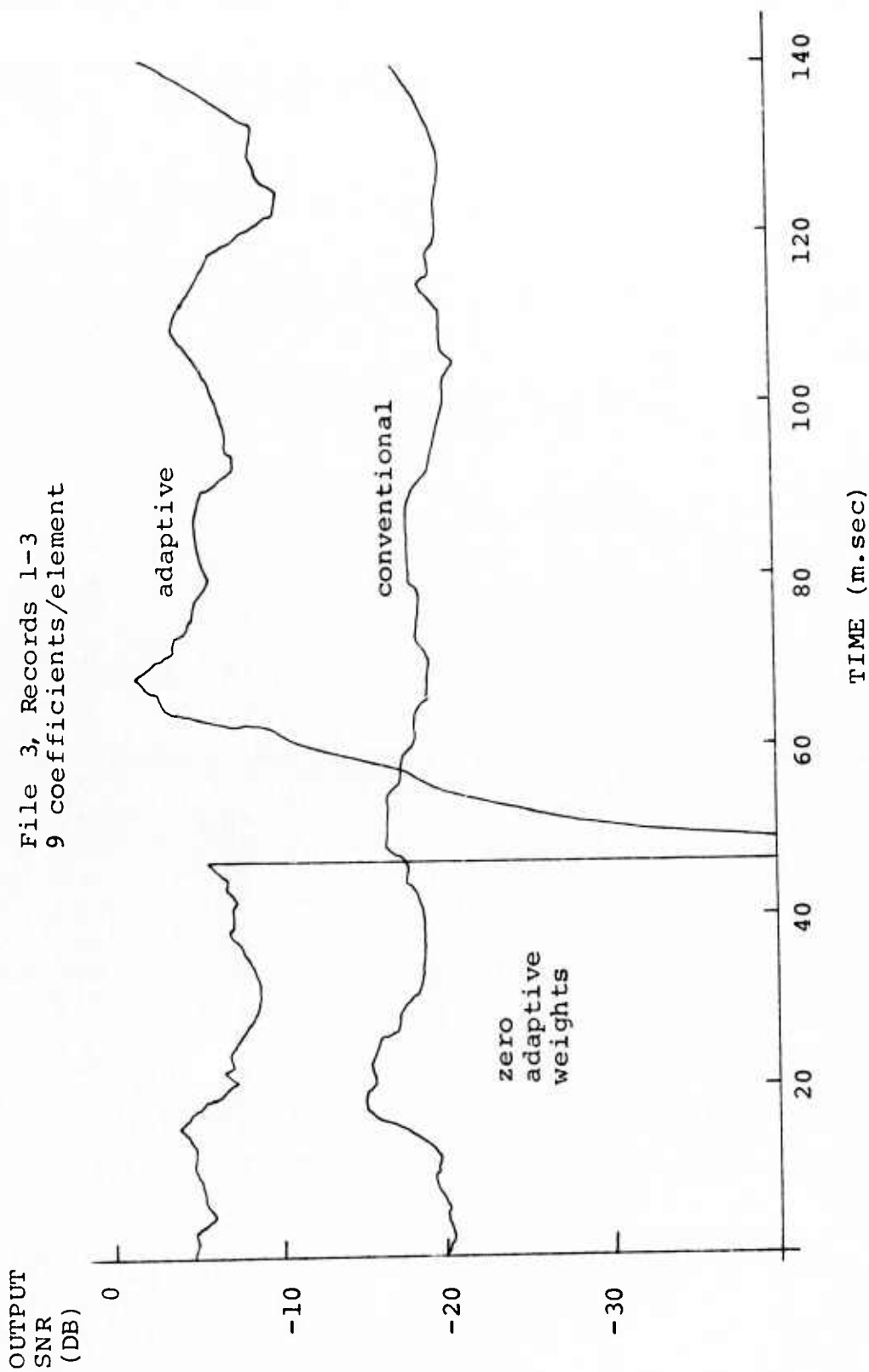
Fig. 26   Time history of output SNR for forward-scatter CW test with
          nine coefficients per element

nine weights per element, respectively. The large transient observed near 45 m. sec was produced by setting the adapted weights to zero. In both cases, the observed recovery time was about 20 m. sec. A summary of the output SNR improvement provided by adaptive processing on File 3 is shown in Table III. Gain only adaptation provides on the order of 3 db improvement while nine coefficients per element produces greater than 10 db. improvement.

B   BACKSCATTER CW TESTS

Output SNR calculations were also carried out for data recorded using backscatter CW transmissions. Figures 9 and 10 illustrate the azimuth/frequency content of these data under both high (File 7) and low (File 8) input SNR conditions. A desired signal was generated using a 100 Hz offset repeater at Bearden. The equivalent downconverted value at the Los Banos receiver output was then 400 Hz. Note that an image frequency line appears at 600 Hz due to the use of a double sideband modulator. For purposes of the following discussion, only the 400 Hz line was taken as the desired output signal.

A time history of the SNR measured at the output of both a conventional beamformer and an adaptive signal processor operating on File 8 with 5 adaptive weights per antenna element α = 0.4 is shown in Fig. 27. The SNR in this plot was computed as the ratio of output power at the desired 400 Hz frequency to total output power. In effect,

60

Table III: Summary of output SNR improvement
provided by adaptive processing of File 3 data.

Tape Record No.	Start time m.sec.	No. of adaptive coefficients/ element		
		1	5	9
1	0	2.7	9.0	11.8
2	64	2.6	9.1	12.9
3	128	5.2	9.0	10.9
4	192	3.0	7.5	9.6
5	256	2.2	10.9	14.3
6	320	5.6	10.9	13.3
7	384	1.4	5.5	8.0
8	448	1.1	6.2	7.9
9	512	5.1	9.7	10.8
10	576	3.0	9.3	11.7
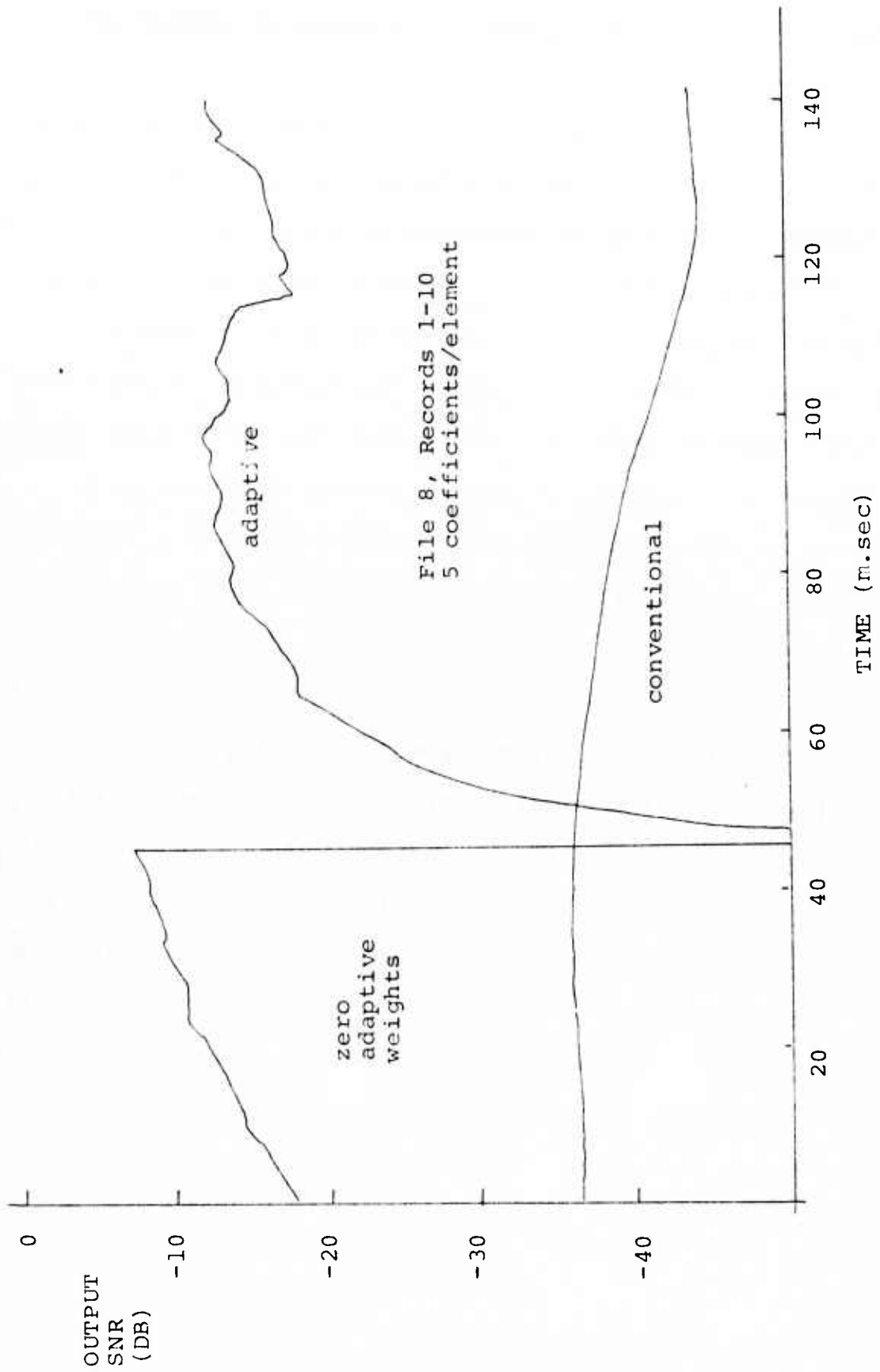
Fig. 27 Time history of output SNR for backscatter CW test with five coefficients per element

62

the quantity measured is the ratio of signal to interference plus clutter plus noise power. The adaptive coefficients were set to zero at time t = 40 m.sec for purposes of measuring the adaptive recovery time. A summary of the improvement offered by the adaptive processor with respect to conventional beamforming is presented in Table IV.

The results obtained in the presence of CW backscatter transmissions were markedly similar to those measured for the forward scatter case. Larger improvements in the backscatter case are primarily due to the clutter rejection provided by the adaptive processor. Figure 28 illustrates this rejection in more detail. A sequence of four azimuth/frequence response curves were computed using the adapted filter coefficients obtained during the experiment shown in Fig. 27. The response at the clutter frequency (500 Hz) is suppressed at all azimuths except borsite.

These experiments were carried out to investigate the performance of the adaptive processor in the presence of an undesired signal (clutter) which was highly correlated with the desired signal. Continuous wave transmissions were used for purposes of providing simple signal formats and were not intended to be representative of operational systems. The results indicated that adaptive processing works well in the presence of clutter and no new operational difficulties were encountered.

63

Table IV: Summary of output SNR improvement
provided by adaptive processing of Files 7 and 8 using
five coefficients per array element

Tape Record No.	Start time m.sec	File 7 improvement	File 8 improvement
1	0	26.1	25.4
2	64	27.3	26.5
3	128	29.1	30.7
4	192	23.2	27.7
5	256	27.5	26.1
6	320	30.5	25.6
7	384	31.3	27.1
8	448	29.6	26.1
9	512	27.4	20.2
10	576	26.2	19.8
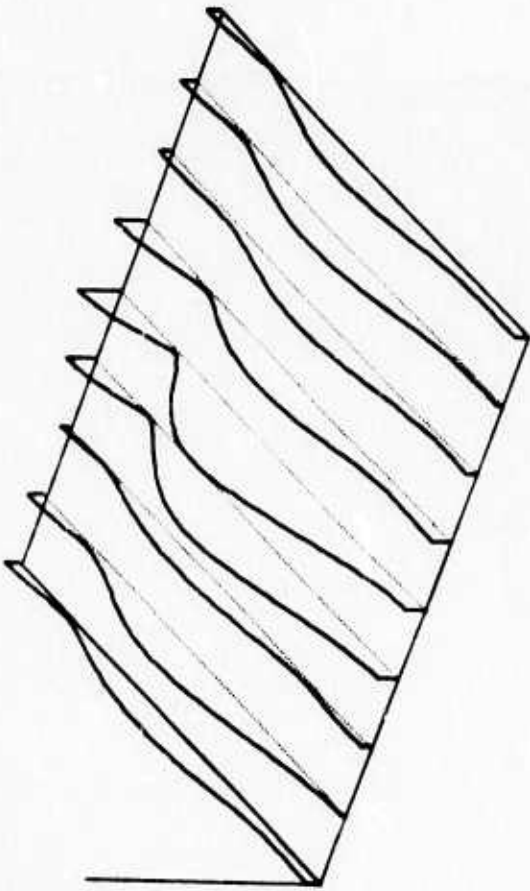
a) File 8, Record 1
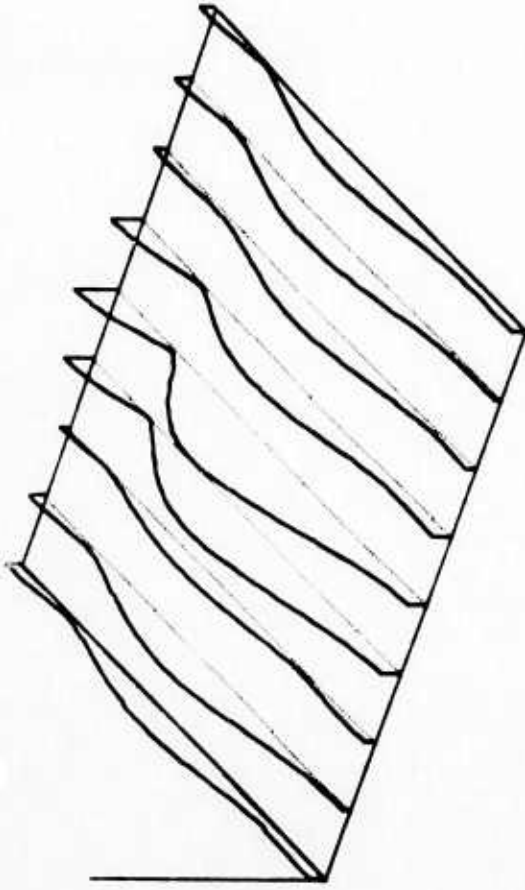
b) **File** 8, Record 2
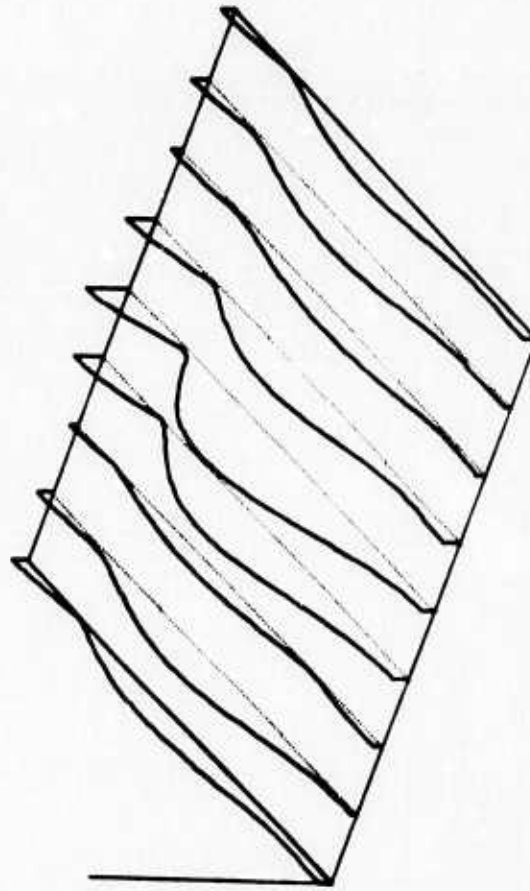
c) File 8, Record 3

d) File 8, Record 4

Fig. 28   Sequential adaptive processor response plots derived from File 8 with five coefficients per element.

65

C   FM/CW RADAR EXPERIMENTS

The data recorded in Files 10, 11, and 12 were taken using the FM/CW transmission format shown in Fig. 5. These data were processed using both a conventional beamformer and the adaptive configuration shown in Fig. 12. Range/doppler maps were computed from the processed outputs using two-dimensional Fourier Transform techniques. Specifically, denoting the kth sample of a processed beam output as $z(k)$, a two-dimensional matrix is constructed in which the nth row contains the beam output samples during the nth sweep. With a 60 Hz sweep rate and a sampling frequency of 1.92 kHz, there are precisely 32 samples per sweep and the matrix is given by,

$$
\begin{bmatrix}
z(0) & z(1) & \cdot \ \cdot & z(31) \\
z(32) & \cdot & \cdot \ \cdot & z(63) \\
\cdot & & & \\
\cdot & & & \\
z[(N-1)32] & \cdot & \cdot \ \cdot & z(32N-1)
\end{bmatrix}
\tag{34}
$$

The number of sweeps N determines the dwell time for the map. In the examples shown below, a value $N = 32$ is used providing a dwell time of 0.533 seconds.

Transforming the rows and columns of this matrix produces a matrix of complex numbers with dimension N x 16. (The reduction from 32 to 16 is due to the use of real-valued samples in the initial array.) After transforming, the mag-

66

nitude of the values in the mth column of the resulting
matrix may be interpreted as the doppler response in the mth
range bin. Thus, with N = 32, the process produces a range/
doppler map with 16 range bins and 32 unambiguous doppler
cells. For the parameters used in this experiment, the range
bin separation was 18.75 km and the doppler cells were sep-
arated by 1.875 Hz.

A range/doppler display was generated from the magnitudes
of the transformed matrix by normalizing with respect to
the root-mean-square noise floor. Figure 29 shows the re-
sults of five successive dwells computed using the data in
File 11. In each case, maps derived from both conventional
and from adaptive beamforming outputs were computed. The
two outputs were generated simultaneously using identical
input signals. The adaptive processor consisted of five
coefficients per element and a value of $\alpha = 0.1$ The steer-
ing vector frequency used was 500 Hz and corresponds to the
range indicated by the arrow. These data contain a clear,
interference-free repeater signal located in the 8th range
cell. The target doppler appears at both +16.9 and -16.9
Hz due to the use of double sideband modulation in the re-
peater. Ground clutter appears in three doppler cells and
is clipped at a value ten times greater than the RMS noise
floor. Display amplitudes are presented on a linear scale
and Hamming windows were applied to the data in both dimen-
sions prior to transforming.

A comparison of adaptive and conventional processing

67
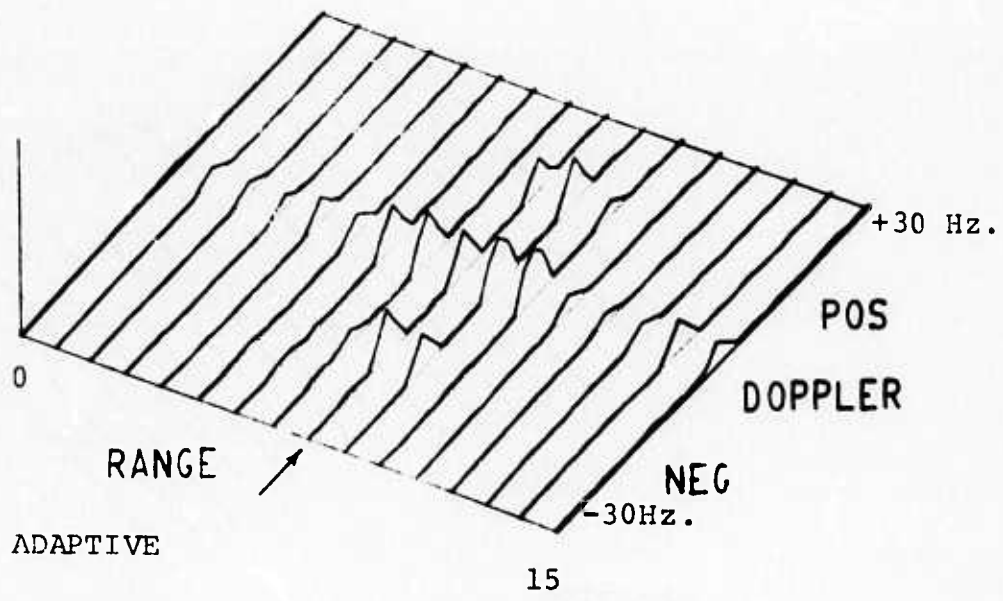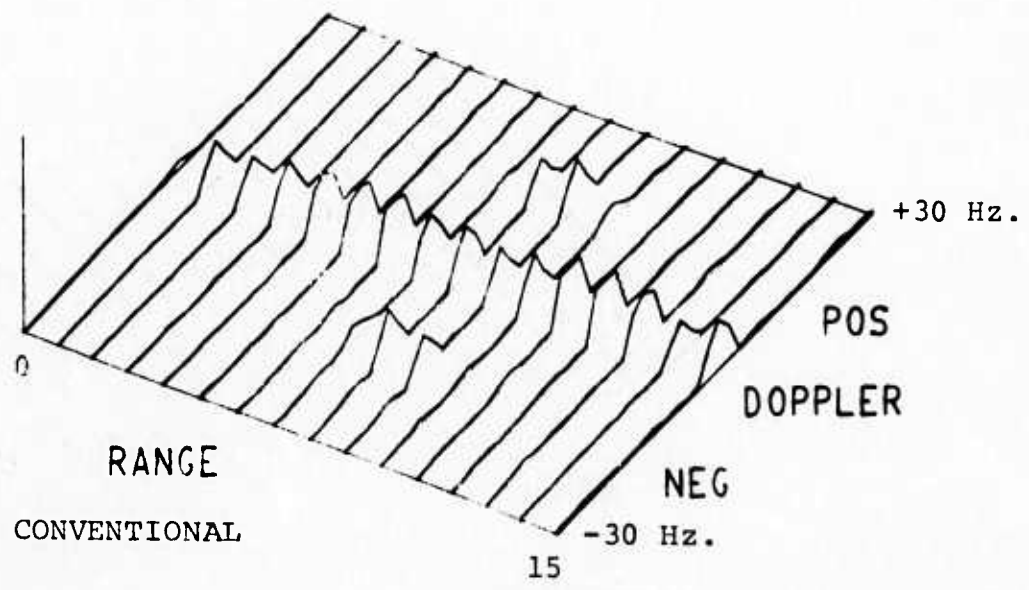
Fig. 29 a)   Range/doppler displays derived from File 11,
             Dwell # 1.
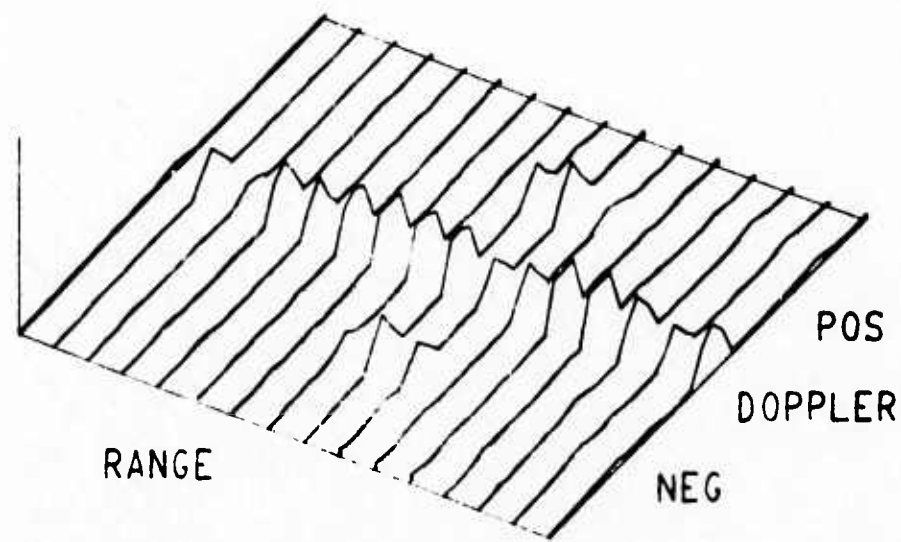
CONVENTIONAL
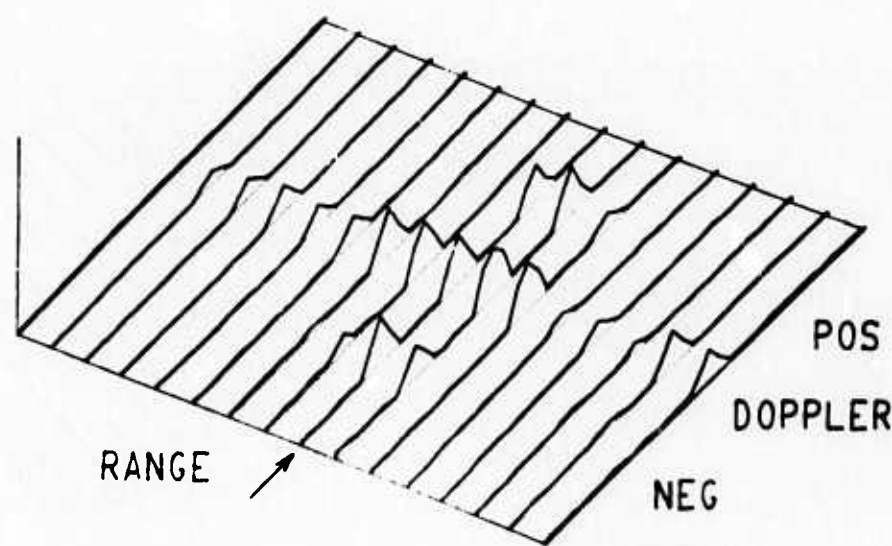
ADAPTIVE

Fig. 29 b) Range/doppler displays derived from File 11,
            Dwell # 2.

69
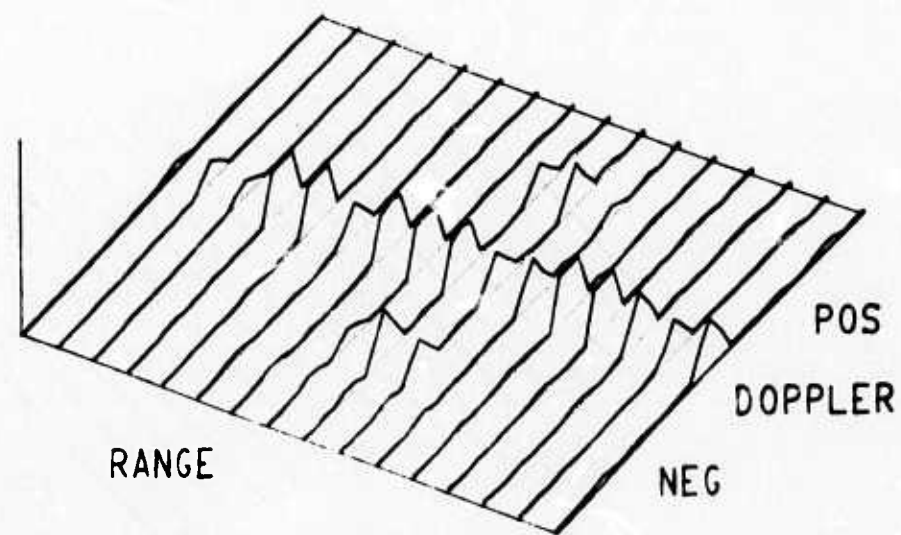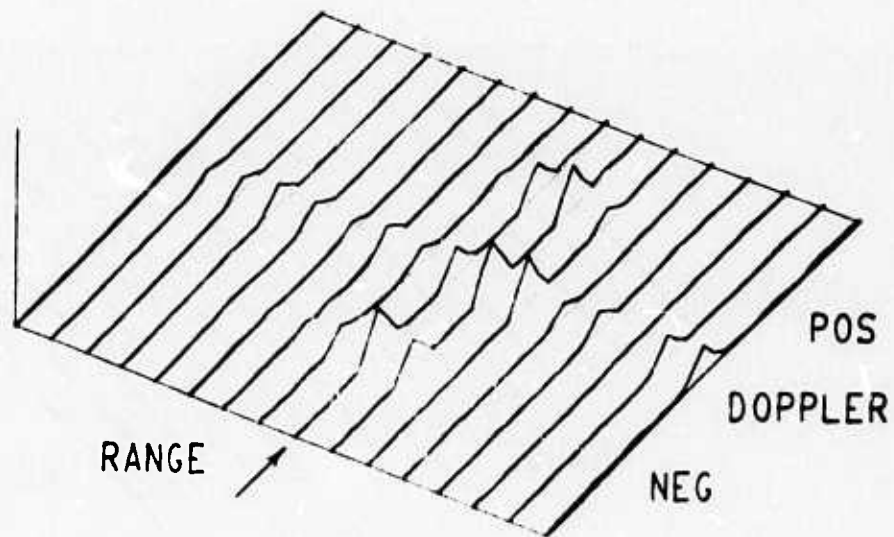
Fig. 29 c) Range/doppler displays derived from File 11,
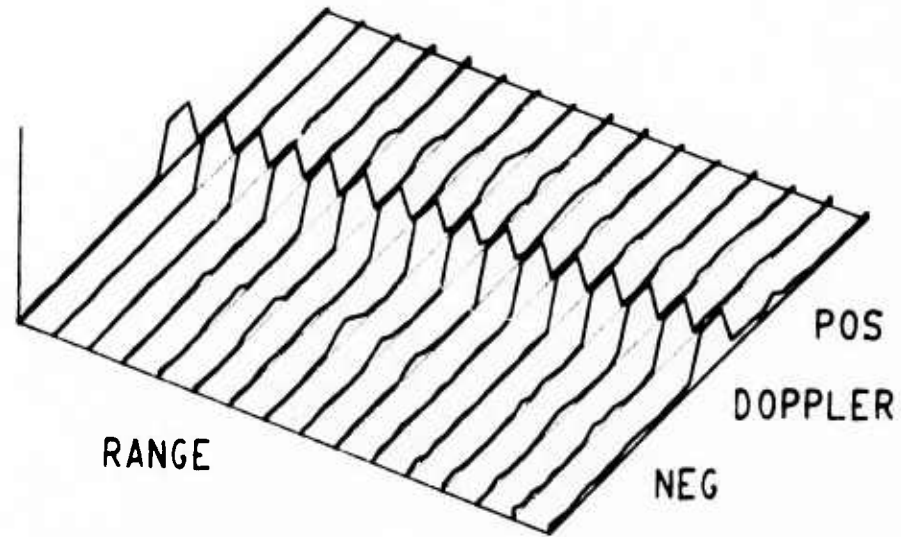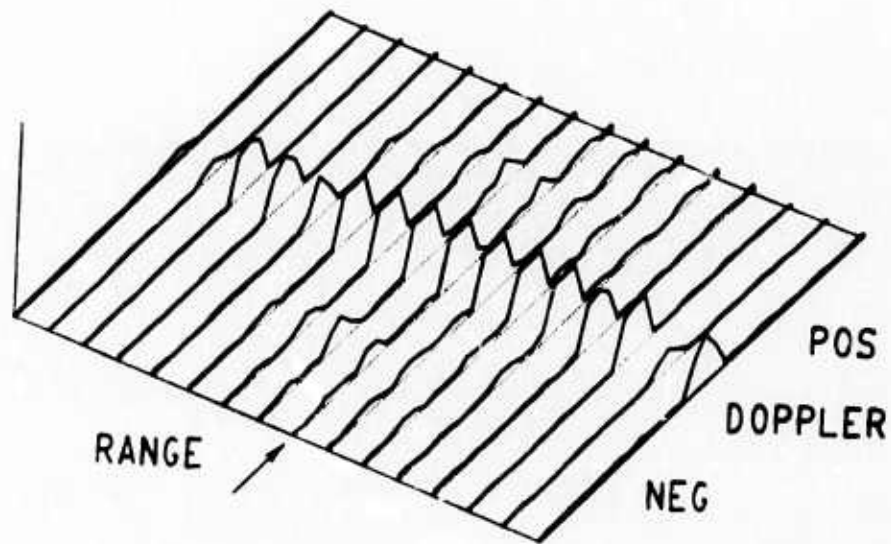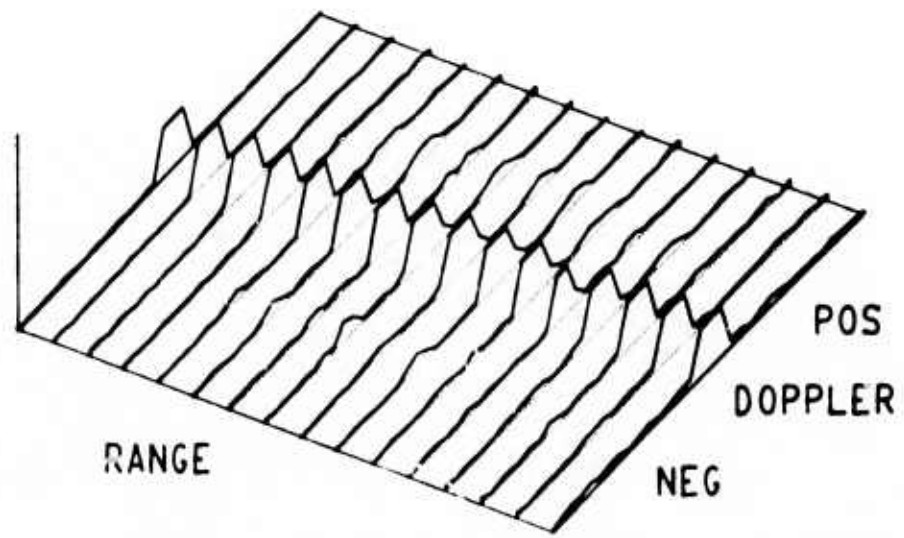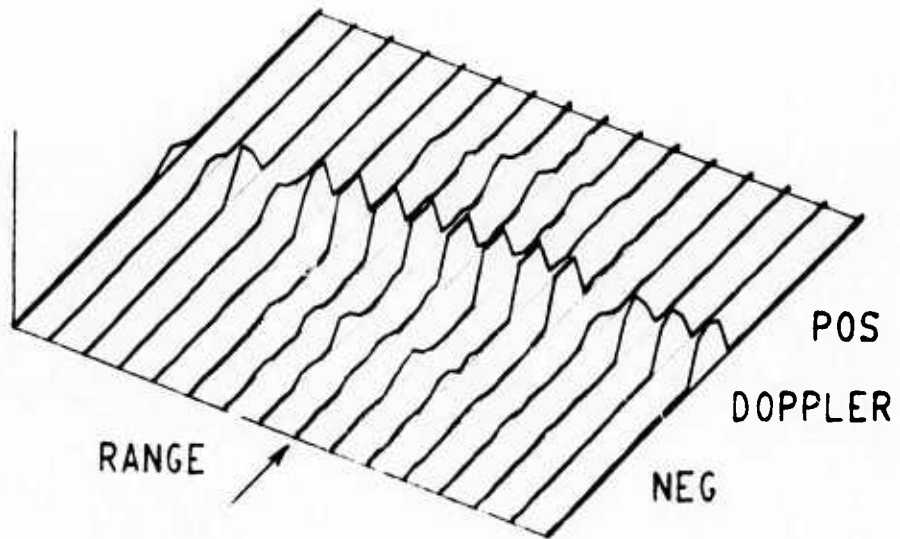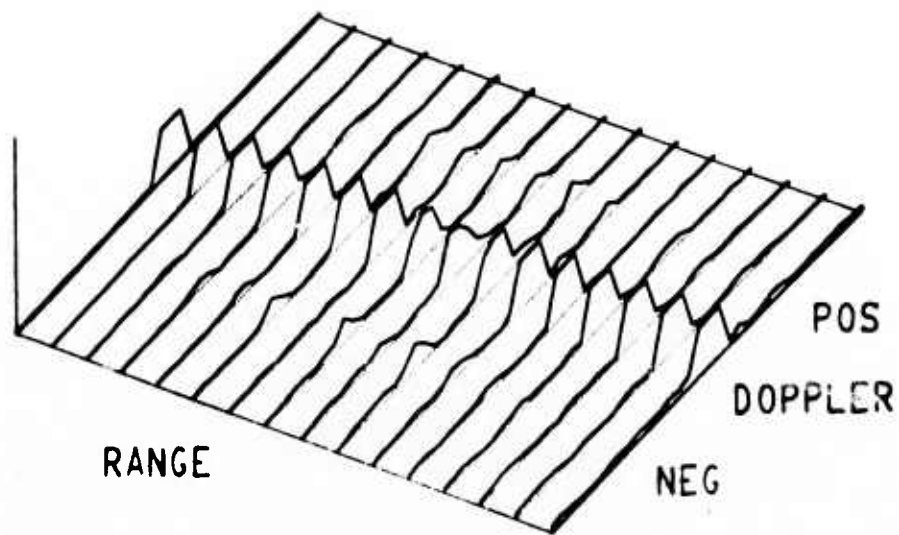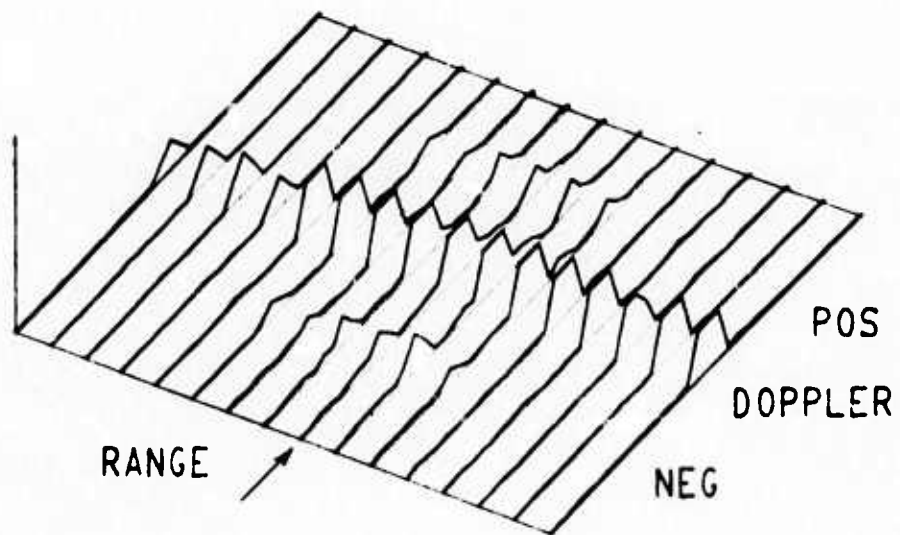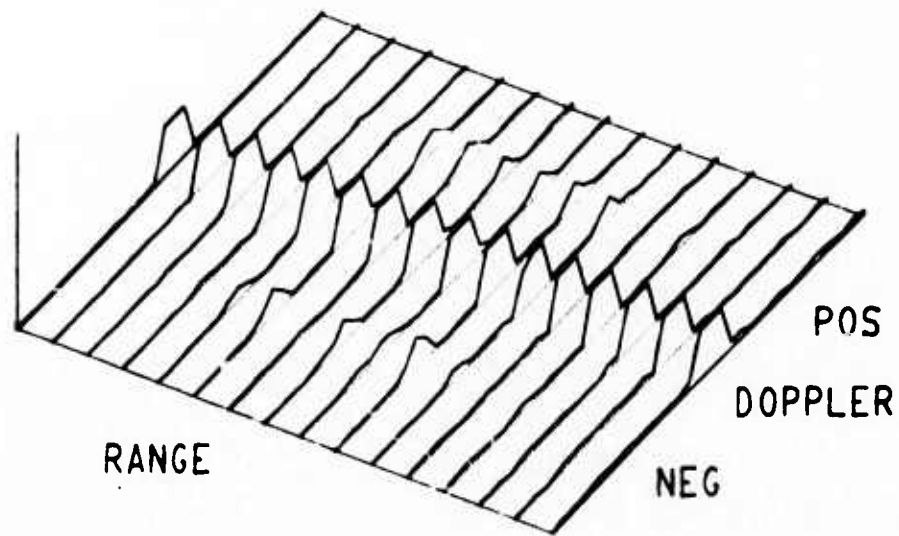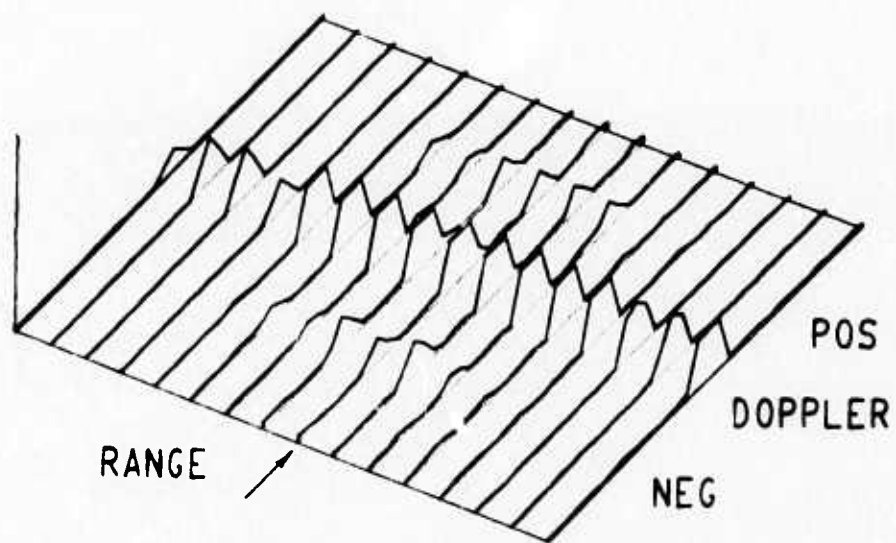   Dwell # 3.
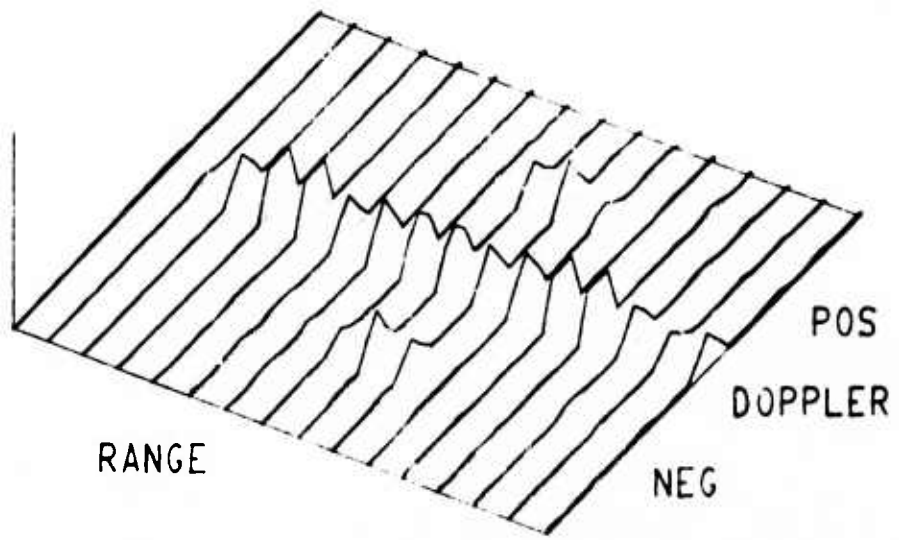
CONVENTIONAL
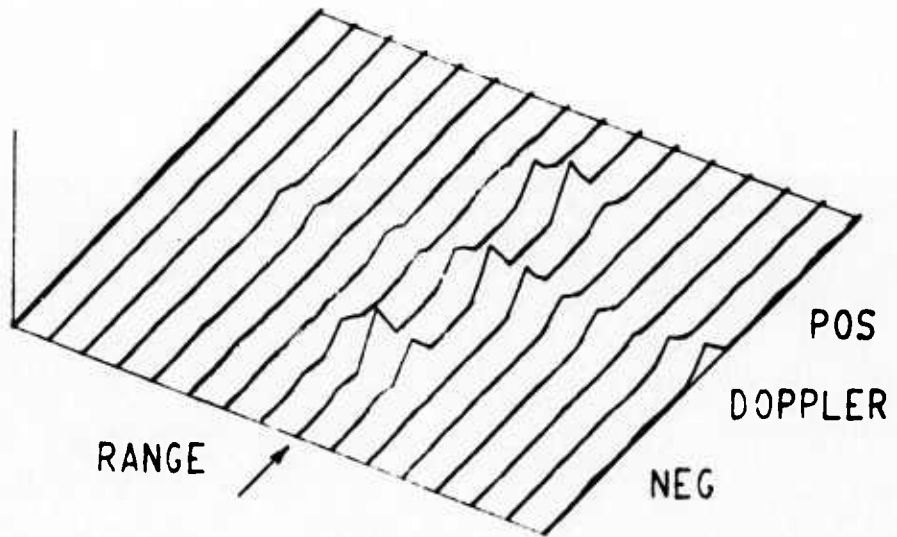
ADAPTIVE

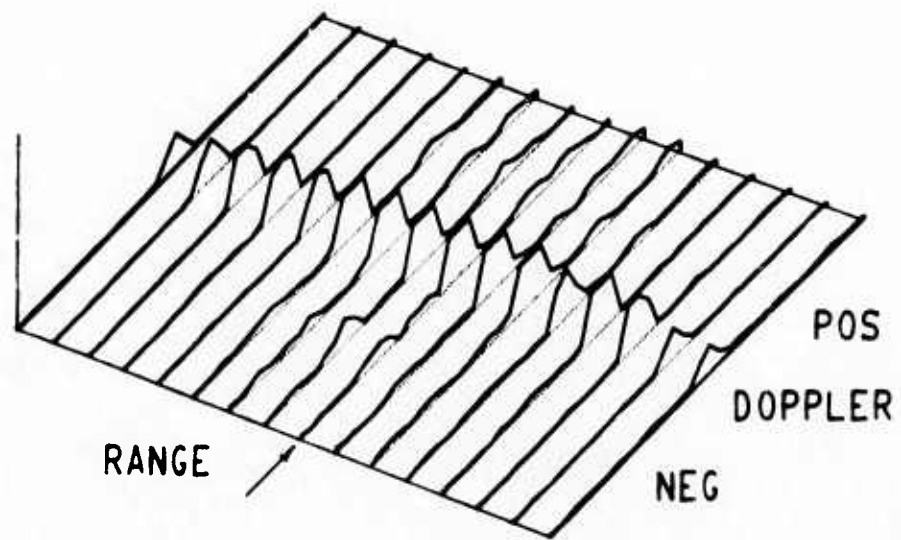Fig. 29 d) Range/doppler displays derived from File 11,
           Dwell # 4.
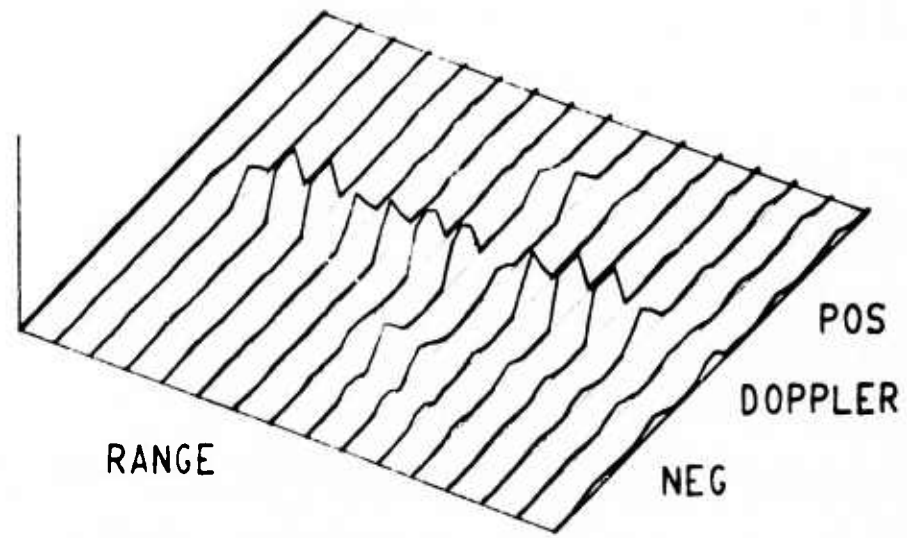
CONVENTIONAL
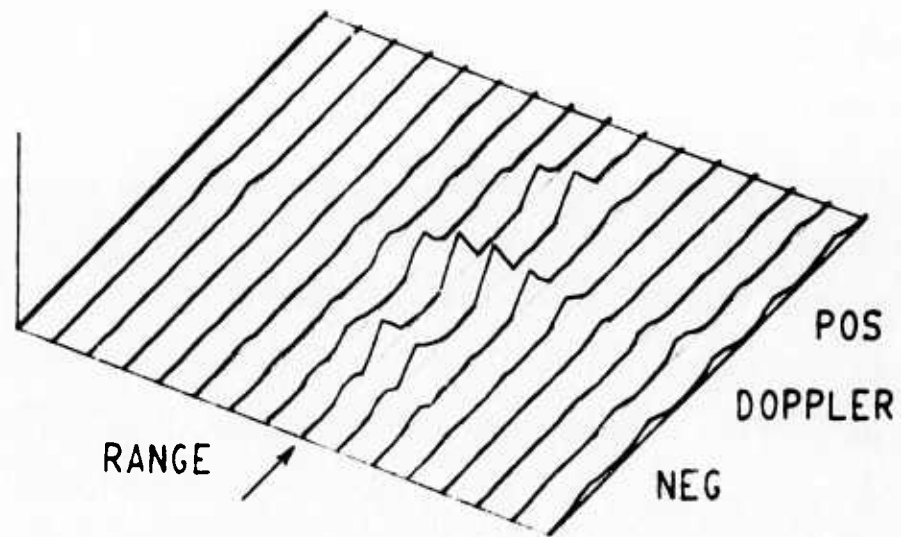
ADAPTIVE

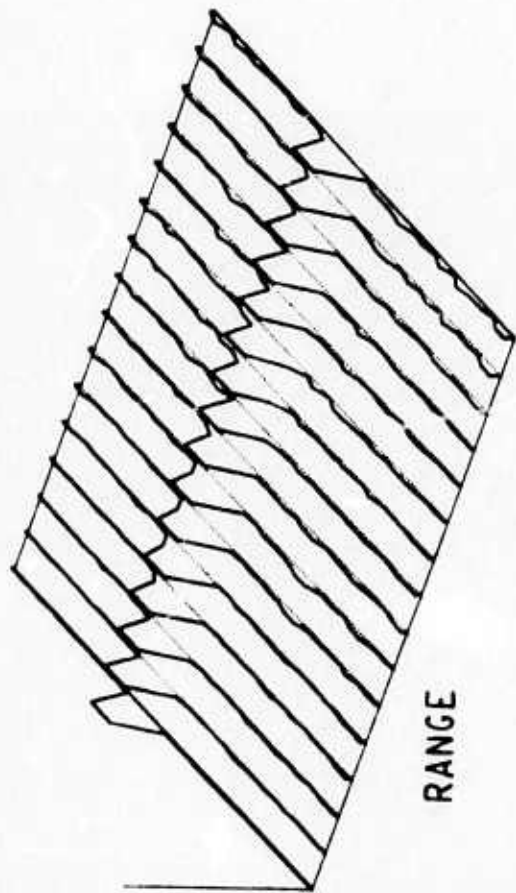Fig. 29 e) Range/doppler displays derived from File 11,
Dwell # 5.

72

using data with a lower signal-to-noise ratio is shown in Fig. 30. Data for these results were obtained from File 10. The filter parameters used to generate this display were identical to those used in Fig. 29. The five dwells shown are time sequential with adaptive and conventional outputs computed simultaneously.

As discussed in Section IV D, the phase and amplitude transient which occurs during frequency flyback in the FM/CW transmission may be expected to affect the performance of the adaptive processor. Figure 31 presents results obtained with a processor, in which adaptation occurred only during the middle portions of the frequency ramp -- i.e. during those periods in which the transient was absent. The two range/doppler maps shown were computed using the same data and filter parameters as used for the first dwells shown in Fig. 30. No apparent advantage was detected for the method.

The effect of variation in the adaptive time constant is illustrated in Figs. 32-39. This sequence of eight successive dwells was computed using the pseudo-operational data recorded in File 12. Examples of adaptation using a 5 weight per element processor with $\alpha = 0.02, 0.10$ and 0.50 are presented. The steering vector frequency selected was 340 Hz and, in effect, optimizes the processor for all doppler frequencies at the range point indicated by the arrow. These results indicate that wide variations in the value of α produce markedly similar adapted range/doppler maps. The average time constants computed from (32) are
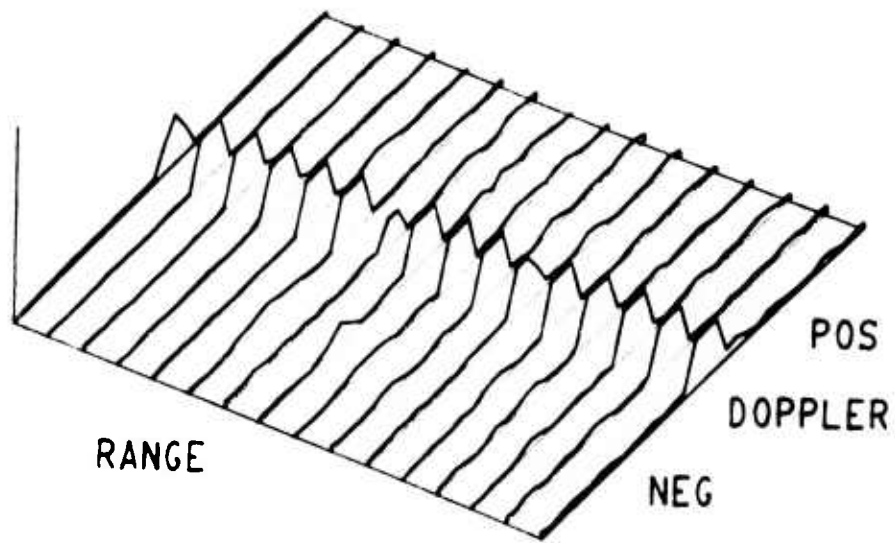
CONVENTIONAL
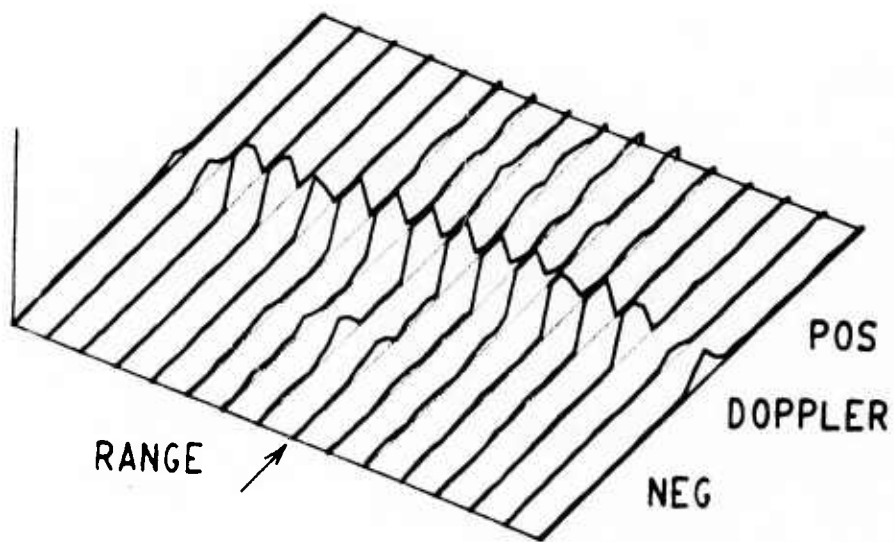
ADAPTIVE

Fig. 30 a) Range/doppler displays derived from File 10, Dwell # 1.

74

CONVENTIONAL

ADAPTIVE

Fig. 30 b)   Range/doppler displays derived from File 10,
              Dwell # 2.

CONVENTIONAL

ADAPTIVE

Fig. 30 c) Range/doppler displays derived from File 10, Dwell # 3.

CONVENTIONAL

ADAPTIVE

Fig. 30 d)   Range/doppler displays derived from File 10,
             Dwell # 4.

77

Fig. 30 e) Range/doppler displays derived from File 10,
Dwell # 5.

a) Adaptive processor, Dwell # 1.
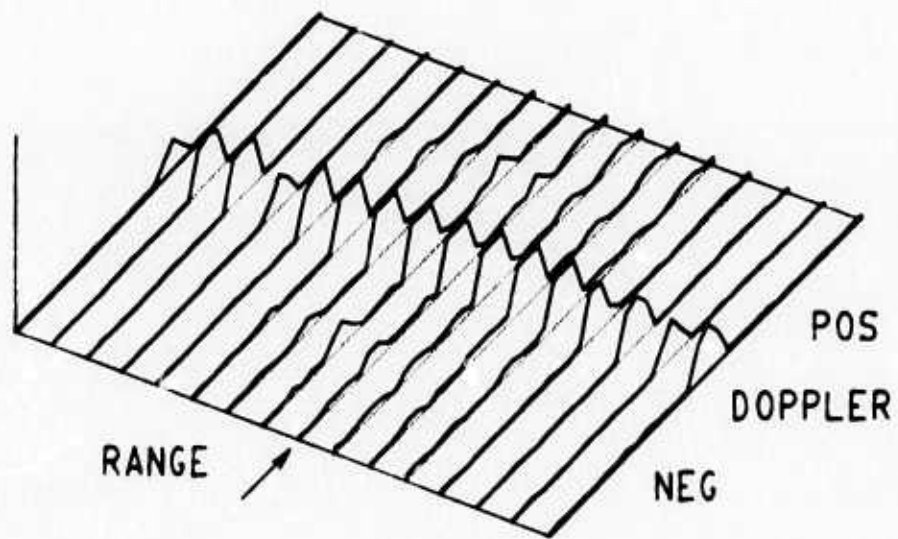
b) Adaptive processor, Dwell # 2.

Fig. 31   Range/doppler displays derived from File 10 using
adaptive algorithm during midsweep only.
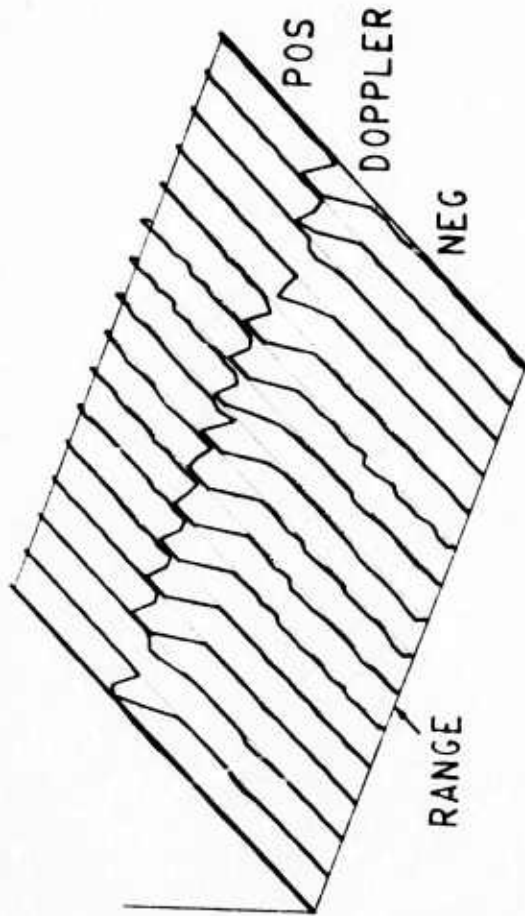
b) Adaptive processor, α = 0.02

d) Adaptive processor, α = 0.50
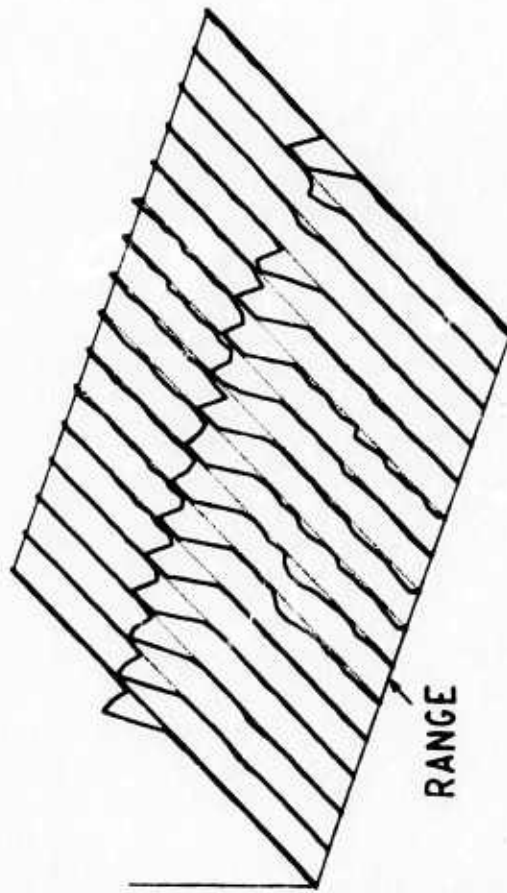
a) Conventional processor
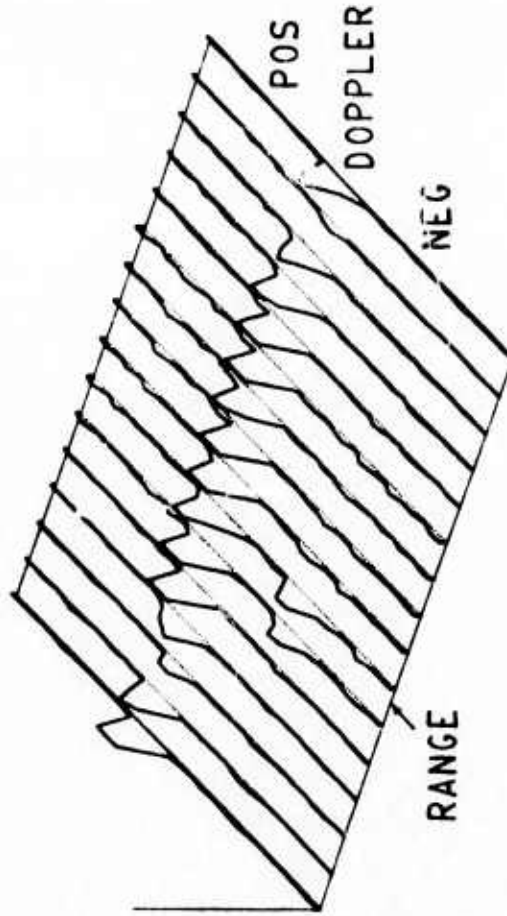
c) Adaptive processor, α = 0.10

Fig. 32 Range/doppler displays derived from File 12, Dwell #1.
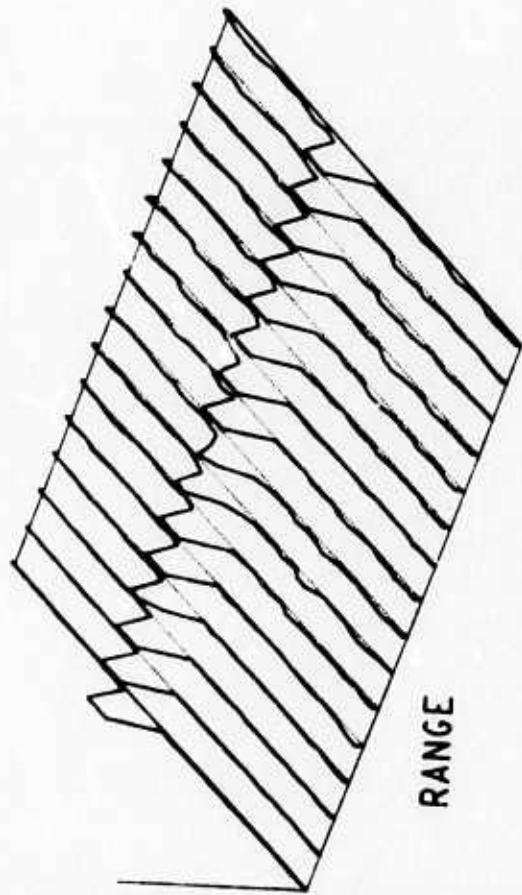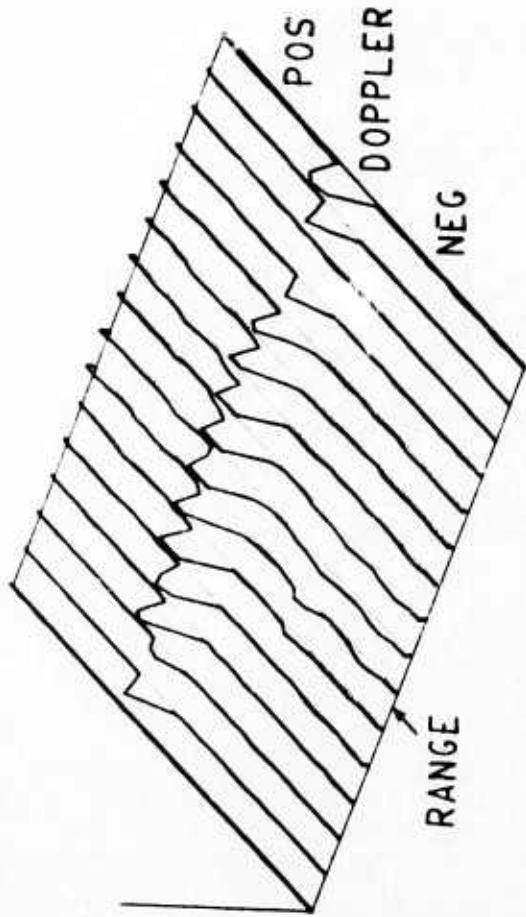
b) Adaptive processor, α = 0.02

d) Adaptive processor, α = 0.50
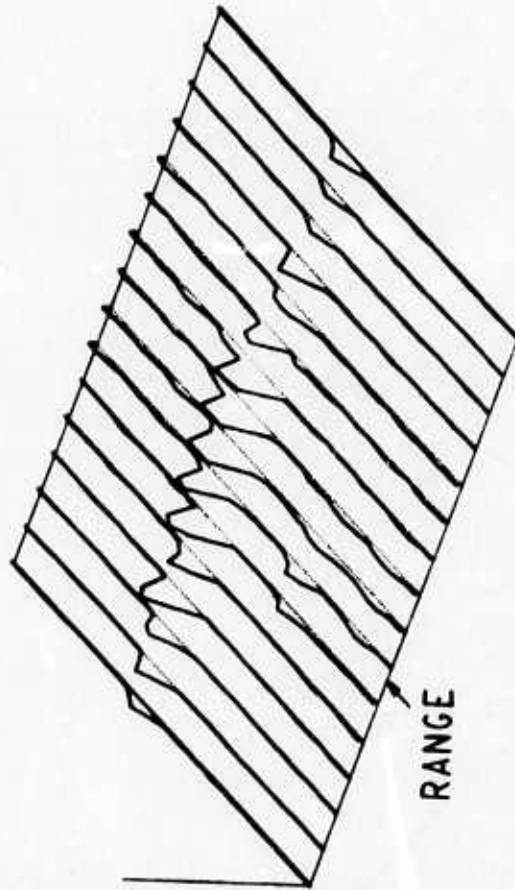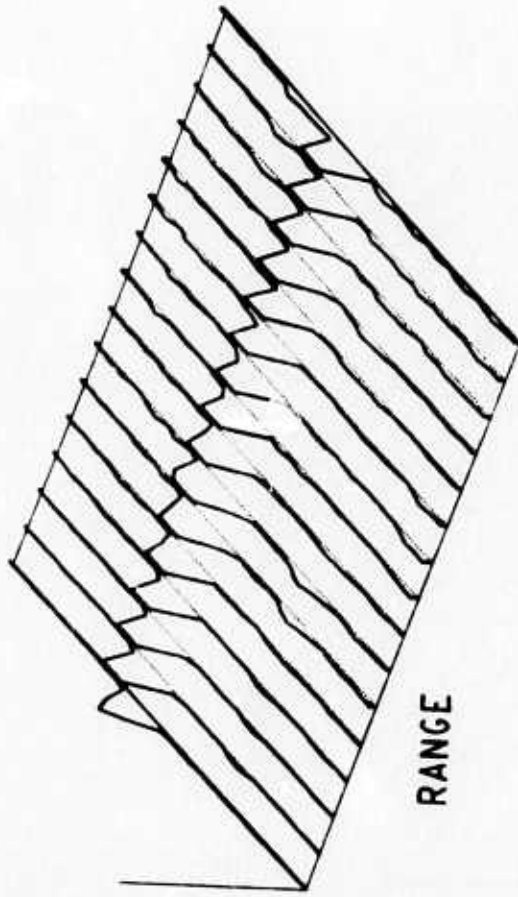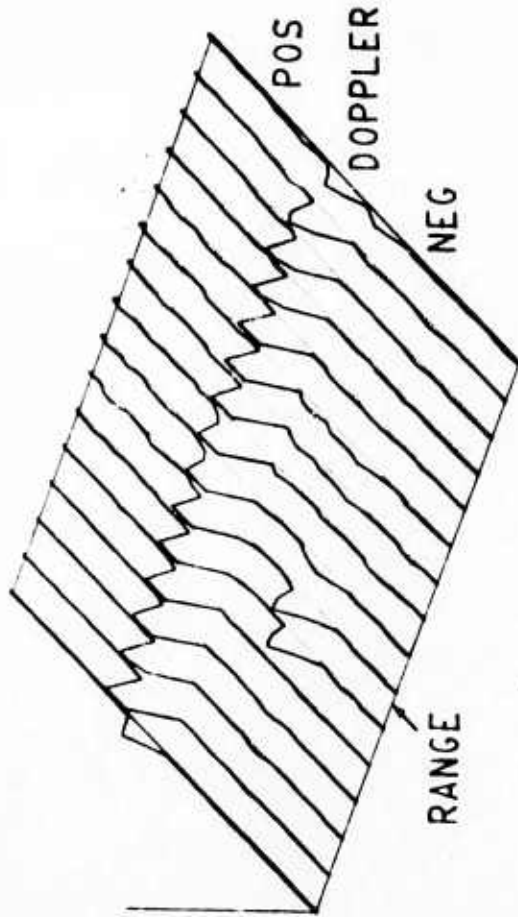
a) Conventional processor
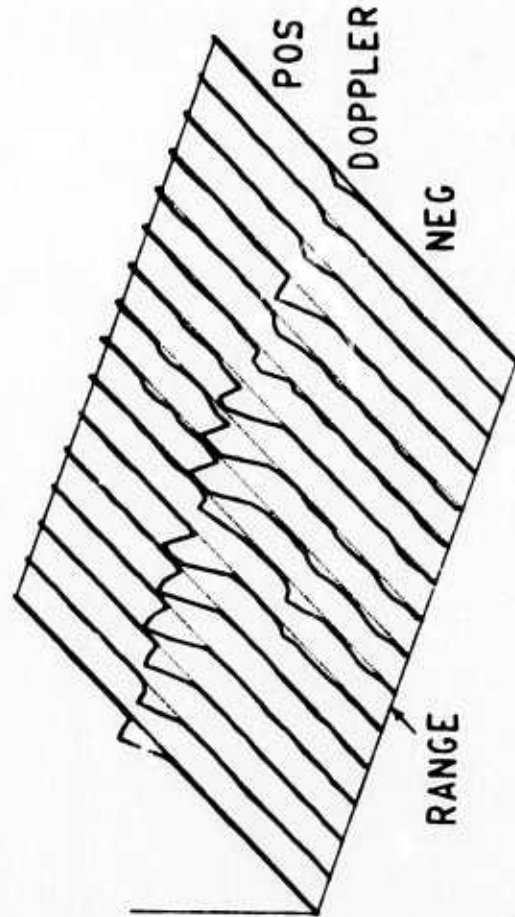
c) Adaptive processor, α = 0.10

Fig. 33   Range/doppler displays derived from File 12, Dwell # 2.
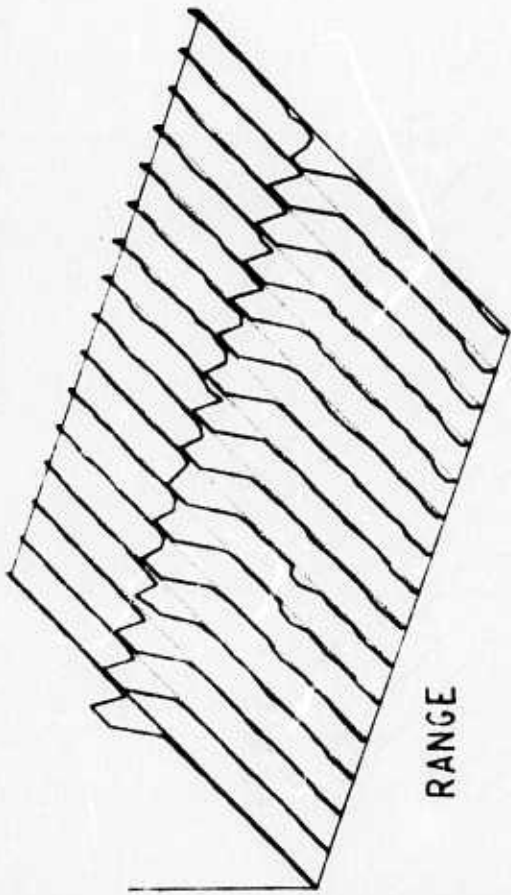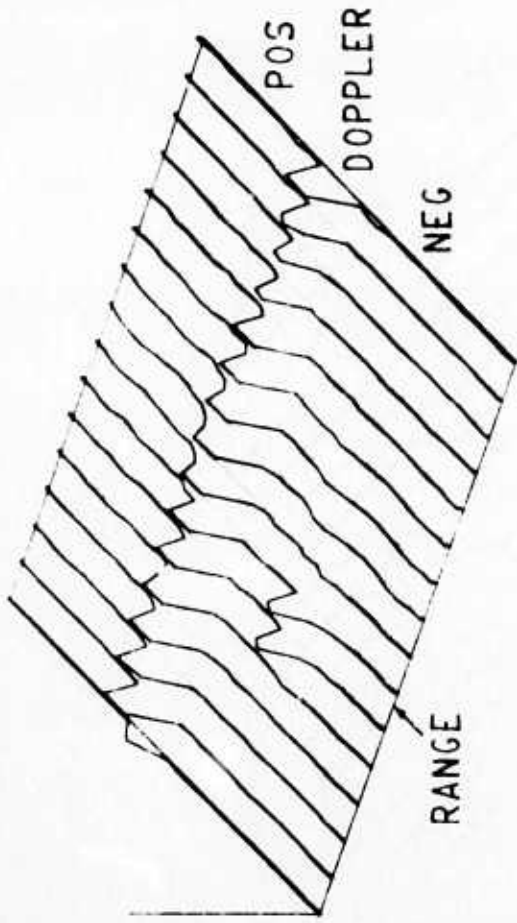
b) Adaptive processor, $\alpha = 0.02$

d) Adaptive processor, $\alpha = 0.50$
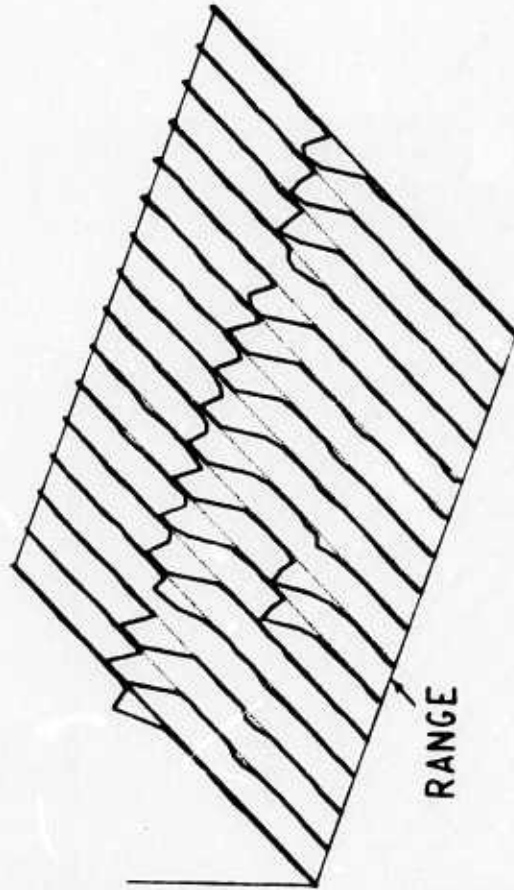
a) Conventional processor
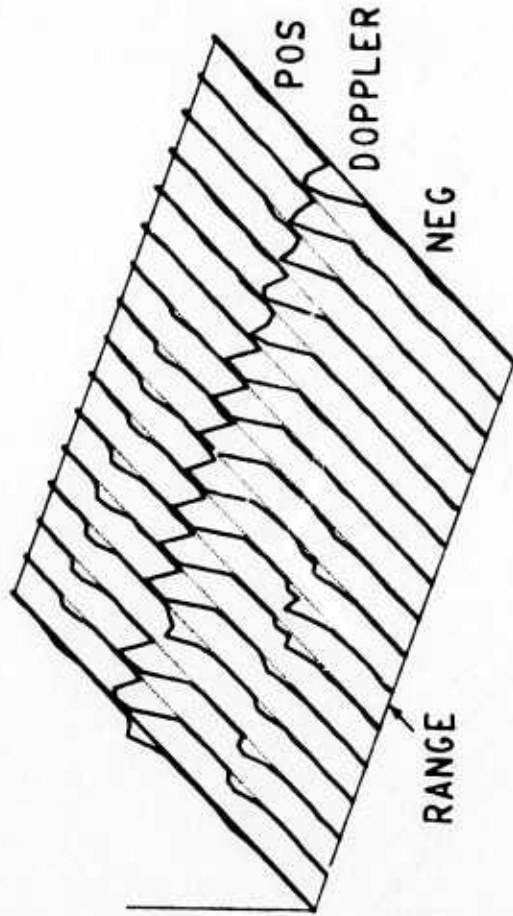
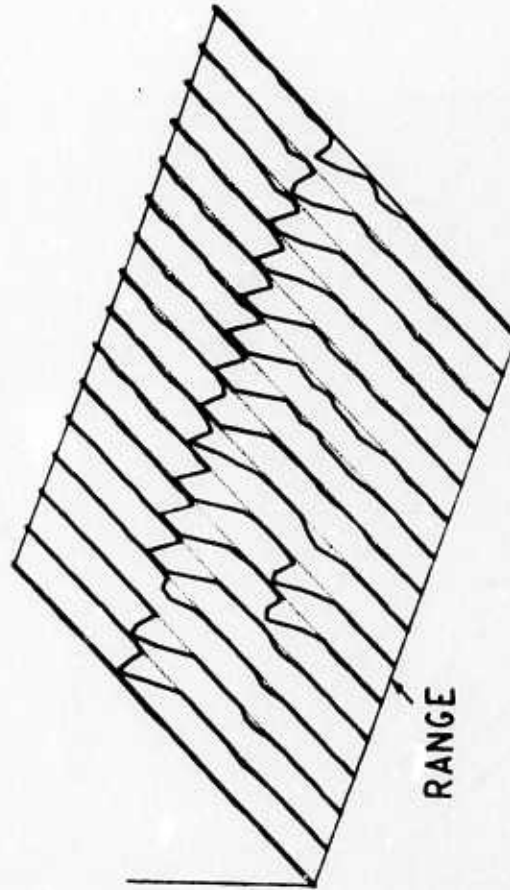c) Adaptive processor, $\alpha = 0.10$

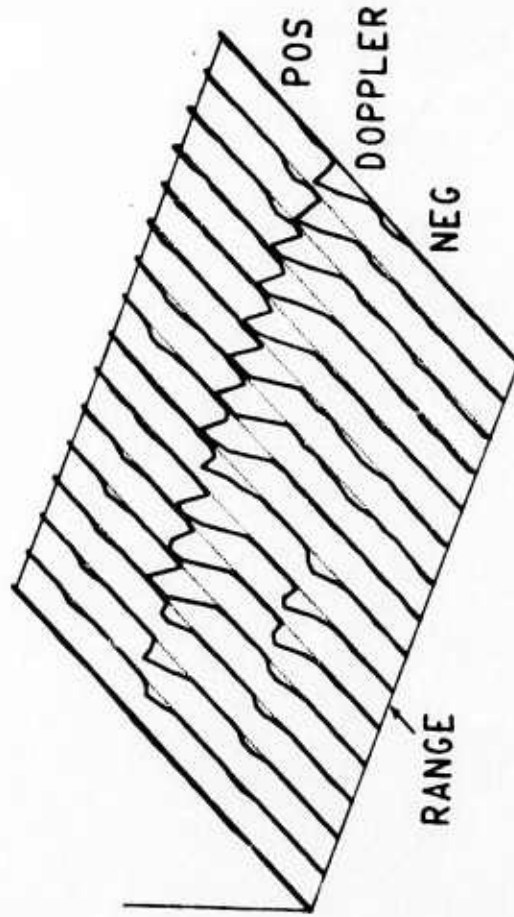Fig. 34   Range/doppler displays derived from File 12, Dwell # 3.

a) Conventional processor
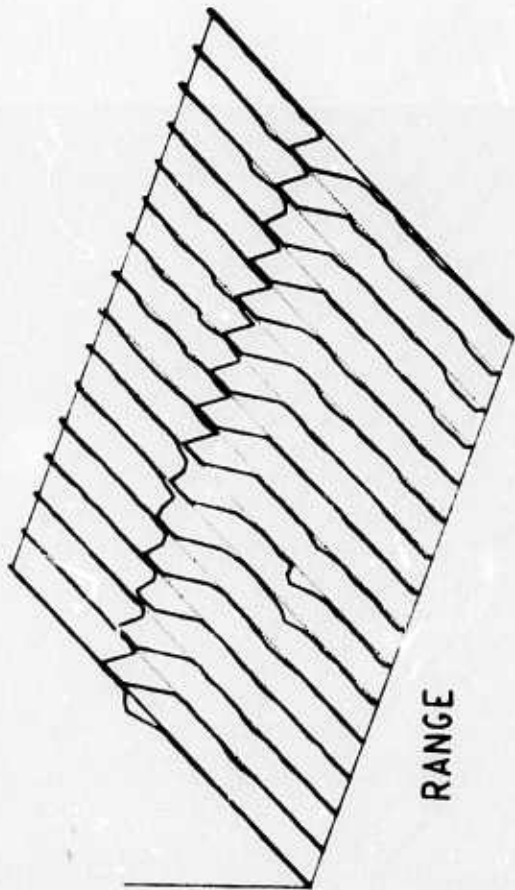
b) Adaptive processor, α = 0.02

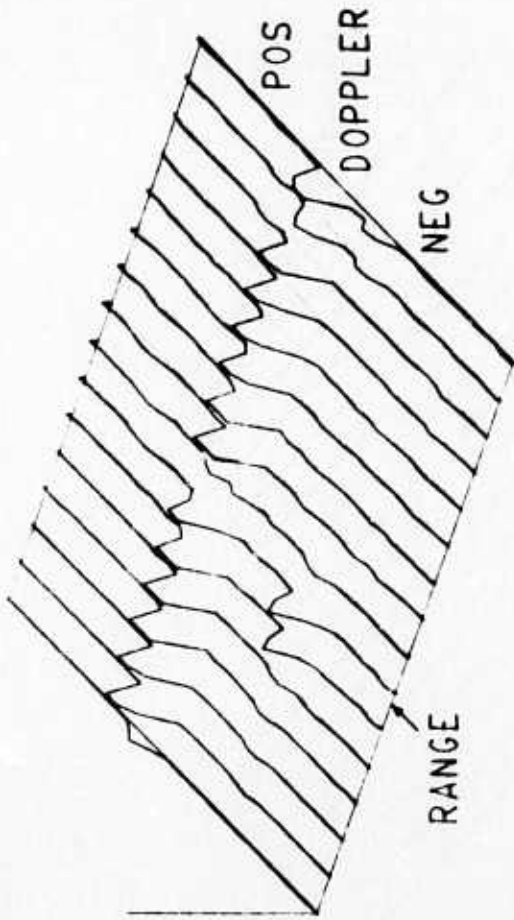c) Adaptive processor, α = 0.10

d) Adaptive processor, α = 0.50

Fig. 35 Range/doppler displays derived from File 12, Dwell # 4.

83

a) Conventional processor

b) Adaptive processor, $\alpha = 0.02$

c) Adaptive processor, $\alpha = 0.10$

d) Adaptive processor, $\alpha = 0.50$

Fig. 36   Range/doppler displays derived from File 12, Dwell # 5.

84

a) Conventional processor

b) Adaptive processor, $\alpha = 0.02$

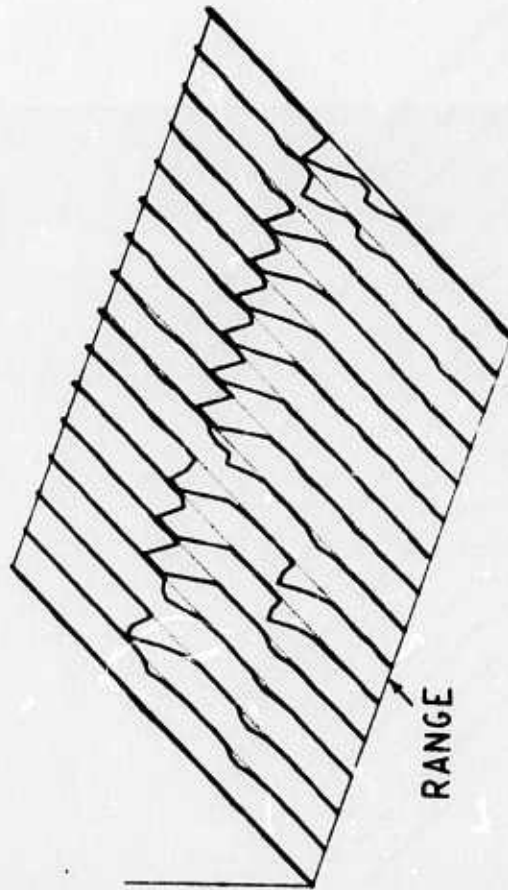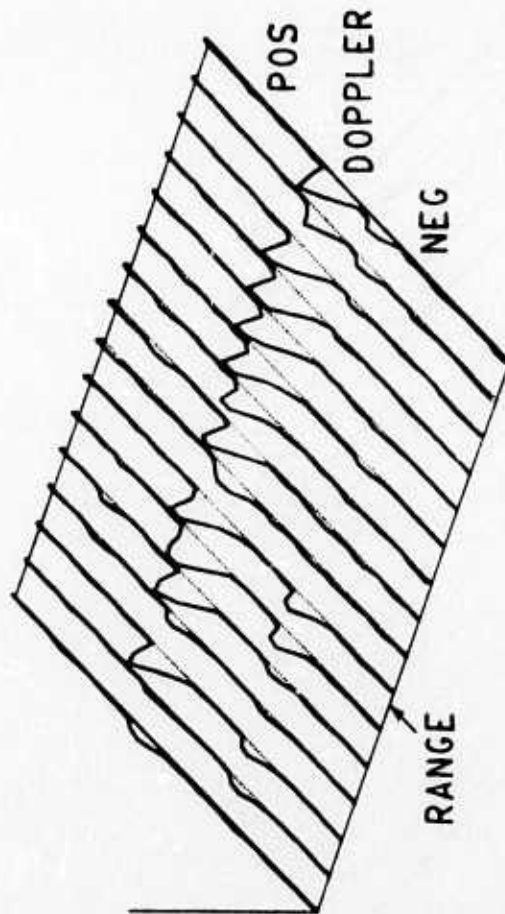c) Adaptive processor, $\alpha = 0.10$

d) Adaptive processor, $\alpha = 0.50$

Fig. 37 Range/doppler displays derived from File 12, Dwell # 6.

a) Conventional processor
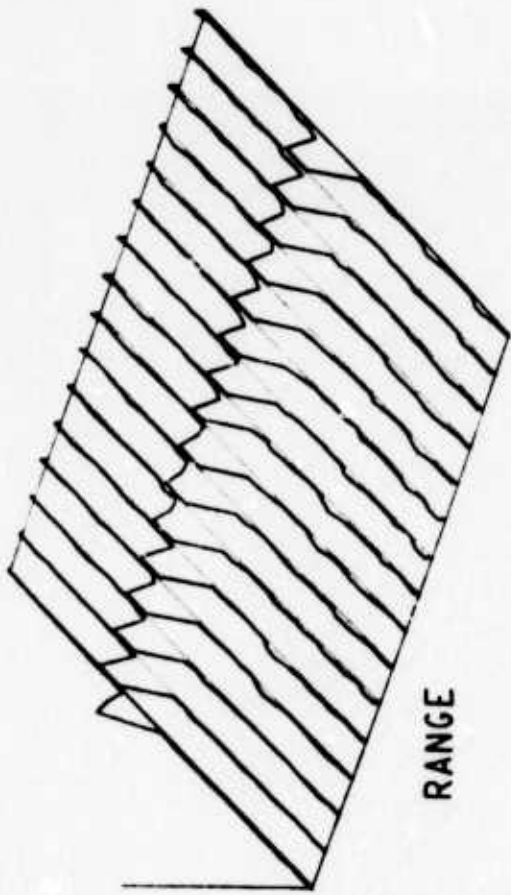
b) Adaptive processor, $\alpha = 0.02$
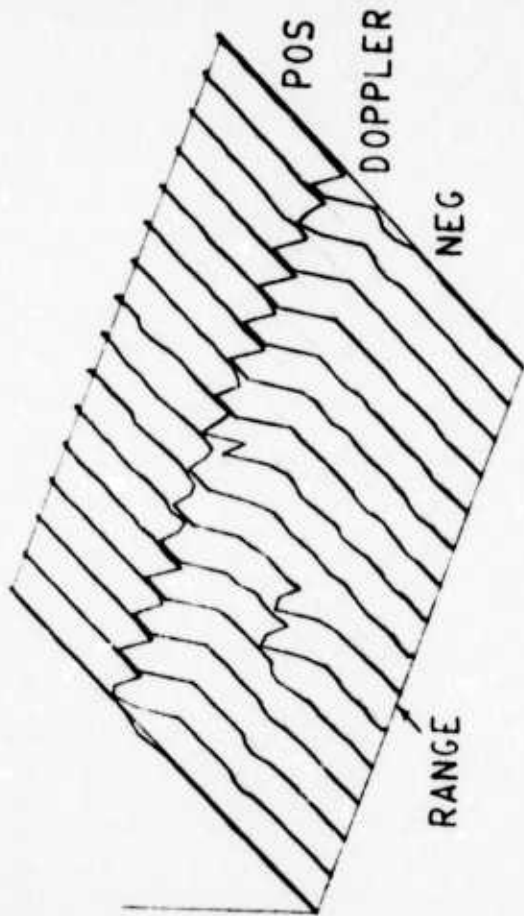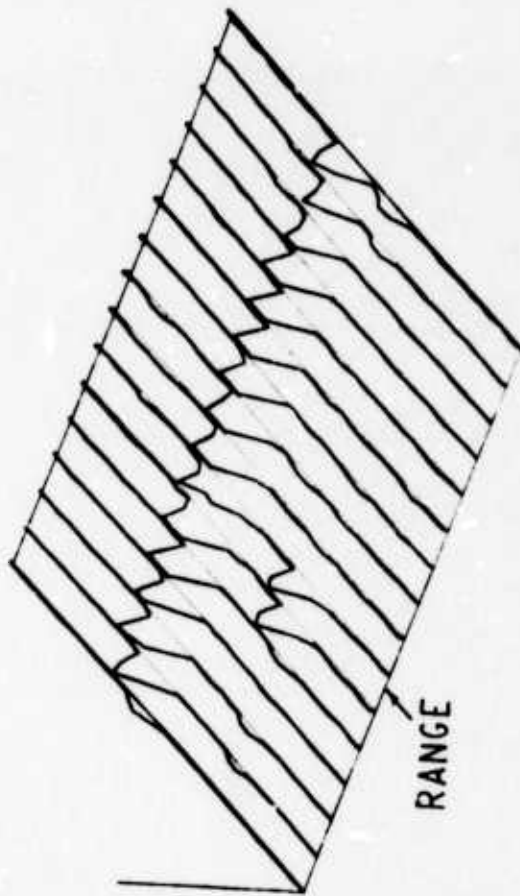
c) Adaptive processor, $\alpha = 0.10$

d) Adaptive processor, $\alpha = 0.50$

Fig. 38 Range/doppler displays derived from File 12, Dwell # 7.

86
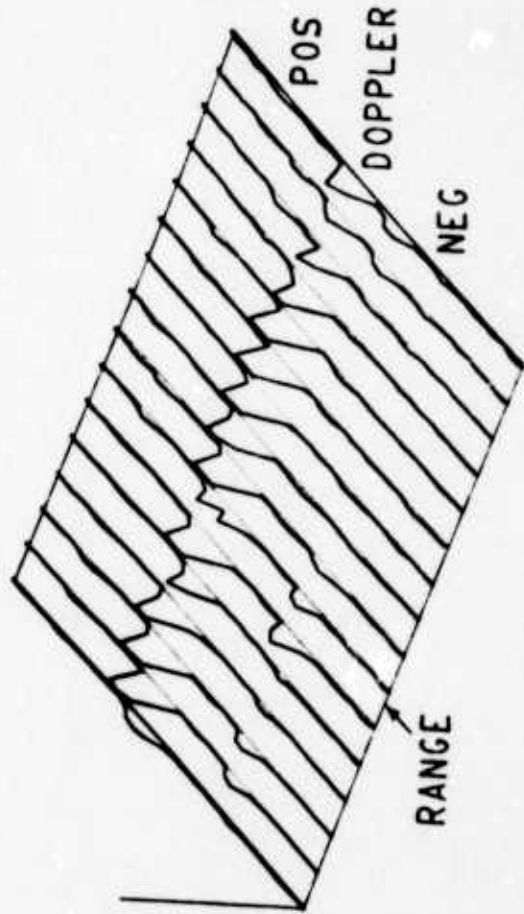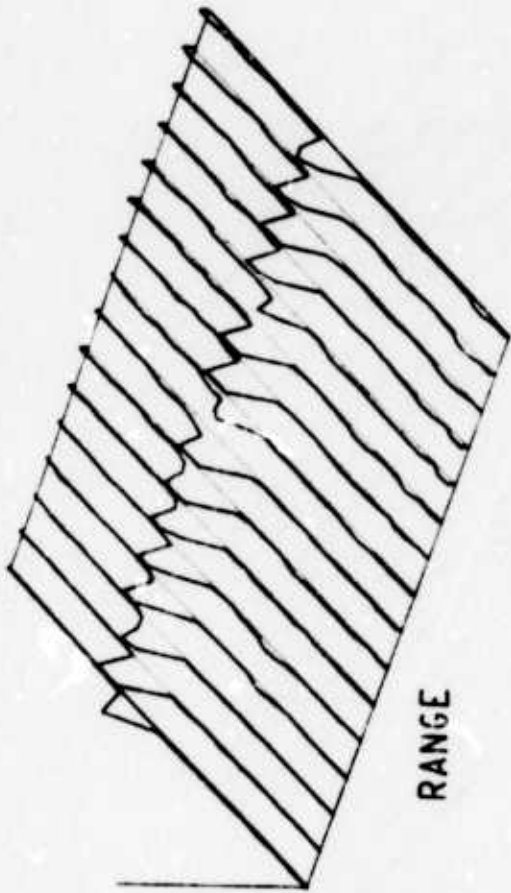
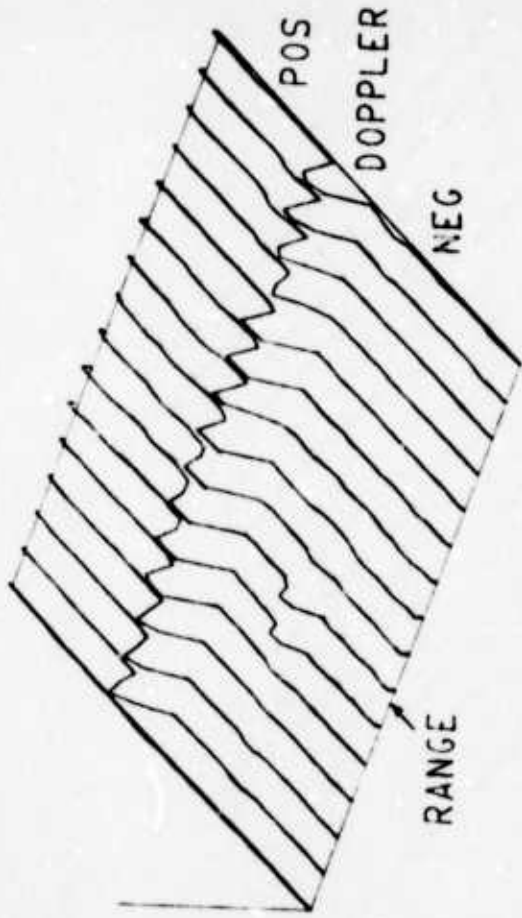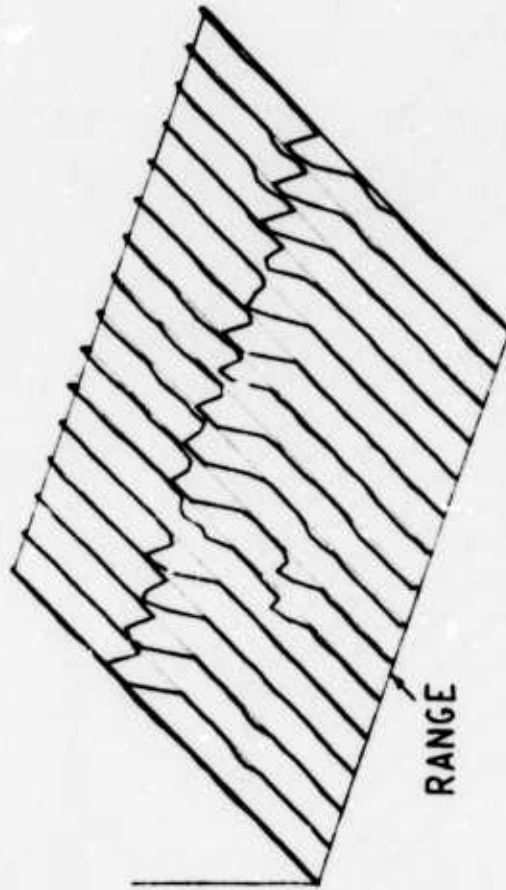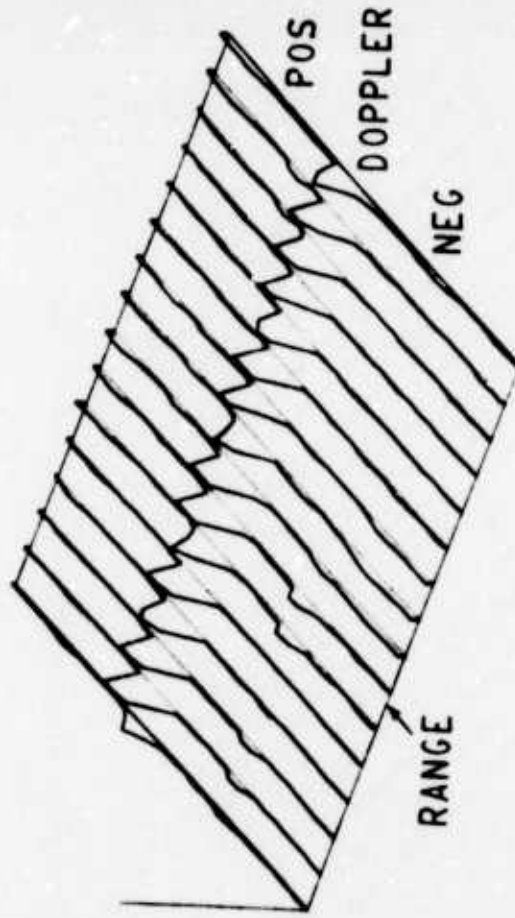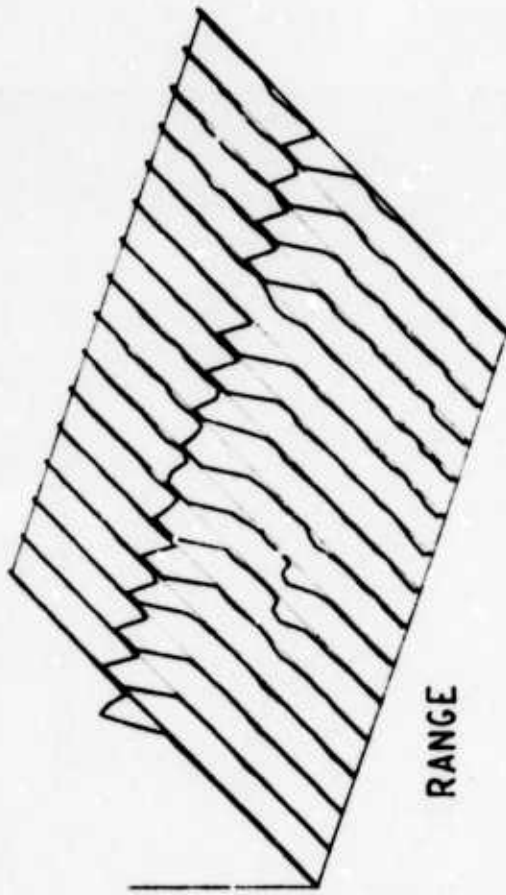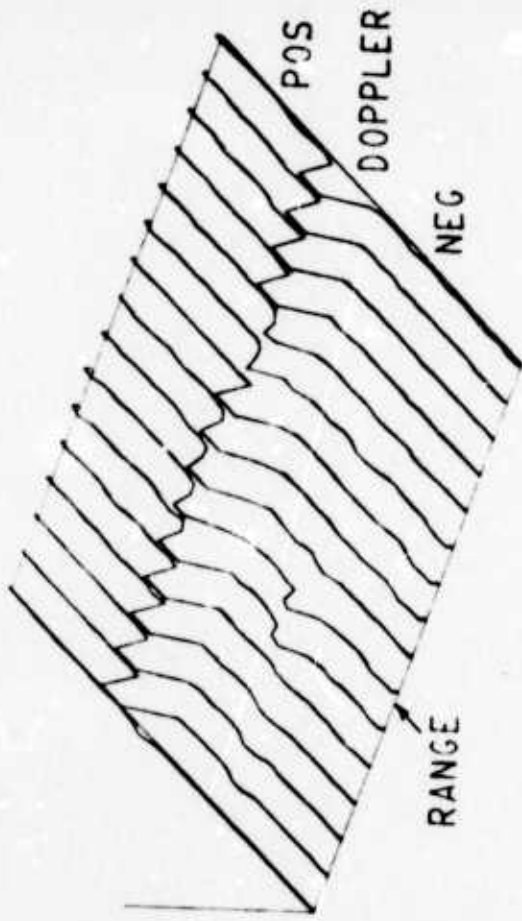b) Adaptive processor, $\alpha = 0.02$

d) Adaptive processor, $\alpha = 0.50$

a) Conventional processor
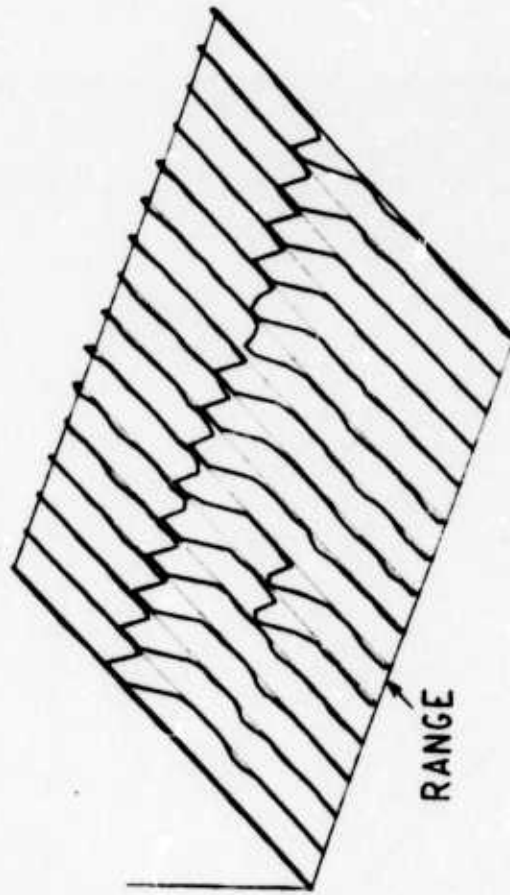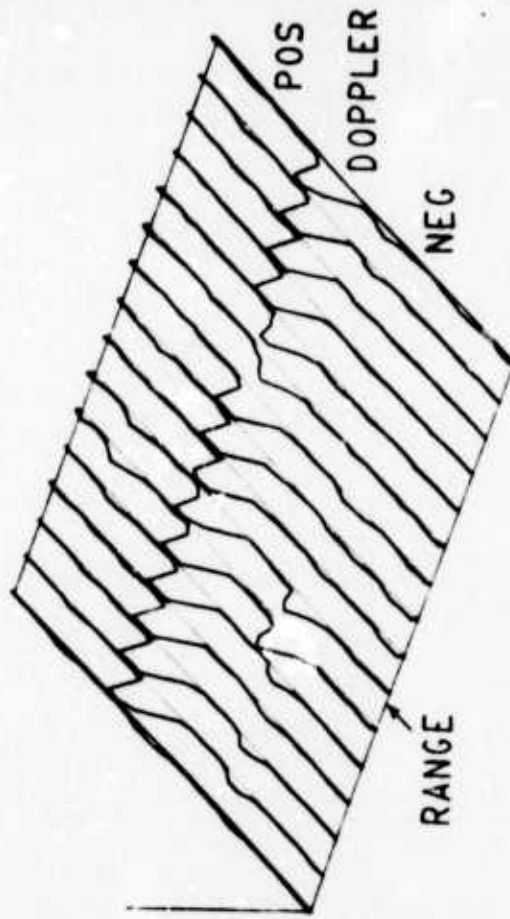
c) Adaptive processor, $\alpha = 0.10$

Fig. 39   Range/Doppler displays derived from File 12, Dwell # 8.

α value	τ_a(m.sec)
0.02	520
0.10	103
0.50	20

Thus, at the smallest value of α used, the time constant was approximately equal to the dwell period. Rapid adaptation may induce an output noise component which is produced by fluctuation of the processor coefficients. An example of this effect at $\alpha = 0.5$ is evident in Fig. (34c).

Computations were also carried out to determine the degree to which the coefficient values were oscillating due to adaptation during this experiment. Mean and root-mean-square (RMS) values for the coefficients were derived using a 128 sample average. The results obtained with $\alpha = 0.1$ are summarized in Table V. Similar tables were constructed for $\alpha = 0.5$ and $\alpha = 0.02$ and the data for all three α values were used to compile an average "coefficient variation" γ as follows

$$\gamma = \frac{1}{KL} \sum_{i=1}^{K} \sum_{j=1}^{L} |M_{ij}/\sigma_{ij}| \qquad (35)$$

where K = no. of elements

L = no. of coefficients/element

M_{ij} = mean of jth coefficient at ith element

σ_{ij} = RMS of jth coefficient at ith element.

The values obtained as a function of α and expressed as a percentage were

α value	γ
0.02	2.26%

88

TABLE V: Mean (M) and RMS (σ) coefficient values obtained using a 128 sample average for Record 1, File 12 with $\alpha = 0.10$

Array Tap No.	ARRAY ELEMENT NO.							
	1		2		3		4	
	M	σ	M	σ	M	σ	M	σ
0	-2.03	0.091	-1.91	0.043	-2.61	0.078	-1.55	0.052
1	0.23	0.042	1.01	0.036	1.81	0.043	0.88	0.050
2	3.06	0.133	2.62	0.101	3.14	0.110	2.91	0.121
3	2.89	0.078	0.36	0.043	0.48	0.025	0.94	0.027
4	-1.51	0.046	-0.88	0.044	-3.66	0.071	-0.78	0.039

$$0.10 \qquad 3.69$$

$$0.50 \qquad 7.75$$

These results indicate that larger values of α produce a greater percentage coefficient oscillation, as expected from the known theory of convergence for the P-vector algorithm. Observation of the range/doppler maps shown in Figs. 32-39 further indicates that γ values the order of 8% induce detectable changes in the map. With $\alpha = 0.1$, the percentage change in coefficients was reduced to less than 4% and no adaptation effects were observed in the range/doppler outputs.

VII DISCUSSION AND CONCLUSIONS

This report has investigated the applicability of adaptive beamforming techniques to HF radar arrays. It has been shown that a simple adaptive algorithm can be used to combine individual received subarray signals within a large array so as to provide an effective increase in the received signal-to-noise ratio relative to conventional beamforming methods. The adaptive processor has been shown to provide combined azimuthal and frequency selectivity within a one kHz. bandwidth centered at about eleven MHz.

Specific results were obtained for the case of forward scatter one-hop ionospherically propagated signals received in the presence of teletype and other interference and noise waveforms. Signal-to-noise ratio improvements observed for this class of signals varied between 3dB, for the case of one adaptive coefficient per subarray element, to about 11 dB for the nine coefficients per element case. Total time taken to adapt from zero weight values to the optimal solution was less than 40 m.sec. for all tests.

Adaptive experiments were also carried out in the presence of CW backscatter signals. These tests demonstrated that adaptation can significantly increase the received SNR of a repeater signal offset by 100 Hz from the clutter. Adaptive performance in the presence of clutter was for all practical purposes identical with that observed in the forward-scatter experiments. Greater than 25 dB improvements against clutter and noise were observed.

Perhaps the most significant results were obtained using FM/CW sweep frequency transmitter waveforms. Range/doppler maps were computed from receiver array output signals using both conventional and adaptive beamforming methods to combine the subarray outputs. Tests were conducted using both known repeater signals and using targets of opportunity. In all cases, the range/doppler display produced with adaptive beamforming was significantly improved over that generated by conventional steering. Specific improvements in excess of 12 dB within a selected range/doppler cell were observed on several occasions (Figs. 33 and 34).

The adaptive algorithm, employed in these studies was originally designed for use in passive sonar receiving arrays and has not been optimized for use in the FM/CW radar environment. The results obtained, however, demonstrate that the procedure is well suited to FM/CW transmissions and steps taken in this research to further optimize the algorithm did not lead to significant performance improvements.

The primary conclusion drawn from the results presented herein is that time-domain adaptation can significantly improve the performance of an HF FM/CW radar system. The procedure may be readily implemented in real time using either special purpose hardware of a fast general-purpose computer. Further research, however, is required to determine the optimal implementation configuration. This research should consider both analog/digital hybrid systems and the all digital approach used in the present study. Additional investigations should also be carried out to determine the optimal subarray geometry for the system.

References

1 L.J. Griffiths and M.J. Larimore, "Adaptive array processing of HF signals propagated over a 2600 km. path," RADC - TR - 73-75 Final Technical Report, January, 1973.

2 Staff, The ARPA-ONR Wide-Aperture High-Frequency Radio Research Facility, Ionospheric Dynamics Group, Radio-science Laboratory, Stanford University, Stanford, California, 1969.

3 L.J. Griffiths, "Final Report: Adaptive antenna processing literature survey," Dept. of Electrical Engineering Report No. 13789, University of Colorado, Boulder, Colo., January, 1972.

4 B. Gold and C. Rader, Digital Processing of Signals, McGraw-Hill, Inc., New York, 1969.

5 J. Capon, R.J. Greenfield, and R.J. Kolker, "Multidimensional maximum-likelihood processing of a large aperture seismic array," Proc. IEEE, Vol. 55, pp. 192-211, January, 1964.

6 O.L. Frost, "Adaptive least squares optimization in subject to linear equality constraints," SU-SEL-70-055, Center for Systems Research, Stanford University, Stanford, California, August, 1970.

7 L.J. Griffiths, "A simple adaptive algorithm for real-time processing in antenna arrays," Proc. IEEE, Vol. 57, No.10, pp. 1696-1704, October 1969.

8 A. Papoulis, Probability, Random Variables and Stochastic Processes, McGraw-Hill, Inc., New York, 1965.

9 K. Senne, "Adaptive linear discrete-time estimation," Ph.D. Dissertation, Stanford University, Stanford, Calif., September, 1968.

10 T.P. Daniell, "Adaptive estimation with mutually correlated training samples," Ph.D. dissertation, Stanford University, Stanford, Calif., September, 1968.